Quantum-Optical Properties of Quantum Dot Based Photonic Crystal Mesoscopic-Cavity

THESIS

Submitted in partial fulfillment
of the requirements for the degree of
DOCTOR OF PHILOSOPHY

by

SAJIA YEASMIN
ID No. 2019PHXF0051H

Under the Supervision of
Prof. Souri Banerjee

and

Under the Co-supervision of
Prof. Aranya B Bhattacherjee

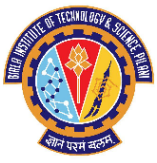

BIRLA INSTITUTE OF TECHNOLOGY AND SCIENCE, PILANI,
2024

BIRLA INSTITUTE OF TECHNOLOGY AND SCIENCE, PILANI

CERTIFICATE

This is to certify that the thesis entitled, **"Quantum-optical properties of quantum dot based photonic crystal mesoscopic-cavity"** submitted by **SAJIA YEASMIN** ID No. **2019PHXF0051H** for the award of Ph.D. of the institute embodies original work done by her under my supervision.

Signature of the Supervisor
Prof. Souri Banerjee
Department of Physics,
BITS-Pilani, Hyderabad Campus.
Date: 18/03/2024

Signature of the Co-Supervisor
Prof. Aranya Bhuti Bhattacherjee
Department of Physics,
BITS-Pilani, Hyderabad Campus.
Date: 18/03/2024

Acknowledgements

I would want to take this occasion to express my sincere gratitude to everyone who assisted me in any manner throughout the course of my research work.

I want to start by expressing my gratitude to my supervisor Prof. Souri Banerjee and my co-supervisor Prof. Aranya Bhuti Bhattacherjee for their guidance, advice and for providing me with a comfortable research environment throughout the course of my doctoral career. I'm grateful for their constant support and value such encouragement which allowed me the freedom to grow independently.

I will always be grateful to Prof. V. Satya Narayana Murthy and Prof. Nirman Ganguly for contributing their recommendations and suggestions as my Doctoral Advisory Committee (DAC).

I am grateful that Birla Institute of Technology and Science, Pilani, Hyderabad Campus offered me an institute fellowship and gave me access to the research facilities for my work. I also want to express my sincere gratitude to the entire team of BITS Pilani, Hyderabad administrators for their support.

I truly appreciate all the professors from the Physics Department at BITS Pilani, Hyderabad Campus for their support and insightful feedback during my doctoral journey. I wish to express my gratitude in particular to Prof. P. K. Thiruvikraman whose disciplined lifestyle inspired me and Prof. Sarmistha Banik and Prof. Kannan Ramaswamy for their encouragement and support. I also like to thank the technical and non-technical members of the Physics Department for their support and productive conversations about my research.

I express my sincere gratitude to my senior colleague and good friend, Mr. Sabur Ahmed Barbhuiya, for his insightful feedback which helped me to enhance the quality of my research work. I shall forever be grateful for his constant support and constructive criticism throughout my doctoral studies.

I want to sincerely thank all my colleagues turned friends in BITS, Pilani, Hyderabad Campus especially Aishwarya, Prajakta, Yash, Urjjarani, Anamika, Suraj, Waseem, Nobleson, Haridev, Sreeshna, Nilofar, Geetika, Greeshma, Akhil, Akshay, Viswa, Pallavi, Lubna,and Anuradha for

their wonderful company, support, and best wishes throughout my doctoral career. I thank them for all the love and laughter and making me feel home away from home.

I would like to thank my beloved parents for their constant blessings and support in every stage of my life. I thank them for believing in me and encouraging me always. I'm forever indebted to both of your contribution to my life. I also thank my aunt, Shahida for keeping her blessed hand upon me since my childhood and loving me like her own child. I also thank my dearest elder brother, Irfan for his pure love, encouragement and blessings without which this academic journey would not have been possible. I would also like to thank my best friend turned sister, Sabanam Talukdar for being there for me in all the highs and lows of my career. I thank her for walking by my side like a constant shield which gave me strength and courage. Last but not least, I would like to express my heartfelt gratitude to my school friends Sneha, Purbasha, Sabina, Suraiya and Salma for their moral support over the past 18 years.

Above all, I am always thankful to the Almighty for his immense blessings, and mercies, and for offering me good health and spiritual strength to complete my academic career.

Abstract

Optical and mechanical nanoscale devices are being combined to create a new class of hybrid systems. Mechanically tunable optical resonators and radiation pressure-driven optical resonators are two kinds of optomechanical devices that can be summed up based on their principles for interaction. Photonic crystal (PhC) cavities have received a lot of attention in sensing applications due to their excellent quality factors, tiny mode volumes, and superior on-chip integrability with waveguides/circuits. An integrated PhC cavity coupled to an optomechanical system benefits from the optomechanical interaction by offering a fascinating platform for ultrasensitive sensors to measure displacement, mass, force, and acceleration. In our study, we propose a few theoretical models which are experimentally feasible for quantum information processing and sensing applications and discuss the physical interpretations of their novel outcomes. PhC cavities based on optomechanical interaction offer extraordinary potential for developing lab-on-a-chip devices and show a bright future for further controlling light propagation in the field of nanophotonics.

Cavity optomechanics is an evolving field of study where the radiation pressure of the confined cavity photon is employed to establish a coherent coupling between the optical modes of the cavity and the mechanical modes of the oscillating membrane. Achievements like gravitational wave detectors, ultrahigh-precision measurements, quantum information processing, entanglement, optomechanically induced transparency (OMIT) and four-wave mixing process are examples of how quickly technology has advanced in this area. Due to the nonlinearity between the optical mode and mechanical mode, the optomechanical systems show optical bistability and multistability. This optical phenomena has real-world applications in all-optical switching and memory storage. Optomechanically induced transparency (OMIT) has fascinating applications in quantum information processing, slow light devices, and ultra-sensitive sensors. It offers a method for controlling how light is manipulated, as well as a platform for investigating quantum coherence and control in the interactions between light and mechanical vibrations. Optomechanical systems can also show the extraordinary optical phenomena known as Fano resonance, which depends on quantum coherence and interference. While EIT and OMIT both indicate symmetric line profiles, a Fano resonance

exhibits an asymmetric line profile. In various research and application fields, tunable Fano resonance offers a number of significant advantages. Researchers can control optical responses and increase efficiency in various photonic devices by modifying the Fano resonance to increase or inhibit particular interactions. Significant improvements in nonlinear optical effects can also result by controlling Fano resonance. Applications like frequency conversion, signal processing, and quantum information processing also rely upon this phenomena. All-optical switches can be created which are effective and extremely fast by taking advantage of the asymmetric response of Fano resonances to control light transmission. The potential to modify and control quantum states and quantum entanglement in quantum systems is provided by Fano resonance control which is essential for quantum state engineering and quantum sensing. The nonlinear optical phenomenon known as four-wave mixing (FWM) plays an important role in many areas of photonics, quantum optics, and communication. The technique involves the coupling of several optical waves with a nonlinear medium, which causes a nonlinear mixing of the input waves in order to generate new frequencies. Applications in spectroscopy, nonlinear optics, quantum technologies, and telecommunications show how important the four-wave mixing process is. It is an essential component of recent photonics and optical research because of its potential to create new frequencies and modify optical signals in a nonlinear manner.

Strong light-matter coupling in a hybrid system can be demonstrated through vacuum Rabi splitting. It is possible to create quantum dot-based on-chip devices using any hybrid CQED system that exhibits VRS. In order to do this, non-linearities in hybrid semiconductor cavities may be crucial for coherently manipulating VRS and producing novel, intriguing physics that can be used to realize novel quantum devices.

An in-depth introduction to cavity optomechanics is given in **Chapter 1** with a brief discussion of cavity quantum electrodynamics, quantum dots, photonic crystal cavities, mechanical oscillator, radiation-pressure interaction, and other optical response phenomena. Here, the importance of vacuum Rabi splitting, optical switching capability, optomechanically induced transparency, and four-wave mixing technique are briefly discussed. Additionally, it briefly described numerous

experimental possibilities and the uses of quantum photonics equipment in relation to various nonlinear interactions.

In **Chapter 2**, an overview of the numerical methods used to solve the Heisenberg-Langevin equations of motion is given along with a more or less detailed explanation of the steady state and semiclassical approximation equations. This chapter also gives a very quick summary of the literature required for numerical and analytical calculations to evolution equations.

In the framework of VRS, optomechanical nonlinearities caused by the radiation pressure of light on a mechanical resonator have not been investigated earlier which we thoroughly explored in **chapter 3** and proposed a theoretical model that consists of a hybrid quantum electrodynamics (C-QED) system where a QD-based photonic crystal optomechanical microcavity is coupled to an auxiliary cavity with a single mode waveguide. The auxiliary cavity plays an essential role to explore the system's quantum dynamics. An optical waveguide capable of supporting only a single optical mode connects the system to an auxiliary cavity. We show the possibility to achieve tunable optical bistability, double-bistability, and tristability, which may be used to develop multi-valued logic circuits and all-optical switch systems that will eventually be a part of a large-scale quantum communication platform. Additionally, it has been observed that the proposed system exhibits the Mollow triplet and Fano resonances that have been modified by an optomechanical interaction. The optomechanically induced transparency (OMIT) has been superimposed on the Fano resonance (OMIT-Fano resonance), with the transparency window appearing exactly at the point where the probe detuning equals the resonant frequency of the mechanical oscillator.

We investigated the nonlinear four-wave mixing process, which was yet another unexplored region in C-QED. In **chapter 4**, we have proposed a theoretical model where we examined the optical response properties of a quantum dot (QD) embedded in an optomechanical photonic crystal (PhC) nanocavity which is coherently driven by two-tone laser fields. Our theoretical analysis shows optical bistability, where the steady-state photon number follows a steady increase in the switch's gain by controlling a strong pump field that drives the QD. A strong coupling between a quantized field and matter (e.g. in optical cavities) is a successful approach for conventionally

modifying the dressed state and by altering the field parameters, thereby achieving modulation of the QD dressed state. Additionally, we discuss the influence of exciton-nanocavity coupling strength, Rabi coupling strength, and off-resonant detuning of the laser fields in our proposed system, which generates a tunable four-wave mixing (FWM) signal in the transmission spectra of the output probe field of the system. When strong coupling and high pump power are present simultaneously, the intensity of the FWM signal is considerably changed which causes the formation of an OMIT window and slow light. The theoretical investigation of the proposed system may be useful for on-chip QD-based nanophotonic devices.

We have done a theoretical investigation in **chapter 5** on how a hybrid optomechanical system consisting of double mechanical modes coupled to a photonic crystal (PhC) nanocavity dynamically changes the amplification of the output probe field spectra. A quantum dot (QD) (two-level system) is also incorporated into the PhC cavity, which is simultaneously driven by an external pump and a probe field. We illustrate that the strength of the QD-cavity coupling can control multiple number of transparency windows that develops due to optomechanical interactions. The resonant frequency of the mechanical mode can be employed to precisely measure the Fano profiles of the optical responses. We also show the optical transition from optical bistability to tristability and multistability by varying the system parameter's switching threshold. The results obtained in our study showed us some convenient way to explore all-optical-switching and sensing applications along with optical nonreciprocity in multi-resonator photonic systems.

The conclusion of my research work and a potential overview of the future aspect of the current work are present in **chapter 6**.

Contents

List of Figures

CHAPTER 1

Introduction

In this chapter, the fundamental laws of physics and phenomena are briefly introduced which serves as the thesis's underlying theoretical framework. The prime focus of this chapter is on quantum dot, photonic crystal cavities, cavity quantum electrodynamics (CQED) and radiation-pressure interaction to study different types of optical response properties in different hybrid optomechanical systems.

1.1 Cavity quantum electrodynamics

Cavity quantum electrodynamics (CQED) is the study of interaction between a single mode radiation field and matter which allow the study of various quantum optical phenomena like quantum-classical boundary, quantum entanglement, quantum decoherence etc [1]. The characteristic of all

physical system is that they are open system with a limited degree of coherence. An atom-photon system can achieve quantum coherence over dynamically significant time scales if it is confined within a high-quality cavity, allowing the system to be significantly insulated from the decohering interaction with its surroundings. For quite a long time, CQED has been the fundamental approach for the study of an open quantum system which offers a special framework to rigorously and systematically explore decoherence. The recent progress in CQED experiments is due to the higher degree of coherence which makes them a suitable testing ground for fundamental concepts in quantum control and quantum computation. Light can be confined in optical cavities in a small mode volume, which can result in a strong electric field inside the cavity. Therefore, one can achieve strong light-matter interactions by embedding matter inside the cavity. The perturbation theory can be used to explain the dynamics of the system when the interaction strength is less than the system losses and the coupling between the emitter and cavity field is weak. On the other hand, when the interaction strength is greater than the system losses then a strong coupling regime is attained. The entangled quantum dot (QD) and cavity field eigenstates for such strongly coupled systems are referred to as polaritons, which are hybridised states of light and matter. Recent developments in nanofabrication technologies have made it possible to integrate CQED systems into integrated semiconductor platforms. To confine light in such systems, one uses nanophotonic cavities and quantum confined structures like quantum wells or quantum dots (QD). The potential of semiconductor technology is quite promising where a nano-photonic cavity can have a mode volume below $\sim (\lambda/n)^3$ which is substantially smaller than the mode volumes of Fabry-Perot cavities (usually of the order of 100-1000 λ^3) [2]. The volume that confines the incoming light is known as cavity mode volume and is given by

$$V_c = \frac{\int \epsilon(\vec{r})|\vec{E}(\vec{r})|^2 d^3\vec{r}}{max[\epsilon(\vec{r})|\vec{E}(\vec{r})|^2]}, \tag{1.1}$$

where $\vec{E}(\vec{r})$ is the electric field amplitude and $\epsilon(\vec{r})$ is the dielectric constant of the medium. When a quantum confined structure (QD) is placed inside a cavity where the value of $\epsilon|E|^2$ is maximum then its dipole moment μ, is proportional to the interaction strength between QD and cavity which

is given as,

$$g = \frac{1}{\hbar}\sqrt{\frac{\hbar\omega}{2V_c}}\mu, \tag{1.2}$$

where V_c is the cavity mode volume and g is the QD-cavity coupling strength. The coupled system is said to be in the strong-coupling regime if the interaction strength overcomes the dissipative losses. Here, photon and atom entangle, allowing the interaction between light and matter reversible. This characteristic signature is known as vacuum-field Rabi splitting. Potential applications in solid-state quantum information technology are a major source of the current excitement in the research community.

1.1.1 Jaynes Cumming Model

In 1963, Jaynes and Cummings performed the first detailed analysis of the interaction between a resonant cavity mode and an atom. They investigated the relationship between a two-level quantum mechanical system and a monochromatic electromagnetic field mode. Despite the fact that this model is clearly approximate, it has shown to be essential for understanding the basic interaction between light and matter. In 1984 the first experimental demonstration was done by Rempe, Walther, and Klein which is commonly employed in quantum information processing, particularly in circuit and cavity QED. The interaction between light and matter is described by the Jaynes Cummings model, which contains quantum mechanical framework. When an atom interacts with a single-mode cavity field, it takes the form with ground state atomic levels $|g>$ and excited level $|e>$ as

$$\hat{E} = e\frac{\hbar\omega}{\epsilon_0 V}^{\frac{1}{2}}(\hat{a} + \hat{a}^{\dagger})Sin(kz) \tag{1.3}$$

where e is polarization vector which is arbitrarily positioned. The interaction Hamiltonian is given as,

$$\begin{aligned} H_I =& -\hat{d}.\hat{E} \\ =& -\hat{d}e(\frac{\hbar\omega}{\epsilon_0 V}^{\frac{1}{2}})(a+a^\dagger)Sin(kz) \\ =& \hat{d}g(a+a^\dagger) \end{aligned} \tag{1.4}$$

where $\hat{d} = \hat{d}.e$. The atomic transition operators are written as $\hat{\sigma_+} = |e><g|$ and $\hat{\sigma_-} = |g><e| = \hat{\sigma_+^\dagger}$ and the inversion operator is written as $\hat{\sigma_z} = |e><g| - |g><g|$,where all the operators obeys the Pauli's spin algebra,

$[\sigma_+, \sigma_-] = [\sigma_+\sigma_- - \sigma_-\sigma_+]$

$= |e><e| - |g><g|$

$= \hat{\sigma_z}$.

Therefore, we can write, $[\sigma_+, \sigma_-] = \sigma_z$ and $[\sigma_z, \sigma_\pm] = 2\sigma_\pm$.

Considering the parity, $< e|d|e >= 0 =< g|d|g >$, we can write

$\hat{d} = d\sigma_- + d^\star|e><g|$

$= d\sigma_- + d^\star\sigma_+$

$= d(\sigma_+ + \sigma_-)$

Therefore, the interaction Hamiltonian is written as,

$$H_I = \hbar\alpha(\sigma_+ + \sigma_-)(a+a^\dagger) \tag{1.5}$$

where $\alpha = \frac{dg}{\hbar}$

When we consider the level of energy to be zero in between the states $|g>$ and $|e>$, then the free atomic Hamiltonian can be written as,

$$\begin{aligned} H_A &= \frac{1}{2}(E_e - E_g)\sigma_z \\ &= \frac{1}{2}\hbar\omega_0\sigma_z \end{aligned} \tag{1.6}$$

where $(E_e - E_g) = \frac{1}{2}\hbar\omega_0$.

After excluding the zero-point energy term, the free-field Hamiltonian is expressed as,

$$H_F = \hbar\omega a^\dagger a \tag{1.7}$$

Therefore, the interaction of the quantized electromagnetic field with a single electron atom is described by the total Hamiltonian as

$$\begin{aligned} H &= H_A + H_F + H_I \\ &= \frac{1}{2}(\hbar\omega_0\sigma_z) + \hbar\omega a^\dagger a + \hbar\lambda(\sigma_+ + \sigma_-)(a + a^\dagger) \end{aligned} \tag{1.8}$$

In case of free-field, the operators $\hat{a}$ and $\hat{a^\dagger}$ evolve as,

$\hat{a}(t) = \hat{a}(0)e^{-i\omega t}$

$\hat{a^\dagger}(t) = \hat{a^\dagger}(0)e^{i\omega t}$

Similarly, for the free-atomic case, the operators evolve as $\hat{\sigma_\pm}(t) = \hat{\sigma_\pm}(0)e^{\pm i\omega_0 t}$

As a result, we can observe that Eq. (1.8)'s operator products have the following approximate time dependences which does not conserve energy,

$\sigma_+ a \sim e^{i(\omega_0-\omega)t}$

$\sigma_- a^\dagger \sim e^{-i(\omega_0-\omega)t}$

$\sigma_+ a^\dagger \sim e^{i(\omega+\omega_0)t}$

$\sigma_- a \sim e^{-i(\omega+\omega_0)t}$

If $\omega \approx \omega_0$, then the last two terms change much more quickly than the first two where, unlike the first two terms, the last two terms do not conserve energy. When an atom is moved from a higher energy state to lower energy state, the situation in which a photon is generated is referred to as "$a^\dagger\sigma_-$". Additionally, when an atom is moved from a lower energy state to a higher energy state then a photon is destroyed or annihilated ,such a situation is expressed as "$a\sigma_+$" . In both cases, energy is conserved and the process of an atom changing from a higher to a lower level whilst simultaneously annihilating a photon is described by the term "$a\sigma_-$" which results in a loss of energy of around $2\hbar\omega$, whereas the process described by the term "$a^\dagger\sigma_+$" results in a gain of energy of $2\hbar\omega$ [3]. This result violates the law of conservation of energy where the conserved

energy terms are kept, but the non-conserving energy terms are eliminated in the rotating wave of approximation.

Therefore, the Hamiltonian is simplified as

$$H = \frac{1}{2}(\hbar\omega_0\sigma_z) + \hbar\omega a^\dagger a + \hbar\lambda(\sigma_+ a + \sigma_- a^\dagger) \tag{1.9}$$

The above mentioned Hamiltonian is called as the Jaynes-Cummings Hamiltonian, which explains the behavior of a two-level atom with a single-mode mode field. This Hamiltonian can be calculated with high precision and describes quantum dynamics such as spontaneous emission, periodic recovery of atomic inversion, etc.

1.1.2 Vacuum Rabi splitting (VRS)

In the early 1980s [4], the research of vacuum Rabi splitting (VRS) with its first observation with atoms has been a fascinating area of atomic physics. Vacuum Rabi splitting with a single atom was observed after a decade of gradually improving the Q-factor of the cavity along with lowering its volume. This offered the discipline of atomic cavity QED fascinating opportunities. When a single photon or atom is added to a quantum system, the optical properties change, allowing the study of the quantum-classical boundary. But since atoms can move around and even leave, their coupling is dependent on time. Hence, it was obvious that the next target was to establish a cold atom using atomic traps [5] inside the cavity. The semiconductor equivalent of a two-level system is a semiconductor quantum dot (SQD), which is an extremely small semiconductor crystal that is confined three-dimensionally by a higher-bandgap material [6, 7]. It was demonstrated that, depending on size and form, the sharp emission lines seen from nanometer sampling areas result from transitions between discrete energy levels of the quantum dot. These atom-like transitions were subjected to coherent transient tests, and the Purcell effect was used to amplify and limit their spontaneous emission in microcavities with increasing Q. The requirement for strong coupling on Q is that the vacuum Rabi splitting, caused by a SQD, must be greater than the average of the decay rates of the cavity, κ, and the quantum dot. The strong coupling regime is intriguing

because it makes it possible to conduct nonlinear quantum optics experiments using as few as two photons, control the direction of emission as well as phase of one photon with another, observe single-atom lasing, study and use quantum entanglement, and investigate the boundary between the classical and quantum physics. If the coupling strength between two oscillators of identical energy is greater than the mean of their decay rates then the coupled system has two eigen-energies, with split states as shown in figure 1.1. VRS emerges when one of the oscillators is a two-level system or QD and the other is a high-Q small-volume cavity. The VRS has a numerical value of two times the product of the transition dipole moment and the vacuum field produced by the root-mean-square of the vacuum fluctuations (zero-point energy of 0.5 eV in the cavity mode). A Fabry-Perot interferometer's transmission formula can be easily understood by adding the QD or QW (quantum well) absorption and refractive index. If the absorption is strong and narrow enough, the transmission will become double-peaked. When this splitting occurs in a system with many atoms, it behaves classically, and removing or absorbing one photon has no impact. Although the splitting is completely eliminated when the SQD is removed, the VRS is a fundamentally quantum event if it results from the well-isolated transition of a single atom or SQD. This situation is known as the strong coupling regime of VRS. When the system is pulse stimulated, the strong coupling may be utilised to emit a single photon on request with the photons being indistinguishable from one another because the emission is predictable by adjusting the decay rate of the cavity which is considerably greater than the QD transition dephasing rate. Previously the source of SQD of single photons has functioned in the weak coupling zone of irreversible emission. However, strong coupling is a reversible technique that can be applied to coherently transfer quantum information between QDs and photons.

1.2 Quantum dots

Quantum dots (QDs) are nanostructured semiconductors which can be embedded in other semiconductor materials and has remarkable electrical and optical properties because of the quantum

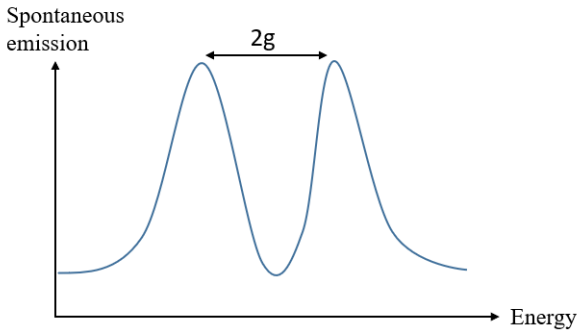

Figure 1.1: The spectrum of VRS for Zero atom-cavity detuning.

confinement of their energy levels where the electrons or any other charge carriers are confined in all three dimensions. Different quantum dot structures can be grown or made using various methods, resulting in confinement length scales that range from 2 to 100 nanometers. The size of the QD determines how differently it behaves optically for a particular material. The size typically falls between a few and tens of nanometers and such small sizes are typically smaller than the thermal electron's de Broglie wavelength. Excitons are the light-induced electron and hole pair that are held together by quantum confinement when QDs are optically excited. Due to their confinement nature, quantum dots (QDs) can only de-excite the carrier along restricted pathways, which results in slow cooling dynamics. [8, 9]. As a result, QDs can be used to extract electrical or chemical-free energy before relaxing to their lowest electronic state. This indicates that such slow cooling behavior in QDs can increase the possibility to generate multiple excitons since the exciton rate becomes similar to the cooling rate. For photo-driven applications using QDs, this chance of numerous excitons per excitation has important ramifications. The density of states in QDs exhibits a Dirac-delta (δ) like function, which reduces the continuous electronic energy bands to discrete quantized states and is denoted as,

$$D(E) = \sum 2\delta(E - E_n) \tag{1.10}$$

where D(E) and E are the corresponding density of state and energy. In quantum dots, the energy gap can be adjusted by changing the QD's dimension [10, 11]. The optical properties of QD are greatly influenced by the electron's quantum state because of the large surface ratio [12, 13]. The energy band structure of the QD exhibits coulomb attraction due to an electron confined in the conduction band and a hole confined in the valance band. A number of methods, including chemical synthesis in a regulated nucleation and growth environment, molecular beam epitaxy (MBE), and MOCVD (metal organic chemical vapour deposition), can be used to make quantum dots. Researchers have been looking at the unique properties of quantum dots in a variety of devices for many years, including LEDs, biological devices, solar cells, spintronics-based devices, etc. The intrinsic properties of QD structures might vary depending on the size, shape, crystallinity, defect and impurities. As a result, the fabrication of QD structures must be carried out in controlled conditions. Excitons within a quantum dot (QD) can either unite or change states both with or without emitting radiation [14]. In order to make QDs processable for usage in various applications, appropriate functionalization procedures must be used. Additionally, in order for a device to function properly, the carriers produced by these materials in response to optical or electrical stimulation must be separated and sent to an appropriate interface. To achieve this, QDs would need to be combined with other materials that would help in the delocalization of excitons as well as the transport of the split electrons or holes [15].

1.3 Photonic crystal cavity

In experiments involving quantum optics, two-dimensional PhC (photonic crystal) structures are commonly used, where a cavity is created by introducing a defect into the periodic structure. The term "photonic crystals" often corresponds to structures with periodic dielectric constants in two and three dimension, whereas distributed Bragg reflectors (DBRs) are used to describe one-dimensional periodic medium [16]. The fundamental characteristics of photonic crystal are significantly altered when a 'defect' is created on it. In other words, when a defect is introduced into

the periodicity of the crystalline structure, a micro/nano cavity surrounded by a highly reflective mirror region is formed which allows the photonic crystal to localize light. According to Vukovi et al.(2002), the defect causes dispersed Bragg reflection to limit light in-plane and complete internal reflection to restrict it out-of-plane and if the size of the cavity has a small mode volume then the electric field produced by a single photon inside the cavity will be substantially enhanced. In general, the structures of photonic crystal devices show high optical confinement over a large frequency range. High optical confinement in a small volume is required to offer a good platform for the optical emission properties, enhancing the luminous atoms by spontaneous emission. Photonic technology has evolved greatly for various applications, either using devices like III-V semiconductor materials, or devices like silicon and silica. Although the fundamental goal is still to produce a single photonic integration which is able to manage any application in a microchip, the latter two materials continue to function as a distinct system. There has been much discussion of the innovations based on theories by Purcell [17, 18] regarding the impact of radiation characteristics brought on by the presence of mirrors. As a result of these ideas a revolutionary concept of photonic crystals [19, 20] came into existence. Photons can be controlled in dielectric periodic structures (Photonic crystal), that show photonic band gap and stopband behavior, in contrast to controlling the electrons that are included for using the electronic properties (of solids), in order to create an electronic band gap. In other words, there is a prohibited gap or band gap due to which photons cannot propagate through the periodic structures. When light is allowed to pass through photonic band gap structures over a certain photon energy range, it reflects back when it hits the periodic structure and is not allowed to propagate, forming the so-called forbidden zone. The optical characteristics of photonic crystal cavity (micro or nano) structures can be described by the ratio Q/V_c, where V_c is the mode volume and Q is the quality factor associated with a specific cavity and its distinctive microwave resonant modes. When light is trapped within a small volume of the order of $(\lambda/2n)^3$, where n is the refractive index of the supplied material, and λ is the emission wavelength, then developing high Q-factor optical cavities (micro or nano) confined in a small volume may be beneficial for fast optical processing. The Q-factor is very helpful in figuring out

how a system will behave qualitatively. A system's quality factor is a non-dimensional parameter that describes the first-order characteristic of an oscillating frequency decaying inside a microcavity. It can be identified by a decrease in the amplitude of the propagating wave through the system throughout the course of an oscillation. The quality characteristics and optical transmission at a specific resonance frequency influence the performance of particular resonances for some telecom applications, like dense wavelength division multiplexing (DWDM). When the Q-factor is higher, there is a slower rate of energy dissipation in relation to the resonant frequencies, which prolongs the life of the oscillations. A pendulum oscillating in the air while suspended on a high-quality bearing, for instance, will have a high Q, whereas a pendulum submerged in oil would have a low Q. The Q-factor in optics is typically given by [21],

$$Q = \frac{2\pi f_r E}{P_d} \tag{1.11}$$

where f_r is the resonant frequency, E is the energy stored in the cavity and P_d is the power dissipated from the cavity given as, $P_d = -\frac{dE}{dt}$. The ratio of the resonance frequency to the bandwidth of the cavity resonance gives the Q-factor as shown in Figure 1.2. The quality factor of a cavity is proportional to the average lifespan of a resonant photon. Resonant systems react much more strongly to frequencies that are close to their resonance frequency compared to other frequencies. When compared to a system with a low-quality factor, a high-quality system resonates with a larger amplitude and exhibits a faster decay in response as the frequency approaches resonance. Hence, the physical explanation of resonance is given by the equation,

$$Q = \frac{f_r}{\Delta f} \tag{1.12}$$

where Δf is the difference in frequency of the total energy stored in the cavity (micro/nano) system

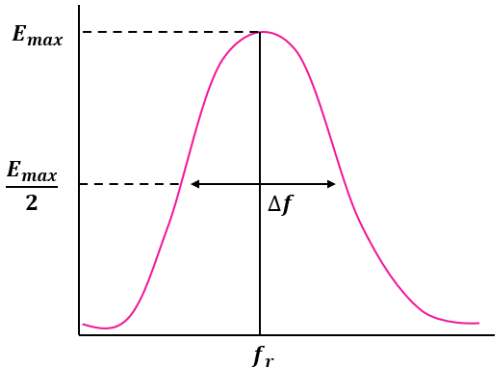

Figure 1.2: Resonance frequency resulting from the structure of a cavity (micro/nano) described by the central resonance frequency and the frequency's bandwidth

1.4 Mechanical Oscillator

The momentum exchange between photons and a mechanical degree of freedom occurs during the radiation pressure interaction between light and matter. The mechanical oscillators used in research feature many degrees of freedom and eigenmodes, whose spectral properties depend on the oscillator's structure, material, and interaction. The spatial structure of a mechanical mode can be defined using a displacement field x(r, t), which in general geometries can be arbitrarily complex. We can expand x(r, t) based on the eigen-modes and the time-dependent amplitudes of the oscillators as

$$x(r,t) = \sum_n A_n(t) x_n(t) \tag{1.13}$$

where $A_n(t)$ is the time-dependent amplitude.

In spite of the fact that mechanical oscillators are often not linear in how they react to applied forces, linearity offers a decent approximation for small deformations that are frequently realized during normal operation. Thus, we model the time-dependent amplitudes to correspond to the damped harmonic transformation given by

$$\ddot{A}_n(t) + \kappa_n \dot{A}_n(t) + {\omega_n}^2 A_n(t) = \frac{F_{ex}}{{m_{ef}}^{(n)}}. \tag{1.14}$$

where κ_n and ω_n represent the damping constant and angular frequency of the n-th eigen-mode, respectively, while ${m_{ef}}^{(n)}$ stands for the corresponding effective mass derived from the mode volume of x_n. F_{ex} represents the total external force (which includes fluctuating Langevin forces and radiation pressure types) acting on a specific mechanical mode. For a single-mode case, we can assume that one can only address a single mechanical eigenmode. The spectral overlap between this mode and its nearby modes is presumed to be negligible. The resonance frequency of this mode is denoted by ω_m, while the energy dissipation rate is denoted by κ_m. We'll designate the oscillation's associated amplitude as $A_n(t)$. The possible eigenmode of a model like the Fabry-Pérot cavity is the center-of-mass oscillation, and the amplitude $A_n(t)$ corresponds to the mirror's displacement from its steady state. Thus, the mirror's overall mass is nearly equal to the effective mass m_{ef} without considering the mass of the mirror. The mechanical oscillator is coupled to its support, which both serves as a thermal environment (often known as a "heat bath") and a source of noise for the mechanical oscillator, which results in the damping described in Eq. 1.14. As originally proposed by Caldeira and Leggett [22], this heat bath is typically represented as a collection of many harmonic oscillators together in a thermal state (at temperature T). A Bose-Einstein distribution governs the mean bath occupation number, given by $n_b(\omega) = \frac{1}{exp(\hbar\omega/k_BT)-1}$ where k_B is the Boltzmann constant. At high-temperature, the mean bath occupation as a function of the mechanical frequency can be roughly estimated as $n_b(\omega_m) \approx k_BT/\hbar\omega_m$. A mechanical oscillator with high-Q and a low-temperature bath is required for low thermal decoherence, and these components can be introduced to an experimental setup through cryogenic cooling. The thermal decoherence rate, often known as the effective decoherence rate, is given by $\bar{n}\kappa_m \approx k_BT/\hbar Q_m$, where $Q_m = \frac{\omega_m}{\kappa_m}$ is the mechanical quality factor. For the quantum analysis of the mechanical oscillator we introduce the position X_m and momentum operators P_m, which satisfy the canonical commutation relations $[X_m, P_m] = i\hbar$ where $i = \sqrt{-1}$. In quantum optics, the non-dimensional quadratures x_m and p_m with $[x_m, p_m] = i$ can be defined in terms of the creation and annihilation operators $a_m^\dagger$, a_m ($[a_m, a_m^\dagger] = 1$)

$$x_m = \frac{a_m + {a_m}^\dagger}{\sqrt{2}}, p_m = \frac{a_m - {a_m}^\dagger}{i\sqrt{2}} \tag{1.15}$$

Additionally, we convert the operators to $X_m = \sqrt{2}x_0 x_m$ and $P_m = \sqrt{2}m_{ef}\omega_m x_0 p_m$ by enhancing the oscillator's zero-point motion, $x_0 = (\frac{h}{2m_{ef}\omega_m})$.

1.4.1 Radiation pressure interaction

Radiation pressure refers to the force applied to any surface that has been exposed to electromagnetic radiation and which can be utilised for cooling atomic motion. Kepler was the first to postulate the concept that light has momentum and can, consequently, generate pressure due to a force known as the radiation pressure force. In the 17th century, he proposed these forces and suggested that radiation pressure seems to be what causes the tail of the comets. When light contacts an object's surface, it then transfers momentum to that object and creates a force known as radiation pressure. The electromagnetic field equation which Maxwell developed in 1873 foresaw the optomechanical effect of electromagnetic fields. Lebedew, Nichols, and Hull were the first to experimentally demonstrate the presence of radiation pressure at the beginning of the 20th century [23]. The transfer of momentum between photons and a mechanical degree of freedom occurs during the radiation pressure interaction between matter and photons. The interaction between the optical mode and mechanical mode in cavity optomechanical systems usually leads to a dispersive coupling, which changes the cavity resonance frequency depending on where the mechanical resonator is placed. In addition to the dispersive regime, there is an optomechanical coupling regime where the mechanical position influences the cavity decay rate [24, 25]. Prior to digging more into the optomechanical interaction, it is important to remember the simple example of a single photon that reflects back from the mirrored surface of a mechanical oscillator. The photon's impact causes a momentum transfer in the oscillator, which allows it to oscillate. In terms of quantum mechanics, the region where the oscillator's maximum displacement exceeds its zero-point motion, $x_{z0} = \sqrt{\frac{\hbar}{2m_{ef}\omega_m}}$, is unquestionably intriguing. In this regime, observations on a mechanical oscillator that is originally in its ground state can demonstrate the impact of photons that has actually occurred, serving as a quantum nondemolition (QND) measurement of the population of photons

in the field. Since, a photon with a wavelength λ has a momentum of h/λ, in the basic scenario where the photon reflects back from the mechanical resonator at normal incidence with unit efficiency, it gives the oscillator a $2h/\lambda$ momentum kick. This momentum kick causes a displacement of $\Delta x = 2h/\lambda m_{ef}\omega_m = 8\pi x_{z0}^2/\lambda$, after a quarter period, assuming the oscillator is significantly underdamped. In order to achieve the quantum regime, mechanisms are required to improve the interaction between the optical field and the oscillator. The conventional methods involve confining the field in a microwave cavity to increase the number of times the photons interact with the oscillator and thereby increasing the optical field's intensity. The amount of incoming incident radiation that impinges on the mechanical membrane determines the radiation pressure. Since photons often exert a very weak force on larger bodies, cavity optomechanical investigations employs an optical cavity as a resonator for the photons. This benefits both the increase in radiation pressure coupling and the increase in effective incident radiation.

1.4.2 Optomechanical coupling

The momentum transfer of photons is a basic process that couples the cavity radiation field's properties to the mechanical motion. The momentum transfer as a result of the reflection that takes place in a Fabry-Perot cavity is the most basic type of radiation-pressure coupling. In a dispersive cavity optomechanical system, the resonance frequency of an optical resonator generally couples nonlinearly to the location of the mechanical membrane. The field that departs the optical resonator carries enough information about the resonance frequency as well as the mechanical position. The optical or microwave field causes radiation pressure that helps in adjusting the position of the mechanical membrane. A change in the mechanical position of a moveable mirror in the Fabry-Perot cavity results in the modification of the resonance frequency of the cavity mode, which enables the description of the interaction Hamiltonian by describing the scaled coupling between the optical field and the mechanical resonator. As shown in Fig. 1.3, we are considering a Fabry-Perot cavity with length L having one end membrane, which is a part of the mechanical oscillator. The motion

of the mechanical oscillator due to radiation pressure interaction changes the length of the cavity to $L(x) = L - x$, where x defines the displacement of the mechanical oscillator from its equilibrium position and the minus sign is arbitrary, which denotes only the positive direction of mechanical vibration. The length of an optical cavity allows a number of longitudinal photonic modes with wavelengths

$$\lambda_j = \frac{2(L-x)}{j} \tag{1.16}$$

where j is the mode number and the mode frequencies are given by,

$$\omega_{c,j}(x) = \frac{2\pi c}{\lambda_j} = \frac{\pi c j}{L-x} \approx \omega_{c,j}(1 + \frac{x}{L}) \tag{1.17}$$

Here, the approximation holds true as long as $L >> x$, which is suitable for the large majority of cavity optomechanical systems, c is the speed of light, and $\omega_{c,j} \equiv \omega_{c,j}(0)$ is the cavity's bare optical resonance frequency where the cavity resonance frequency is denoted by the subscript c. We observe that the mechanical motion of the membrane has a tendency to shift linearly to first order with the resonance frequency of the optical cavity. The change in frequency per meter is measured by the optomechanical coupling strength g_0

$$G = \frac{\delta\omega_c(x)}{\delta x} = \frac{\omega_c}{L} \quad (Fabry - Perot\ \ cavity) \tag{1.18}$$

where we have neglected the mode number j. The Fabry-Perot cavity was the precise example utilised to arrive at Eq. 1.18, and the equation $G = \frac{\omega_c}{L}$ is only applicable to this particular type of cavity geometry. The optomechanical coupling strength is an important and widely applicable property.

1.4.3 Quantum Optomechanical system

Optomechanical systems can be found in a wide variety of physical applications, which can be explained using a simple model like a Fabry-Perot resonator. There are a number of resonances in a Fabry-Perot resonator or etalon, which consists of two highly reflecting mirrors separated by a

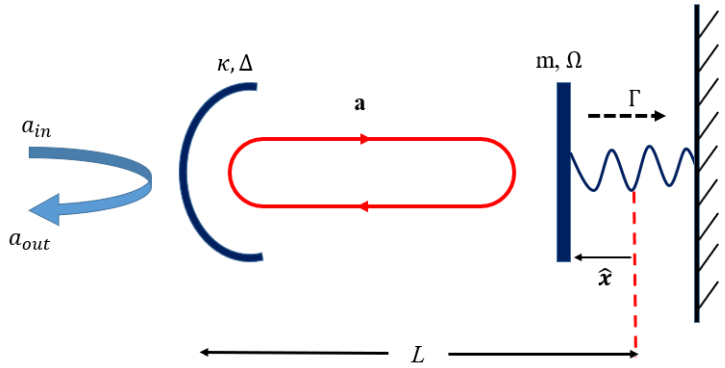

Figure 1.3: Schematic of a cavity optomechanical system

length L. Let us consider, a laser-driven cavity where the displacement of the moveable end mirror, x, determines the optical resonance frequency. The energy of the radiation in a certain cavity mode is calculated by multiplying its energy per quantum $\hbar\omega_c$ by the number of photons $(n(t))$ that are present in the cavity. Therefore,the Hamiltonian of the cavity mode is given by,

$$H_{cav} = \hbar\omega_c(x)n. \tag{1.19}$$

where we consider the cavity frequency's dependency on the mechanical oscillator.

The energy of the mechanical oscillator in absence of the radiation pressure interaction is given by,

$$H_m = \frac{p^2}{2m} + \frac{m\omega_m^2}{2}x^2. \tag{1.20}$$

where p,m are the momentum and mass respectively and ω_m is the resonance frequency of the mechanical oscillator.

When the quantum picture of the system is shown by replacing the classical variables with the corresponding operators $x \to \hat{x}, p \to \hat{p}, n \to a^\dagger a$ that satisfies the canonical computing relations $\hat{H} = \frac{k\hat{q}^2}{2} + \frac{\hat{p}^2}{2m}$ and $[a, a^\dagger] = 1$ then the quantum Hamiltonian is given by

$$H = \frac{p^2}{2m} + \frac{m\omega_m^2}{2}x^2 + \hbar\omega_c(x)a^\dagger a. \tag{1.21}$$

Expanding the frequency to linear order in x and introducing the raising and lowering operators of the mechanical mode as b and b, which also obey the Boson commutation relation $[a, a^\dagger] = 1$, we then write the Hamiltonian as

$$\begin{aligned} \hat{H} &= \hbar(\omega_c + Gx)a^\dagger a + \hbar\omega_m b^\dagger b \\ &= \hbar\omega_c a^\dagger a + \hbar\omega_m b^\dagger b + \hbar g_0 a^\dagger a(b^\dagger + b) \end{aligned} \tag{1.22}$$

The vacuum optomechanical coupling rate is defined by using the relation $\hat{x} = x_{zp}(a^\dagger + a)$ and is given by,

$$g_0 = Gx_{zp} = x_{zp}\frac{\omega_c}{L} \tag{1.23}$$

In every cavity optomechanical structure, the linear dispersive shift of the optical resonance frequency caused by the mechanical motion is measured by the optomechanical coupling strength from the perspective of the cavity field. It quantifies the interaction between a single phonon and a single photon. The optomechanical coupling rate, g_0 is one of the main parameter in the area of quantum optomechanics which has units of $(rads^{-1})$.

The interaction of a moving mirror with the radiation field is basically a nonlinear process that involves three operators (three-wave mixing) and the interaction Hamiltonian is given as,

$$H_{int} = -\hbar g_0 a^\dagger a(b + b^\dagger) \tag{1.24}$$

The resonance frequency ω_c of the optical cavity is greater than the other system parameters in most cavity optomechanics experiments. The total Hamiltonian,H_{total} also contains terms for fluctuations (influx of thermal phonons), dissipation (photon decay and mechanical friction), and driving by an external field. The input-output framework [26] and the equations of motion are the most effective ways to formulate these effects. In this regime, it is appropriate to modify the optical mode by applying a rotating frame at the incident laser frequency ω_L. By using the unitary transformation $\hat{U} = exp(i\omega_L a^\dagger at)$, the driving terms become time-independent and a new Hamiltonian ($\hat{H} = \hat{U}\hat{H}\hat{U}^\dagger - i\hbar\hat{U}\partial\hat{U}^\dagger/\partial t$) is formed,

$$H_{Tot} = \hbar\Delta_a a^\dagger a + \hbar\omega_m b^\dagger b - \hbar g_0 a^\dagger a(b^\dagger + b) \tag{1.25}$$

where $\Delta_a = \omega_c - \omega_L$ is the cavity-laser detuning.

1.4.4 Input-output theory for an optical cavity

The quantum fluctuations introduced into the cavity from any coupling point, like the input mirror, can be easily modelled using input-output theory. An electromagnetic resonator's energy can be expressed as a complex field amplitude, $\alpha(t)$, where $|\alpha(t)|$ gives the number of photons inside the resonator at time t. The energy in the resonator decays as the field amplitude changes.In general, the cavity decay rate κ can have two factors:

$$\kappa = \kappa_{ex} + \kappa_{in} \tag{1.26}$$

where κ_{ex} is the loss rate related to the incident coupling of radiation field with the cavity mirror and κ_{in} is the loss rate inside the cavity, which includes all the scattering and absorption losses behind the first mirror as well as the transmission losses at the second cavity mirror. Also, there will be no trace of the photon passing through the κ_{in} decay channel.

For open quantum systems, the input-output theory states that the field that is reflected back from the Fabry-Perot cavity is provided by,

$$a_{out}(t) = a_{in}(t) - \sqrt{\kappa_{ex}}a(t) \tag{1.27}$$

In case of a two sided cavity, an additional term $\sqrt{\kappa_{ex}^{(2)}}a_{in}^{(2)}$ is included for the transmission from the second mirror. We can assume the input field $a_{in}(t)$ to be a stochastic quantum field which represents a coherent laser drive in addition to the fluctuating vacuum electric field coupled to the cavity at time $'t'$.

Both the input noise operator and its adjoint follows the correlation and commutation relations [26] given below

$$[a_{in}(t), a_{in}^{\dagger}(t')] = \delta(t - t') \tag{1.28}$$

$$[a_{in}(t), a_{in}(t')] = [a_{in}^{\dagger}(t), a_{in}^{\dagger}(t')] = 0 \tag{1.29}$$

where $\delta(t)$ is the Dirac delta function.

Given that the input noise is assumed to be in a thermal condition, the correlation relations are:

$$< a_{in}^{\dagger}(t)a_{in}(t') >= \bar{n}\delta(t - t') \tag{1.30}$$

$$< a_{in}(t')a_{in}^{\dagger}(t) >= (\bar{n}+1)\delta(t-t') \tag{1.31}$$

$$< a_{in}(t)a_{in}(t') >=< a_{in}^{\dagger}(t)a_{in}^{\dagger}(t') >= 0 \tag{1.32}$$

Initially, when no mechanical mode is considered, the quantum stochastic differential equation is written as,

$$\dot{a}(t) = -\frac{i}{\hbar}[a(t), H] - \frac{\kappa}{2}a(t) + \sqrt{\kappa_{ex}}a_{in} + \sqrt{\kappa_{in}}f_{in}. \tag{1.33}$$

Suppose we are not considering the noise properties, but instead concentrate on the classical average quantities $< a >$. In the presence of a monochromatic laser field, whose amplitude is given by $< a_{in} >$, we can first solve Eq. (1.33) for the steady-state amplitude. For vacuum state ($< f_{in} >= 0$), steady state is given as,

$$< a >= \frac{\sqrt{\kappa_{ex}} < a_{in} >}{\kappa/2 - i\Delta_a} \tag{1.34}$$

In frequency range,

$$< a(\omega) >= \frac{\sqrt{\kappa_{ex}} < a_{in}(\omega) >}{\kappa/2 - i(\omega - \Delta_a)} \tag{1.35}$$

where ω refers to the Fourier frequency of the input field's fluctuations around its laser frequency ω_L.

The expression relating the incident laser field to the intracavity field indicates the optical susceptibility written as,

$$\chi_{op}(\omega) \equiv \frac{1}{\kappa/2 - i(\omega - \Delta_a)} \tag{1.36}$$

The steady-state population inside the cavity ($\bar{n} =< a^{\dagger}a >$) i.e., the average number of photons propagating inside the cavity is given by,

$$\bar{n}_{cav} = | < a > |^2 = \frac{\kappa_{ex}P}{[\kappa^2/4 + \Delta_a^2]\hbar\omega_L}. \tag{1.37}$$

Here, P is the input power injected into the cavity where, $P = \hbar\omega_L| < a_{in} >^2 |$.

Using Eq. (1.34) in Eq. (1.27), the reflection amplitude can be written as,

$$R = \frac{< a_{out} >}{< a_{in} >} = \frac{(\kappa_{in} - \kappa_{ex})/2 + i\Delta_a}{(\kappa_{in} + \kappa_{ex})/2 + i\Delta_a} \tag{1.38}$$

The square of reflection amplitude $|R|^2$ gives the probability of reflection from the cavity.

$$|R|^2 = \frac{(\kappa_{in} - \kappa_{ex})^2/4 + \Delta_a^2}{(\kappa_{in} + \kappa_{ex})^2/4 + \Delta_a^2} \tag{1.39}$$

If the external coupling κ_{ex} is greater than the cavity losses ($\kappa_{ex} >> \kappa_{in}$) then the cavity is called over-coupled and $|R|^2 \approx 1$. Therefore, the pump photons leave the cavity through the second mirror without being absorbed or lost.

If $\kappa_{ex} = \kappa_{in}$, then such situation is referred to as critical coupling where $R(\Delta_a = 0) = 0$ on resonance which indicates that either the input power is completely dissipated inside the resonator or the input power is completely transmitted through the second mirror.

If $\kappa_{ex} << \kappa_{in}$, then such cases is referred to as under-coupling and is linked to cavity losses that are primarily caused by intrinsic losses. This coupling condition is unfavourable for many studies since it causes a loss of information.

1.5 Optomechanical bistability

In some nonlinear optical systems, a specific input state might have more than one output state. Optical bistability refers to the event where two stable output intensities are achievable for a given input intensity, and optical multistability, in a broader sense, refers to the event in which two or more stable output states are possible [27]. In the year 1969, Szöke et al. made the first theoretical description of optical bistability and its experimental observations by using an absorptive nonlinearity. For the case of a refractive nonlinearity, Gibbs et al. [28] experimentally observed optical bistability in 1976. A nonlinear medium is positioned inside a Fabry-Perot cavity to create the bistable optical devices which is the subject of this research. A schematic illustration of such a device is illustrated in figure 1.4. To further understand this phenomenon, let's first review the conditions that must be met. When a continuous wave laser beam is incident on an optical cavity, like a Fabry-Perot cavity, it experiences partial reflection, absorption, and transmission. Following are the two cavity situations that can be thought about :

1. In the case of empty cavity without any absorbent material, the detuning and fineness of the cavity determines the ratio of transmitted power to incident power, which is constant.

2. In the case of filled cavity with absorbing material the Fabry-Perot resonator contains a nonlinear medium in order to build a bistable optical device. Here, the field amplitude of the

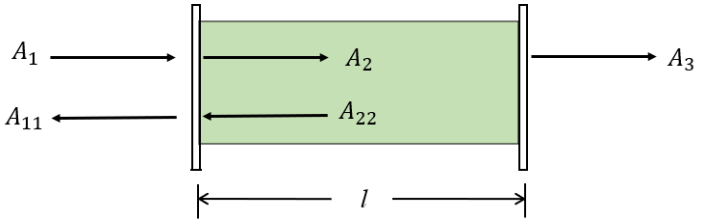

Figure 1.4: Schematic of a Fabry-Perot interferometer with a nonlinear medium inside is a bistable optical device.

incident wave is represented by $A1$, the reflected wave by $A11$, the waves going forward and backward inside the interferometer by $A2$ and $A22$, and the transmitted wave is denoted by $A3$. If the cavity mirrors are identical and lossless, the relationship between amplitude reflectance ρ and transmittance τ and their corresponding intensity reflectance R and transmittance T is given by the expression,

$$R = |\rho|^2 and T = |\tau|^2, \tag{1.40}$$

where

$$R + T = 1 \tag{1.41}$$

A connection between the incident and internal fields can be seen through the boundary conditions of the form

$$A_2{}' = \rho A_2 e^{2ikl-\alpha l}, \tag{1.42}$$

$$A_2 = \tau A_1 + \rho A_2{}'. \tag{1.43}$$

In these equations, we presume that the field amplitudes are determined on the inner surface of the left mirror. Both the intensity absorption coefficient α and the propagation constant, $\kappa = \frac{n\omega}{c}$, are considered to be real quantities, including its both linear and nonlinear effects. We assume that the nonlinear material's and the medium around the resonator's linear refractive indices are the same. Additionally, we assume that the values k and α are spatially invariant under a mean-field approximation. Consequently, the above equations (1.42) and (1.43) can be derived as

$$A_2 = \frac{\tau A_1}{1 - \rho^2 e^{2ikl-\alpha l}}. \tag{1.44}$$

The above mentioned equation is known as Airy's equation which describes the properties of a Fabry-Perot interferometer. Suppose that the light intensity inside the interferometer has a sufficient nonlinear effect on k or α (or both). In that situation, as anticipated by the equation above, the transmitted wave's intensity will show bistability. The two essential conditions for producing such optical phenomena are the medium's nonlinearity and the optical feedback action. Optical bistability can be classified as dispersive or absorptive based on whether the feedback occurs by an intensity-dependent refractive index or through an intensity-dependent absorption, respectively.

1.5.1 Absorptive bistability

Let's start by taking a look at the case where the amplitude of the wavevector k is assumed to be constant while only the absorption coefficient is believed to have a nonlinear dependence on the field intensity. In order to simplify the analysis below, we assume that the spacing l between the mirrors is adjusted to tune the cavity to resonance with the applied field. In this case, a real quantity R is equal to the factor $\rho^2 e^{2ikl}$ in the denominator of the equation (1.44). Additionally, we assume that $\alpha l << 1$, which allows us to ignore the spatial fluctuation of the field's intensity inside the cavity and supports the use of the mean-field approximation. In all of these circumstances, Airy's equation (1.44) becomes,

$$A_2 = \frac{\tau A_1}{1 - R(1 - \alpha l)}. \tag{1.45}$$

A similar equation for the relationship between the incident and circulating intensities $I_i = 2n\epsilon_0|A_i|^2$ is given by

$$I_2 = \frac{\tau I_1}{1 - R(1-\alpha l)^2}, \tag{1.46}$$

$$I_2 = \frac{1}{T}\frac{I_1}{(1+C)^2}, \tag{1.47}$$

Here, C is a dimensionless parameter known as cooperation number, where $C = \frac{R\alpha l}{1-R}$.

We now suppose that the parameter C and the absorption coefficient α are dependent on the amount of light that enters the interferometer. In order to keep things simple, we consider that the absorption coefficient satisfies the relationship that applies to a two-level saturable absorber,

$$\alpha = \frac{\alpha_0}{1 + \frac{I}{I_s}}, \tag{1.48}$$

where I and I_s is the local and saturation intensity respectively and α_0 is the unsaturated (low intensity) absorption coefficient [27]. The input-output properties of an optical bistable system

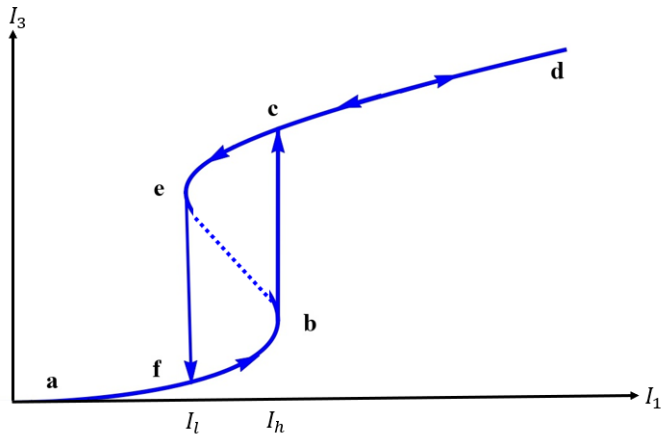

Figure 1.5: Schematic of an optical bistable input-output system.

are illustrated in figure (1.5). The section of the curve with a downward slope, where the output intensity rises and the input intensity falls, is shown as a dashed line. This plot point is not stable, which is intuitively expected and supported by a linear steady-state study. If the system is at first in

this shape, the aggregation of minor perturbations will cause it to swiftly switch to the other stable solutions. Further information is provided on the hysteresis loop of the bistable figure. Suppose the input intensity I_1 begins at zero and increases to I_h over time. The output intensity is therefore determined by the lower branch of the solution, which is the section that is terminated by points a and b. Once the input intensity has been raised further, the output intensity must travel to point c and trace out the region of the curve denoted by the letters c to d. If the intensity gradually decreases, the system will remain on the upper branch, and the curve part from e to d will regulate the output intensity. As the input intensity crosses the value I_l, the system changes to point f, and when the input intensity reaches zero, it follows the curve from f to a.

1.5.2 Refractive bistability

The dispersive nonlinearity of a medium leads to the second kind of bistability. Optical bistability can be categorized as either dispersive or absorptive depending on what causes the feedback, a refractive index or an intensity-dependent absorption. However, since both absorptive and refractive systems may be significant at the same time, it is obvious that this distinction is not precise. Even though one of them may produce a nonlinear effect that is noticeably larger than the other, they are always related on a more fundamental level. In contrast to an absorptive analog, a dispersive system dispersive system, in contrast to an absorptive analog, consists of a Fabry-Perot etalon filled with a medium whose refractive index varies proportionally to the radiation intensity. The cavity is initially configured at a low transmission state that is nearly in resonance. The refractive index of the medium is thus determined by the total intensity inside the cavity, which is proportional to the transmitted intensity. Consequently, the refraction varies with the increase of radiation in the cavity changing the frequency of the cavity. When the cavity resonance gets close to the radiation frequency, a slight increase in input intensity will result in a substantial change in the intensity of the transmission and the cavity. As a result, the refractive index of the medium is further decreased, bringing the cavity even closer to resonance. When the cavity resonance gets close to the radiation

frequency, a slight increase in input intensity will result in a substantial change in the intensity of the transmission and the cavity. As a result, the refractive index of the medium is further decreased, bringing the cavity even closer to resonance. In accordance with the change in the medium's index of refraction, the output will eventually suffer a runaway effect. When that happens, the output will suddenly increase in value before levelling off at the transmitted intensity.

1.5.3 Optical switching

The detection of optical bistability requires both the cavity feedback and a nonlinear medium. Therefore, the medium might be a material having an intensity-dependent refractive index, and the feedback is created by placing the material inside a Fabry-Perot cavity. Now, let's investigate an illustration of an optical switching device, as shown in figure (1.6). Here, we examine a Fabry-

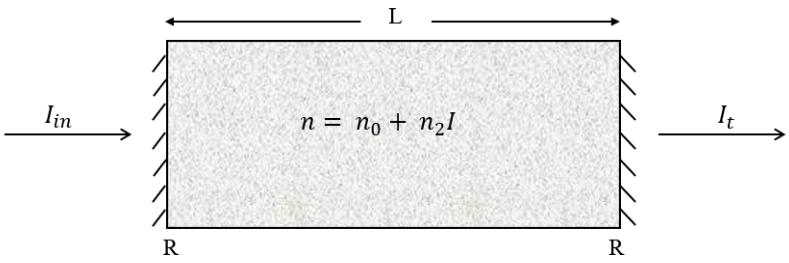

Figure 1.6: In a Fabry-Perot interferometer with length L and mirror reflectivity R, the incident and transmitted intensities are I_{in} and I_t, respectively.

Perot cavity with a length (L), a refractive index (n), and mirror reflectivity (R). Assuming a signal field with input intensity I_{in} is applied to the cavity where the transmission (T) of the optical cavity is measured by the relation between input and output intensity I_t which is given by

$$T = \frac{1}{1 + FSin^2\phi_0}, \tag{1.49}$$

where is the wavelength of the radiation, $F = \frac{4R_\alpha}{1+{R_\alpha}^2}$ stands for the cavity finesse factor with mirror reflectivity coefficient R_α, and the initial detuning, which stands for the linear round-trip phase shift is represented as $\phi_0 = \frac{2\pi}{\lambda} n_0 L$. Let's now examine the conditions that result in a nonlinear phase shift in greater detail. As the linear refractive index (n_0) turns non-linear (n_2), equation (1.46) is modified as,

$$n(I_{int}) = n_o + n_2 I_{int}, \tag{1.50}$$

where I_{int} denotes the cavity's interior intensity. In this instance, a nonlinear phase shift develops as,

$$\phi = \frac{2\pi}{\lambda} n_2 I_{int} L. \tag{1.51}$$

The equation of transmission (Airy function), which includes both linear and non-linear phase shifts, is given as,

$$T = \frac{1}{1 + FSin^2(\phi_0 + \phi)}. \tag{1.52}$$

The relationship between internal intensity I_{int} and transmitted intensity I_t is given by,

$$R_B I_{int} = I_t, \tag{1.53}$$

where $R_B = \frac{2\pi n_2 L}{\lambda}$ is the reflectivity of the cavity mirrors and $I_t = T I_n$.

Therefore, from Eq.(1.49) and (1.50), we have,

$$R_B I_{int} = \frac{I_{in}}{1 + FSin^2(\phi_0 + \phi)}. \tag{1.54}$$

Hence, the final equation is given as,

$$\phi = \frac{I_{in}}{1 + FSin^2(\phi_0 + \phi)}. \tag{1.55}$$

By plotting a ϕ vs $I_{int}$for various parameter values we can obtain several bistable hysteresis graphs. However, the calculation above, which illustrates the situation of a single input field, is slightly oversimplified, which draws attention to an essential concept: Strongly linearly absorbed nonlinear optical materials can provide a nonlinear phase shift as big as radians, required for high-contrast all-optical switching. The application of some materials for all-optical switching is not possible,

even theoretically, because their effective interaction lengths are longer than the actual length of the non-linear medium. Stegeman and Miller (1993) [29] provided an excellent overview of all-optical switching.

1.6 Optomechanically Induced Transparency (OMIT)

The ability of light fields in mechanically deformable microcavities to couple the optical and mechanical degrees of freedom via radiation pressure offers an intriguing link between nanophotonics and nanomechanics. Over the past few years, this capability has gained increasing attention due to its significant applications in gravitational-wave detection [30], the creation of macroscopic-scale quantum entanglement [31], and the observation of mechanical motion [32]. Cavity optomechanics investigations have recently reached the resolved sideband limit, where the mechanical sidebands of the optical mode reside outside its linewidth. It has been demonstrated that when the input field is red-detuned from the cavity resonance, during which the photons usually absorb a phonon from the mechanical oscillator and disperse upward to the cavity resonance, the intracavity optical field can modify the effective loss factor of mechanical modes and subsequently cause mechanical cooling via the optomechanical interaction. This condition is comparable to the laser cooling of atomic and molecular motion in an optical cavity [33]. A number of phenomena resulting from the coherent interaction of optical fields with atoms have analogs in cavity optomechanics due to the mechanical effects of light. The coherent interaction of the intracavitary field and mechanical oscillator via radiation pressure, for instance, causes optomechanical systems to exhibit a mechanical analog of the Autler-Townes splitting, and it has also been shown that quantum interference in the phonon excitation pathways leads to an optomechanical analog of electromagnetically induced transparency which is known as optomechanically induced transparency (OMIT). The first theoretical [34] prediction of optomechanically produced transparency was made in April 2010, and a few months later, it was experimentally [35] confirmed. The apparent drop in the absorption spectrum regulated by the control laser beam and a comparable interaction Hamiltonian involving

electromagnetically induced transparency in a three-level atomic system indicates the phenomena corresponds to quantum interference.

1.6.1 Standard structure of OMIT

The optomechanical system as illustrated in figure(1.7) usually consist of a high-Q optical cavity where the mechanically deformable limit is observed as a moving mirror and as a result, it describes the mechanical oscillator with its effective mass m and angular frequency Ω_m. The energy of cavity

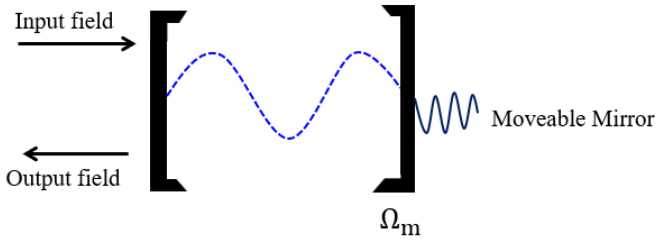

Figure 1.7: A standard schematic model of an optomechanical system, where the displacement of the end mirror of a Fabry-Perot cavity is defined as the mechanical degree of freedom.

optical mode is given by the Hamiltonian,

$$H_{cav} = \hbar\omega_a a^\dagger a \tag{1.56}$$

where $a^\dagger(a)$ is the creation(annihilation) operator of the cavity field and ω_a is the resonance frequency of the cavity.

Hamiltonian of mechanical oscillator,

$$H_{mech} = \frac{p^2}{2m} + \frac{m{\Omega_m}^2 x^2}{2} \tag{1.57}$$

where $\hat{x}$ and $\hat{p}$ are the position and momentum operators of the mechanical oscillator respectively.

Now, the mechanical oscillator can be quantised by introducing the bosonic annihilation and creation operator as

$$b^\dagger = \frac{(m\Omega_m x - ip)}{2m\Omega_m x_{ZPF}}, \tag{1.58}$$

$$b = \frac{(m\Omega_m x + ip)}{2m\Omega_m x_{ZPF}}. \tag{1.59}$$

where $x_{ZPF} = \sqrt{\frac{\hbar}{2m\Omega_m}}$ represents the zero point fluctuation amplitude of the mechanical oscillator.

Therefore, the Hamiltonian which represents the mechanical oscillator's uncoupled free energy is given by

$$H_{mech} = \hbar\Omega_m(b^\dagger b + 1/2) \tag{1.60}$$

with commutation relation $[b, b^\dagger] = 1$.

According to the rotating wave approximation, the following Hamiltonian can adequately represent the photon hopping process that the input lasers use to drive the intracavity field

$$H_{drive} = i\hbar\sqrt{\eta\kappa}\sum s_j(a^\dagger e^{-i\omega_j t} - ae^{i\omega_j t}) \tag{1.61}$$

Here, $\eta = \frac{\kappa_{ex}}{\kappa}$ is the dimensionless coupling parameter with intrinsic decay rate κ_0 and external cavity decay rate κ_{ex}, where the total total decay rate is given by $\kappa = \kappa_0 + \kappa_{ex}$. Also, $s_j = e^{-i\theta_j}\sqrt{P_j/\hbar\omega_j}$ is the normalized amplitude of the j-th cavity field. P_j is the power of the j-th cavity mode with phase and frequency given by θ_j and ω_j respectively.

The intracavitary photon may exert radiation pressure on the cavity wall once the optical fields inside the cavity get excited, which will modify the position of the mechanically deformable membrane. The motion of the cavity wall also affects the behavior of the intracavity field because of its sensitivity where the radiation pressure depends on the position of the cavity wall, resulting in a feedback-backaction that will couple the cavity field and the mechanical oscillator [36]. Through mechanical effects, such optomechanical interaction cancan significantly alter the cavity field. The Hamiltonian representing the non-relativistic optomechanical interaction is given by

$$H_I = \hbar G X a^\dagger a \tag{1.62}$$

where G is the optomechanical coupling parameter, which may be derived from the electromagnetic wave equation [37] and has a time-varying boundary condition. In terms of bosonic creation(annihilation) operators, the interaction Hamiltonian described above can be expressed as

$$H_I = \hbar g_0 (b^\dagger + b) \tag{1.63}$$

where $g_0 = G x_{ZPF}$ denotes the single photon optomechanical coupling parameter.

In the optically induced transparency arrangement, an optomechanical system is driven by a strong pump field and a weak probe field with amplitudes s_1 and s_2 and frequencies ω_1 and ω_2 as illustrated in figure (1.8). While the probe laser field is resonant to the cavity mode, the control field is introduced at the red-detuned sideband of the cavity resonance.

The total Hamiltonian is given by

$$H = H_{cav} + H_{mech} + H_I + H_{drive} \tag{1.64}$$

where the driving term H_{drive} is formed by adding $H_{control} = i\hbar\sqrt{\eta\kappa}s_1(a^\dagger e^{-i\omega_1 t} - a e^{i\omega_1 t})$ with $H_{probe} = i\hbar\sqrt{\eta\kappa}s_2(a^\dagger e^{-i\omega_2 t} - a e^{i\omega_2 t})$.

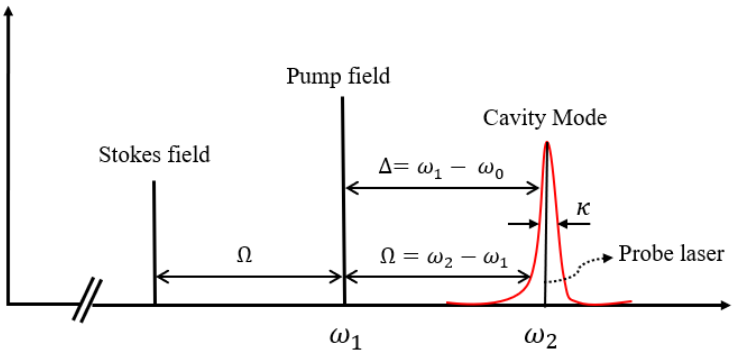

Figure 1.8: Optomechanically induced transparency in the standard frequency range.

The Heisenberg-Langevin equations can be used to explain the dynamics of intracavity fields and mechanical motion by using the total Hamiltonian and adding the noise term. Therefore, the

equation of motion for both the cavity and mechanical mode is obtained as,

$$\frac{d\hat{a}}{dt} = (-i\omega_0 - iGx - \kappa/2)\hat{a} + \sqrt{\eta\kappa}\sum s_j e^{-i\omega_j t} + \sqrt{\tilde{\eta}\kappa}\hat{a}_{in}, \tag{1.65}$$

$$m(\frac{d^2}{dt^2} + {\Omega_m}^2 + \Gamma_m\frac{d}{dt})\hat{x} = -\hbar G a^\dagger a + \hat{F_{th}}. \tag{1.66}$$

where $\hat{a_{in}}$, and $\hat{F_{th}}$ represents the quantum noise operators for cavity and mechanical modes which follows $< a_{in}(t){a_{in}}^\dagger(t') >$ = $\delta(t-t')$, $< a_{in}(t) = 0 >$. Here, $\hat{\eta} = 1 - \eta$. Also, $< F_{th}(t){F_{th}}^\dagger(t') >$ = $\Gamma_m \int e^{-i\omega(t-t')}[coth(\hbar\omega/2k_BT) + 1]d\omega/2\pi\Omega_m$ and $< F_{th}(t) >$ = 0 [35] and the damping terms for the cavity and mechanical mode are described classically as $-\kappa/2$ and $m\Gamma_m\frac{dx}{dt}$ respectively.

1.6.2 Steady-state dynamics of OMIT

In the weak coupling regime ($g_0 << \kappa$) of a single photon, the operators can be simplified by their expectation values $a(t) =< a(t) >$ and $x(t) =< x(t) >$. In the semi-classical condition, the Heisenberg Langevin equation is written as,

$$\frac{da}{dt} = [i(\Delta - Gx) - \kappa/2]a + \sqrt{\eta\kappa}\sum s_j e^{-i\Omega t}, \tag{1.67}$$

$$m(\frac{d^2}{dt^2} + {\Omega_m}^2 + \Gamma_m\frac{d}{dt})x = -\hbar G a^\dagger a, \tag{1.68}$$

where, $\Omega = \omega_2 - \omega_1$. The above equations (1.67) and (1.68) admit a steady-state solution when the probe laser is removed and only the control field of amplitude s_1 is incident into the cavity where the solutions are given as,

$$\bar{a} = \frac{\sqrt{\eta\kappa}s_1}{i\bar{\Delta} + \kappa/2}, \tag{1.69}$$

$$\bar{x} = \frac{\hbar G|\bar{a}|^2}{m{\Omega_m}^2}, \tag{1.70}$$

where $\bar{\Delta} = \Delta - Gx$, and $\Delta = \omega_1 - \omega_0$.

After the light enters the cavity, the system reaches a steady state ($\bar{a}$, $\bar{x}$) in a matter of nanoseconds, as defined by the mechanical oscillator's decay rates. Optomechanical dynamics can display

a bistable behaviour (one input with two possible stable outputs) in its steady-state optical response when the control field is strong enough, as a result of the nonlinear feedback mechanism. While trying to examine optomechanically generated transparency the bistable region needs to be avoided since unstable dynamics always take place in that region.

1.6.3 Theoretical model of OMIT

In order to witness optomechanically induced transparency, optomechanical bistability must be absent and the probe field must be significantly less than the control field which allows the probe field to be regarded as a steady-state perturbation. By taking the steady state approach $a = \bar{a} + \delta a$ and $x = \bar{x} + \delta x$, the Langevin equation can be solved in linearized form as,

$$\frac{da}{dt} = (i\bar{\Delta} - \kappa/2)\delta a - iG\bar{a}\delta x + \sqrt{\eta\kappa}s_2 e^{-i\Omega t}, \tag{1.71}$$

$$m(\frac{d^2}{dt^2} + {\Omega_m}^2 + \Gamma_m \frac{d}{dt})\delta x = -\hbar G(\bar{a}\delta a^* + \bar{a}^*\delta a). \tag{1.72}$$

According to the physical model, the probe field is viewed as a perturbation of the steady state while the control field provides a solution for the system at a steady state($\bar{a}$, $\bar{x}$). Equation (1.71) and (1.72) can be solved analytically by using the ansatz:

$$\delta a = A^- e^{-i\Omega t} + A^+ e^{i\Omega t}, \delta x = X e^{-i\Omega t} + X^* e^{i\Omega t}. \tag{1.73}$$

This, along with the input-output relation $S_{out}(t) = S_{in}(t) - \sqrt{\eta\kappa}a$, between the input and output fields, ultimately results in the analytical expression of the probe laser's transmission [35] given as,

$$t_p = 1 - \frac{1 + if(\Omega)}{\kappa/2 - i(\bar{\delta} + \Omega) + 2\bar{\Delta}f(\Omega)}\eta\kappa, \tag{1.74}$$

where, $f(\Omega) = \hbar G^2|\bar{a}|^2\chi(\Omega)/[\kappa/2 + i(\bar{\Delta} - \Omega)]$ and $\chi(\Omega) = 1/m({\Omega_m}^2 - \Omega^2 - i\gamma_m\Omega)$. In terms of optomechanical interaction term g_0, can be written as $f(\Omega) = \hbar {x_{ZPF}}^2 {g_0}^2|\bar{a}|^2\chi(\Omega)/[\kappa/2 + i(\bar{\Delta} - \Omega)]$.

A transmission window on resonance ($\Omega = \Omega_m$) with a window width of $\Gamma_m + 4{g_o}^2|\bar{a}|^2/\kappa << \kappa$ can be seen in the transmission of the probe field as a function of probe detuning Ω.

1.6.4 Physical origin of OMIT

A time-varying radiation-pressure force is caused by the beat of the probe field and the control field when the beat frequency is given by $\Omega = \omega_2 - \omega_1$. When the mechanical resonance frequency and the beat frequency are equal ($\Omega \approx \Omega_m$), the mechanical resonator is forced into resonance and begins to oscillate coherently. The optical sidebands are then produced on the cavity field as a result of the mechanical oscillation, producing photons at frequencies $\omega_1 + n\Omega_m$ where n is an integer that represents the optical sideband's order. In the resolved sideband limit (for the case of a strong control field), the first-order sideband ($n = 1$) is dominant and it has the same frequency as the probe field. A transparency window in the transmission is produced due to the cancellation of the intracavity field as a result of the destructive interference between the first-order sideband and the probe field. Probe excitations in OMIT are transformed into mechanical oscillations and then returned to the probe field. Therefore, the probe cannot continue to exist in the cavity. A standard Λ-type three-level system with three states $|0_a, 0_b>$, $|0_a, 1_b>$, and $|1_a, 0_b>$ can well describe the effect of optomechanically induced transparency as shown in figure (1.9) where a and b stands for the cavity photon and phonon states, respectively.

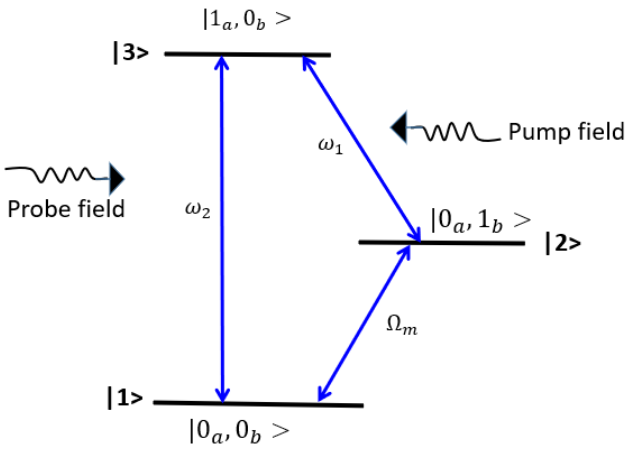

Figure 1.9: Standard energy level diagram of OMIT

This is comparable to the situation of electromagnetically induced transparency (EIT) in atomic systems. When the resonance condition of the system is satisfied, the coupling of the probe field shows the transition $|0_a, 0_b > \rightleftharpoons |1_a, 0_b >$. However, the coupling of pump field or the control field shows the transition $|0_a, 1_b > \rightleftharpoons |1_a, 0_b >$. Optomechanically induced transparency results from a destructive interference of these two excitation paths when the condition, $\Omega = \Omega_m$ is fulfilled.

1.7 Four-wave mixing process

Four-wave-mixing (FWM), also known as four-photon-mixing (FPM), is a nonlinear optical phenomenon in which four distinct waves or photons interact with one another as a result of the material's third-order nonlinearity. As a result, as the waves propagate through the waveguide, new waves with sum and difference in frequencies are produced. Many optical telecommunications applications, including wavelength conversion and optical switching, can benefit from the application of FWM. According to the quantum mechanical theory, the atom simultaneously produces two new photons while annihilating two existing photons. Since only the virtual states of the atom are involved, the process must adhere to the laws of energy and momentum conservation. The phase-matching condition results from momentum conservation. The correct alignment of the waves' phases is a critical factor in determining the efficiency of the FWM. Consequently, the fibre dispersion affects the FWM efficiency. The use of material with zero dispersion in transmission systems is a serious challenge. However, the FWM can be efficiently suppressed if the transmission system exhibits substantial local dispersion, which is the situation with dispersion-managed systems.

All four-wave mixing processes are described in terms of three electromagnetic fields interacting to create a fourth field. If we think about how each field interacts with each other within a dielectric medium, we can physically comprehend how this process works. The first input field induces an oscillating polarisation in the dielectric, which reradiates with some phase shift dictated by the damping of the individual dipoles which is just the conventional Rayleigh scattering that is

accounted for by linear optics. By applying a second field, the dielectric will also become polarized, and the interference of the two waves leads to harmonics in the polarisation at the sum and difference frequencies. The application of a third field shall also drive the polarisation, which will beat with the other input fields, the sum frequencies, and the difference frequencies. The beating between the sum and the difference in frequencies causes the fourth field in four-wave mixing.

In this section we consider the response of a two-level system in the simultaneous presence of a strong optical field (called as pump field) and one or more weak optical fields (called as probe field). As illustrated in figure 1.10, one determines how the presence of the pump field modifies the medium's response to the probe field. Usually, both the intensity and frequency ω of the pump field, as well as the frequency detuning δ between the pump and probe field, can be used to determine the transmission of the probe field. It is possible to learn more about the dipole transition moments and the T_1 and T_2 relaxation times from the outcomes of such studies.

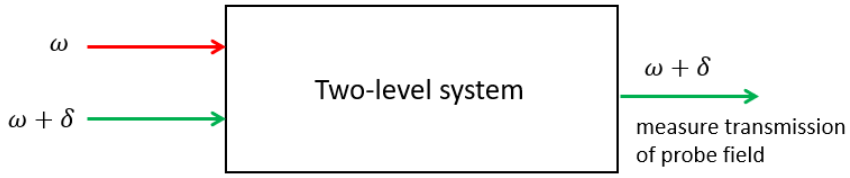

Figure 1.10: Setup for saturation spectroscopy

The multi-wave mixing experiment illustrated in part (a) of Figure 1.11 is yet another illustration of the interactions taken into consideration in this section. Here, the pump field at a frequency ω and the probe field at a frequency $\omega+\delta$ are co-propagating through the medium. For such a structure, the four-wave mixing process illustrated in part (b) of the figure 1.11 becomes phase-matched which results in the formation of the symmetric sideband at frequency $\omega - \delta$. The response of the two-level system at frequency $\omega + \delta$ and $\omega - \delta$ can be determined using the perturbation theory [27] for low intensities of the pump field. The existence of the pump field in this limit is found to somewhat reduce the absorption (and dispersion) that the probe field experiences in the structure of

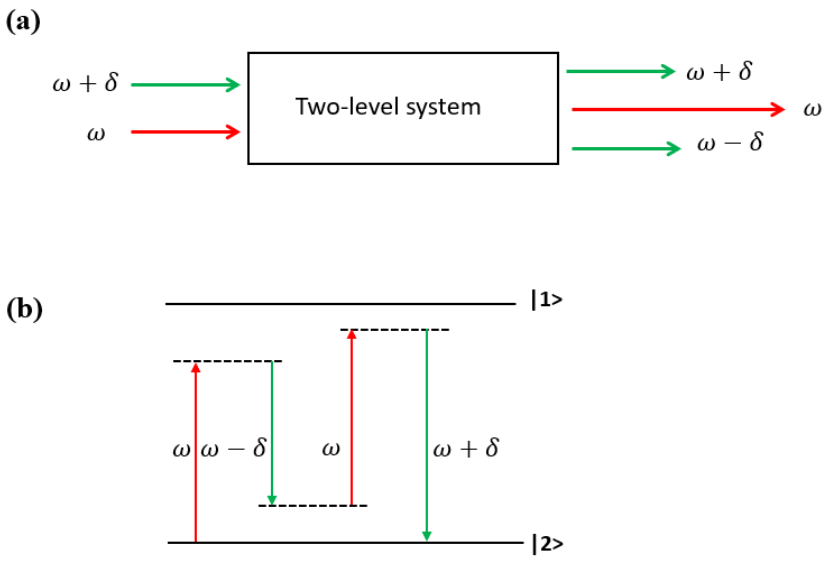

Figure 1.11: (a) Four-wave mixing process. (b)Four-wave mixing process described by the energy level

Fig. 1.10. It is also observed that the intensity of the sideband formed at frequency $\omega - \delta$ increases quadratically with the increase of the pump intensity for the structure of Fig. 1.11. When the intensity of the pump field rises to a point where perturbation theory is insufficient to adequately describe the interaction, the nature of these nonlinear processes is significantly modified. When the Rabi frequency Ω of the pump field exceeds both the transition linewidth $1/T_2$ and the pump wave's detuning Δ from the system (two-level) resonance, then these processes of higher orders become essential. In this situation, the pump field dramatically modifies the system's energy levels, causing novel resonances in the absorption and mixing responses. We will discover that these novel resonances can be activated when the pump-probe detuning δ is approximately comparable to $\pm\Omega_g$, where Ω_g is the generalised Rabi frequency.

1.8 Outline of the Thesis

The first of the six chapters that make up this thesis gives a quick review of the basic ideas about the cavity quantum electrodynamics (CQED), quantum dot, photonic crystal cavities, and radiation-pressure interaction to study different types of optical response properties in different hybrid optomechanical systems. It provides a brief explanation of different optical phenomena that take place in a photonic crystal optomechanical system as well as the various modes that can be coupled to the optical system. Chapter two is a description of the mathematical techniques and tools that were adopted to understand the dynamics of different optomechanical systems. The absorptive and dispersive behaviour in the transmission spectra of the output probe field is also discussed in order to determine the dynamics of various coupling parameters in resonant and off-resonant conditions. It is possible to address the issue analytically by using a mathematical framework that transforms the Hamiltonian into the rotating wave approximation frame of reference. In addition, the Heisenberg equations of motion are also discussed, which are essential for studying the dynamics of the proposed systems. However, the mean-field approximation is introduced while neglecting the correlation between the operators.

As a result of the nonlinear interaction between the primary cavity and the secondary cavity as well as the mechanical oscillator, the process of energy transfer between optical and mechanical modes has been greatly enhanced, as discussed in chapter three. A strong pump field and a weak probe field is incident on the primary cavity to determine the optical response properties of the system. In chapter four we theoretically investigated the optical response characteristics of a quantum dot placed in an optomechanical photonic crystal (PhC) nanocavity, which is driven by two-tone fields. It has been greatly discussed how the off-resonant coupling between the exciton and the PhC nanocavity causes the four-wave mixing signal to vary significantly. Furthermore, we have obtained significant optical response properties of a hybrid system consisting of a QD-based photonic crystal nanocavity coupled to two nanomechanical membrane. This study focuses on multi-OMIT and Fano resonances along with optical multistability, which are efficient and controllable optical responses.

CHAPTER 2

Methods and formulation

In this chapter, a variety of methodologies and techniques are used to explain the dynamics of the theoretical framework that was implemented to support the thesis are explained.

2.1 Rotating wave approximation

The rotating wave approximation in quantum optics is important for avoiding the fast oscillating terms of the Hamiltonian given as

$$\int e^{\pm in\theta} d\theta = \frac{e^{\pm in\theta}}{\pm in} \approx 0. \qquad (if\ n \to \infty) \tag{2.1}$$

The Hamiltonian H must be transferred to a rotating frame with frequency ω_0 in order to achieve H_{rot} given as,

$$H_{rot} = U^{\dagger}HU + i\frac{\partial U^{\dagger}}{\partial t}, \tag{2.2}$$

where U represents the unitary operator.

For a basic Jaynes-Cummings model of a two-level system interacting with a cavity, the Hamiltonian is denoted by the equation: $H = \hbar\omega_a a^{\dagger}a + \frac{\hbar}{2}\omega\sigma_z + \hbar g(\sigma_+ + \sigma_-)(a + a^{\dagger})$.

The Hamiltonian is frequently thought of as being transformed into a rotational frame with frequency ω_0. Now, selecting U to enter the rotating frame as, $U = e^{-i\omega_0 t a^{\dagger}a}\ e^{-i\omega_0 t\sigma_z}$. Therefore,

$$U^{\dagger}HU = e^{i\omega_0 t(a^{\dagger}a+\sigma_z)}(\hbar\omega_a a^{\dagger}a + \frac{\hbar}{2}\omega\sigma_z + \hbar g(\sigma_+ + \sigma_-)(a + a^{\dagger}))e^{-i\omega_0 t(a^{\dagger}a+\sigma_z)} \tag{2.3}$$

Now, applying

$$e^{\alpha A}Be^{-\alpha A} = B + \alpha[A, B] + \frac{\alpha^2}{2!}[A, [A, B]] + ..., \tag{2.4}$$

and

$$[a, a^{\dagger}] = 1 \tag{2.5}$$

Using the above transformation, the first term of the Hamiltonian H is given as,

$$\begin{aligned} &e^{i\omega_0 t(a^{\dagger}a+\sigma_z)}\hbar\omega_a a^{\dagger}ae^{-i\omega_0 t(a^{\dagger}a+\sigma_z)} = \hbar\omega_a a^{\dagger}a + i\omega_0 t[a^{\dagger}a + \sigma_z, \hbar\omega_a a^{\dagger}a] \\ &+ \frac{(i\omega_0 t)^2}{2!}[a^{\dagger}a + \sigma_z, [a^{\dagger}a + \sigma_z, \hbar\omega_a a^{\dagger}a]] + ... \end{aligned} \tag{2.6}$$

Since, $[a^{\dagger}a + \sigma_z, \hbar\omega_a a^{\dagger}a] = 0$,

$$e^{i\omega_0 t(a^{\dagger}a+\sigma_z)}\hbar\omega_a a^{\dagger}ae^{-i\omega_0 t(a^{\dagger}a+\sigma_z)} = \hbar\omega_a a^{\dagger}a \tag{2.7}$$

Similarly,

$$e^{i\omega_0 t(a^{\dagger}a+\sigma_z)}\omega\sigma_z e^{-i\omega_0 t(a^{\dagger}a+\sigma_z)} = \frac{\hbar}{2}\omega\sigma_z, \tag{2.8}$$

$$e^{i\omega_0 t(a^{\dagger}a+\sigma_z)}ae^{-i\omega_0 t(a^{\dagger}a+\sigma_z)} = e^{-i\omega t}a, \tag{2.9}$$

$$e^{i\omega_0 t(a^\dagger a+\sigma_z)}a^\dagger e^{-i\omega_0 t(a^\dagger a+\sigma_z)} = e^{i\omega t}a^\dagger, \tag{2.10}$$

$$e^{i\omega_0 t(a^\dagger a+\sigma_z)}\sigma_+ e^{-i\omega_0 t(a^\dagger a+\sigma_z)} = e^{i\omega t}\sigma_+, \tag{2.11}$$

$$e^{i\omega_0 t(a^\dagger a+\sigma_z)}\sigma_- e^{-i\omega_0 t(a^\dagger a+\sigma_z)} = e^{-i\omega t}\sigma_-, \tag{2.12}$$

$$i\frac{\partial U^\dagger}{\partial t} = -\omega_0(a^\dagger a + \sigma_z). \tag{2.13}$$

Therefore, the final Hamiltonian is written as,

$$H_{rot} = \hbar(\omega_a - \omega_0)a^\dagger a + \hbar(\frac{\omega}{2} - \omega_0)\sigma_z + \hbar g(e^{-i\omega t}a + e^{i\omega t}a^\dagger)(e^{-i\omega t}\sigma_+ + e^{i\omega t}\sigma_-). \tag{2.14}$$

Under the rotating wave approximation, neglecting the fast oscillating term, $\omega + \omega_0$, we obtain

$$H_{rot} = \hbar\Delta_a a^\dagger a + \hbar\Delta\sigma_z + \hbar g(\sigma_+ a + \sigma_- a^\dagger), \tag{2.15}$$

where $\Delta_a = \omega_a - \omega_0$ and $\Delta = \frac{\omega}{2} - \omega_0$.

2.2 Heisenberg Equation of motion

Let us consider the time-dependent wavefunction $\psi(t)$ and a linear operator $\hat{o}$. The expectation value of the linear operator is given by,

$$< \hat{o} >=< \psi(t)|\hat{o}|\psi(t) > \tag{2.16}$$

$\frac{d<\hat{o}>}{dt}$ can be written as follows [26]

$$\frac{d < \hat{o} >}{dt} = \frac{d}{dt} < \psi(t)|\hat{o}|\psi(t) > . \tag{2.17}$$

As we know

$$i\hbar\frac{d}{dt}|\psi(t) >= \hat{H}|\psi(t) >, \tag{2.18}$$

$$i\hbar\frac{d}{dt}|\psi(t) >=< \psi(t)|H^\dagger = \frac{i}{\hbar} < \psi(t)|\hat{H}. \tag{2.19}$$

Using the above equations

$$\frac{d}{dt} < \hat{o} >= \frac{1}{i\hbar} < \hat{o}\hat{H} - \hat{H}\hat{o}|\psi(t) > + < \psi(t)|\frac{\partial o}{\partial t}|\psi(t) >, \tag{2.20}$$

$$\frac{d}{dt} < \hat{o} >= \frac{1}{i\hbar} < [\hat{o}, \hat{H}] > + \frac{\partial o}{\partial t}. \tag{2.21}$$

The relationship established by equation (2.21) can be used to derive a significant assumption. If the operator $\hat{o}$ has no explicit time dependency then $< \frac{\partial o}{\partial t} >= 0$.

Thus, the equation of motion gives

$$\frac{\partial}{\partial t} < \hat{o} >= \frac{1}{i\hbar} < [\hat{o}, \hat{H}] > . \tag{2.22}$$

By using the commutation relation, $[a, a^\dagger] = 1, [\sigma_-, \sigma_z] = 2\sigma_-$ and $[\sigma_+, \sigma_z] = -2\sigma_+$, where σ_z, σ_+ and σ_- are Pauli matrix, we solve the Jaynes Cumming's Hamiltonian of equation (2.15) mentioned above.

$$\dot{a} = \frac{i}{\hbar}[H, a], \tag{2.23}$$

$$\dot{a} = -i\omega_a a - g\sigma_- - \kappa a, \tag{2.24}$$

$$\dot{\sigma_z} = \frac{i}{\hbar}[H, \sigma_z], \tag{2.25}$$

$$\dot{\sigma_z} = i2g(a^\dagger\sigma_- - \sigma_+ a) - \gamma\sigma_z, \tag{2.26}$$

where γ and κ are respectively the decay rates of the atom dipole and the cavity field.

2.3 Semi-classical approximation

The steady-state dynamics of the hybrid system are investigated in the present work, and semi-classical approximations are essential for understanding this procedure. The semiclassical approximation of a system can be achieved by taking the expectation value of the equation of motion [26]. The operator's inner product of the type $< \hat{0}\hat{p} >$ in this approximation can be replaced with

$< \hat{0} >< \hat{p} >$. The approximation is based on the presumption that the product of the fluctuation term for each operators $< (\hat{0} - < \hat{0} >)(\hat{p} - < \hat{p} >) >$ is smaller than $< \hat{0} >< \hat{p} >$. In order to derive equations of motion, each instance of an operator must be described along with its corresponding expectation value which can be done by using Heisenbergs equation of motion in the mean field approximation. Since it is not necessary to take into account the correlation between two degrees of freedom, he Jaynes Cummins Hamiltonian's equation of motion in a mean field approximation can be written as,

$$< \dot{a} >= -i\omega_a < a > -g < \sigma_- > -\kappa < a >, \tag{2.27}$$

$$< \dot{\sigma_z} >= i2g(< a^\dagger >< \sigma_- > - < \sigma_+ >< a >) - \gamma < \sigma_z > . \tag{2.28}$$

The use of this technique for the handling of nonlinear optical media with high photon densities has shown to be important in the literature [38]. Carusotto validated the effectiveness of this method by comparing the outcomes to exact calculations [39]. The accuracy of approximations is compromised when a single photon has the power to significantly change a device's optical response in the photon blockade domain [40]. It is at this point when photons' quantum properties become important.

2.4 Steady-state solution

In stable states with small oscillation from the variables, we consider the steady state solution. For this case, our focus is on small fluctuations that are close to a few classical stable states. We assume that the system enters a steady state at time t. The equation of motion is then used to calculate an average over a period of time. In this case, the variable's temporal derivative is taken to be zero. As a result, the Jaynes Cumming Hamiltonian's equation of motion in the steady state approximation can be expressed as

$$0 = -i\omega_a < a_s > -g < (\sigma_-)_s > -\kappa < a_s >, \tag{2.29}$$

$$0 = i2g(< a_s^\dagger >< (\sigma_-)_s > - < (\sigma_+)_s < a_s >) - \gamma < (\sigma_z)_s > . \tag{2.30}$$

where the steady-state solution of the operators are $a_s, (\sigma_-)_s$ and $(\sigma_z)_s$.

CHAPTER 3

A QD-based hybrid photonic crystal optomechanical microcavity with tunable multistability and Fano resonances

We study the optical behaviour of a quantum dot (QD) embedded in a photonic crystal (PhC) optomechanical cavity in a hybrid cavity quantum-electrodynamics (C-QED) system. A single optical mode-supporting waveguide connects the system to an auxiliary cavity. We show how it is possible to produce tunable optical bistability, double-bistability and tristability which can be used to develop multi-valued logic circuits and all-optical switch systems that will eventually be a part of a large-scale quantum communication platform. Additionally, it has been observed that the proposed system displays the Mollow triplet and Fano resonances that have been modified by an optomechanical interaction.

3.1 Introduction

The study of enhanced interactions between photons and quantum emitters found within a small volume is called cavity quantum electrodynamics (C-QED) [41, 42]. One of the primary advantages of C-QED has been the ability to coherently control the spontaneous emission of the quantum emitter, which is now known as the Purcell effect [43]. A unique quantum phenomena known as vacuum Rabi splitting (VRS) [44], which has been experimentally verified in a variety of C-QED systems, is caused by the reversible interaction between quantum emitters and photons in the strong coupling regime. In order to categorize the dynamics of the emitter-photon system as having a weak or strong coupling, three separate characteristic time scales are defined by the parameters of the cavity mode decay rate, non-resonant decay rate, and emitter-photon coupling strength [45]. Auxiliary-cavity-assisted VRS has recently been performed in a hybrid photonic crystal (PhC) nanocavity integrated with a quantum dot (QD). The findings showed that the auxiliary cavity was essential for controlling the dynamics of the system [46]. It is important to note that solid-state optical emitters are well suited for quantum sensing applications due to their quantum mechanical features. These quantum technologies depend on being able to include optical emitters into solid-state networks. Faron et al. [47] have successfully created quantum devices using GaAs photonic crystals and InAs quantum dots (QD). There have also been numerous published theoretical and experimental studies based on linking a quantum dot to a nano-phC cavity [48, 49].

Due to recent technical developments, quantum optomechanics has demonstrated significant promise in examining both the storage and transport of quantum information and, as a result, constructing sensitive quantum sensors in addition to testing the fundamentals of quantum physics [26]. It is interesting to note that a system exhibiting optical bistability could reveal all optical switching characteristics [50]. Drummond and Walls proposed the first quantum theory of optical bistability in a dispersive cavity based on cubic nonlinearity in the polarisation [51]. Optomechanical systems can exhibit optical multistability because of the intrinsic nonlinearity brought on by the interaction between the two systems. Another helpful and fascinating phenomenon known as optomechanically induced transparency (OMIT) is seen in cavity optomechanical systems. It

is similar to electromagnetically induced transparency (EIT), which is demonstrated in quantum optics [34, 35]. OMIT has been revealed in a nanobeam cavity optomechanical system based on photonic crystals. The Fano resonance is a distinct asymmetric line profile in the probe absorption spectra that differs from the symmetric profile of EIT/OMIT [52]. Through careful manipulation of optical signals, the OMIT phenomenon has been proven to be effective for storing information in mechanical oscillators [53]. Techniques for creating optical semiconductor cavities with high-quality factors have prepared the way for studying cavity quantum electrodynamic phenomena in solid-state systems, such as quantum dots inside photonic crystals [54, 55]. Quantum photonic applications such as optical switching and networks for processing quantum information have been made possible by further integrating quantum optical networks based on quantum dots placed inside photonic crystal cavities [47]. Photonic crystal cavities with a high quality factor and small mode volume can be integrated seamlessly with circuitry and waveguides on a chip [56]. On the other hand, a new type of device based on opto-mechanical interaction in photonic crystal give a promising platform for sensing application [56]. In this chapter, we discuss the new physics and applications that result from the combination of a mechanical resonator, a solid-state optical cavity, and a quantum emitter. Our objective is to demonstrate that QD-PhC cavities with optomechanical interactions provide several opportunities to further control the optical response in nanophotonics. In this chapter, we discuss the new physics and applications that result from the combination of a mechanical resonator, a solid-state optical cavity, and a quantum emitter. Our objective is to demonstrate that QD-PhC cavities with optomechanical interactions provide several opportunities to further control the optical response in nanophotonics. We believe that this study has never been attempted before.

3.2 Theoretical framework

Our proposed design is based on single quantum dot embedded in an optomechanical photonic crystal (PhC) nanocavity coupled to another PhC auxiliary cavity via a single mode waveguide

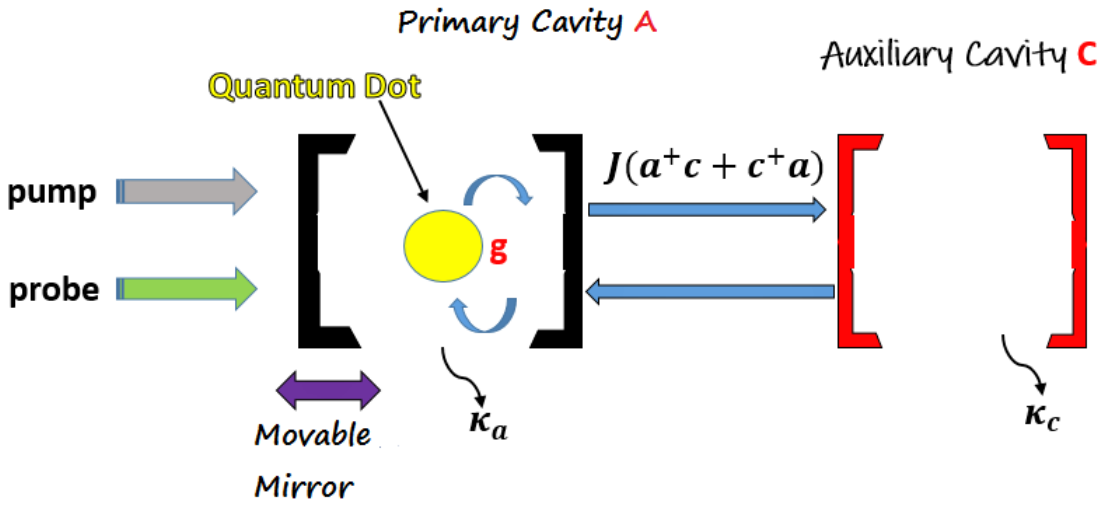

Figure 3.1: Schematic diagram of the proposed hybrid photonic crystal based opto-mechanical system. An embedded quantum dot is interacting with the mode of the primary optomechanical cavity. The primary cavity is coupled to the auxiliary cavity via a waveguide.

as shown in Fig 3.1. Small regions of disorder (artificial defects) in the photonic crystal(PhC) can serve as high-Q factor resonant optical cavities. A high Q-factor and small modal volume V are an essential pre-requisite for strong light-matter interactions [57]. The semiconductor heterostructure consisting of InAs QD (with QD density ranging from zero to 3 per μm^2) embedded in gallium arsenide (GaAs) photonic crystal structure can be fabricated by well developed experimental techniques [47, 58, 59, 60]. Experimental procedures of designing and fabricating a PhC cavity integrated opto-mechanical system have also been recently reviewed [56]. The coupling between the primary cavity "A" and the auxiliary cavity "C" is via exchange of energy with strength J. The coupling strength J can be tuned by varying the distance between the two cavities [61] . At low temperatures, the QD may be approximated as an artificial two-level atom consisting of the ground state and the first excited state(single exciton) [62, 63]. The two level QD can be characterized

by the pseudospin -1 operators $\sigma^{\pm}$ and σ^{z}. The optical mode of the primary cavity is driven by a pump laser with frequency ω_p whereas the optical response of the hybrid system is probed by a weak laser of frequency ω_s .

The Hamiltonian of the proposed system is given by:

$$H = H_0 + H_I + H_d, \tag{3.1}$$

where,

$$H_0 = \hbar\omega_a a^{\dagger}a + \hbar\omega_c c^{\dagger}c + \hbar\omega_b b^{\dagger}b + \frac{\hbar\omega_e}{2}\sigma^{z}, \tag{3.2}$$

$$H_I = \hbar g(\sigma^{\dagger}a + a^{\dagger}\sigma^{-}) + \hbar J(a^{\dagger}c + c^{\dagger}a) - \hbar g_{om}a^{\dagger}a(b^{\dagger} + b), \tag{3.3}$$

$$H_d = \hbar E_p(a^{\dagger}e^{-i\omega_p t} + ae^{i\omega_p t}) + \hbar E_s(a^{\dagger}e^{-i\omega_s t} + ae^{i\omega_s t}). \tag{3.4}$$

Here, H_0 is the bare Hamiltonian with the first term being the energy of the primarily cavity optical mode with resonant frequency ω_a and the second term is the energy of the auxiliary cavity mode with frequency ω_c . The third term in H_0 represents the energy of the mechanically compliant distributed Braggs reflector (DBR) with frequency ω_b and the last term is the energy of the two-level QD with resonant frequency ω_e . The Hamiltonian H_I is the interaction Hamiltonian with the first term denoting QD-primary optical field interaction with strength g. The second term in equation (3.3) describes the energy exchange between the primary and the auxiliary cavity whereas the last term represents the optomechanical interaction term between the primary optical mode and the mechanical mode of the movable DBR with single photon optomechanical strength g_{om}, the Hamiltonian H_d describes the coherent driving and the probe field. The first term in H_d is the driving of the primary cavity "A" at the rate E_p while the second term denotes the probe with Rabi frequency E_s . Finally a,c and b denotes the annihilation operators of the primary cavity mode, auxiliary cavity mode and the mechanical mode, respectively.

In a frame rotating at the pump frequency ω_p, the Hamiltonian of equations (3.1)-(3.4) is rewritten as,

$$H_{RWA} = \hbar\Delta_a a^\dagger a + \hbar\Delta_c c^\dagger c + \hbar\omega_b b^\dagger b + \frac{\hbar\omega_e}{2}\sigma^z + \hbar g(\sigma^\dagger a + a^\dagger \sigma^-) + \hbar J(a^\dagger c + c^\dagger a)$$
$$-\hbar g_{om} a^\dagger a(b^\dagger + b) + \hbar E_p(a^\dagger + a) + \hbar E_s(a^\dagger e^{-i\delta t} + a e^{i\delta t}), \quad (3.5)$$

where, $\Delta_a = \omega_a - \omega_p$ is the primary cavity-pump field detuning,

$\Delta_c = \omega_c - \omega_p$ is the auxiliary cavity-pump field detuning,

$\Delta_e = \frac{(\omega_e - \omega_p)}{2}$ is the exciton-pump detuning,

and $\delta = \omega_s - \omega_p$ is the probe- pump detuning.

Now, using $i\hbar\dot{O} = [O, H]$ (O is any operator), we obtain the Heisenberg equations of motion for the various degrees of freedom for our hybrid system as,

$$\dot{a} = -(i\Delta_a + \frac{\kappa_a}{2})a - ig\sigma^- - iJc + ig_{om}a(b^\dagger + b) - iE_p - iE_s e^{-i\delta t}, \quad (3.6)$$

$$\dot{b} = -(i\omega_b + \frac{\kappa_b}{2})b + ig_{om}a^\dagger a, \quad (3.7)$$

$$\dot{c} = -(i\Delta_c + \frac{\kappa_c}{2})c - iJa, \quad (3.8)$$

$$\dot{\sigma^-} = -(i\Delta_e + \Gamma_2)\sigma^- + iga\sigma^z, \quad (3.9)$$

$$\dot{\sigma^z} = -\Gamma_1(\sigma^z + \frac{1}{2}) + 2ig(a^\dagger\sigma^- - \sigma^\dagger a). \quad (3.10)$$

Here, $\kappa_a, \kappa_b, \kappa_c$ are the decay rates of primary cavity, mechanical mode and auxiliary cavity respectively. Also $\Gamma_1(\Gamma_2)$ is the exciton relaxation rate (dephasing rate).

Equations (3.6)- (3.10) will form the basis of ours future analysis in the next section of the steady-state behaviour of the system.

3.3 Optical Multistability: tunable switching

To understand the conditions under which the system exhibits bistable or tristable behaviour, we analyze the steady state solutions of equations (3.6)-(3.10). We take $a_s, b_s, c_s, \sigma_s^-$ and σ_s^z as the average values of the operators a , b , c , σ^- and σ^z respectively under the condition of strong

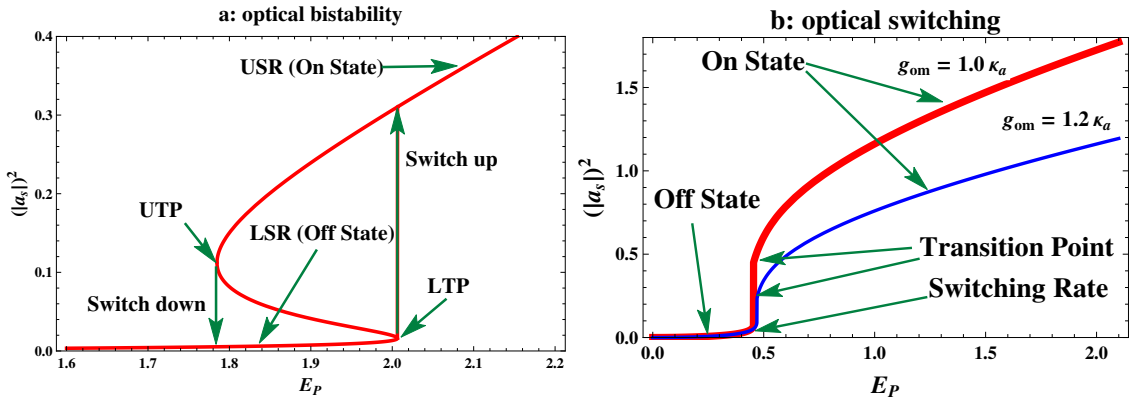

Figure 3.2: a: Optical bistabilty (typical S shaped curve) obtained from eqn.(16). The plot shows intracavity photon number $|a_s|^2$ as a function of E_P. The parameters used are: $\Delta_e = 1.5\kappa_a$, $\Delta_a = 0.5\kappa_a$, $\Delta_c = 1.5\kappa_a$, $\kappa_c = \kappa_a$, $\Gamma_1 = 0.65\kappa_a$, $\Gamma_2 = 0.33\kappa_a$, $g = 10\kappa_a$, $g_{om} = 0.7\kappa_a$, $\omega_b = 1.5\kappa_a$, $J = 2.0\kappa_a$, $\kappa_b = 0.0001\kappa_a$. (b): Steady state plot of $|a_s|^2$ as a function of E_P for two different values of $g_{om} = 1.0\kappa_a$ (thick solid line) and $g_{om} = 1.2\kappa_a$(thin solid line). The parameters used are: $\Delta_e = \Delta_a = \Delta_c = 1.5\kappa_a$, $\kappa_c = \kappa_a$, $\Gamma_1 = 0.65\kappa_a$, $\Gamma_2 = 0.33\kappa_a$, $g = 3.5\kappa_a$, $\omega_b = 1.5\kappa_a$, $J = 0.88\kappa_a$, $\kappa_b = 0.001\kappa_a$. The abbreviations used have the following meaning: USR: Upper Stable Region, LSR: Lower Stable Region, LTP: Lower Transition Point, UTP: Upper Transition Point.

optical driving field ($E_p >> E_s$). The steady state solutions are obtained by equating the time derivatives of equations (3.7) - (3.10) to zero. This yields ,

$$a_s = \frac{-i[g\sigma_s^- + Jc_s - g_{om}a_s(b_s^* + b_s) + E_p]}{(i\Delta_a + \frac{\kappa_a}{2})}, \tag{3.11}$$

$$c_s = \frac{-iJa_s}{(i\Delta_c + \frac{\kappa_c}{2})}, \tag{3.12}$$

$$b_s = \frac{ig_{om}|a_s|^2(-i\omega_b + \frac{\kappa_b}{2})}{(\omega_b^2 + \frac{\kappa_b^2}{4})}, \tag{3.13}$$

$$\sigma_s^- = \frac{iga_s}{(i\Delta_e + \Gamma_2)}[-\frac{1}{2}\frac{A_1}{(A_1 + A_2|a_s|^2)}], \tag{3.14}$$

$$\sigma_s^z = [-\frac{1}{2}\frac{A_1}{(A_1 + A_2|a_s|^2)}], \tag{3.15}$$

where, $A_1 = \Gamma_1(\Delta_e^2 + \Gamma_2^2)$ and $A_2 = 4g^2\Gamma_2$.

Note that if g=0, $\sigma_s^z = -\frac{1}{2}$, i.e, in the absence of the light-QD coupling, the two-level QD stays in its ground state. By substituting the value of σ_s^-, c_s, b_s into Equation(3.11), we obtain the mean number of photons as,

$$P_5x^5 + P_4x^4 + P_3x^3 + P_2x^2 + P_1x = P, \tag{3.16}$$

where ,

$x = |a_s|^2 4,\ P = \frac{E_p^2 A_1^2}{\Delta_a^2 + \frac{\kappa_a^2}{4}},\ P_1 = \psi_1^2 + \phi_1^2 - A_{12}, P_2 = 2(\psi_1\psi_2 + \phi_1\phi_2) - A_{22},$

$P_3 = (\psi_2^2 + \phi_2^2 + \psi_1\psi_3 + \phi_1\phi_3),\ P_4 = 2(\psi_2\psi_3 + \phi_2\phi_3), P_5 = \psi_3^2 + \phi_3^2,$

$A_{12} = \frac{2E_p^2 A_1 A_2}{\Delta_a^2 + \frac{\kappa_a^2}{4}},\ A_{22} = \frac{E_p^2 A_2^2}{\Delta_a^2 + \frac{\kappa_a^2}{4}},\ \psi_1 = A_1 - \alpha_1 - \beta_1 A_1,\ \psi_2 = A_2 - \beta_1 A_2 - \gamma_1 A_1,$

$\psi_3 = -\gamma_1 A_2, \phi_1 = \alpha_2 + \beta_2 A_1,\ \phi_2 = \beta_2 A_2 + \gamma_2 A_1,\ \phi_3 = \gamma_2 A_2,$

$\alpha_1 = \frac{g^2 A_1(\Delta_e\Delta_a - \frac{\kappa_a\Gamma_2}{2})}{2(\Delta_e^2+\Gamma_2^2)(\Delta_a^2+\frac{\kappa_a^2}{4})},\ \alpha_2 = \frac{g^2 A_1(\Delta_e\frac{\kappa_a}{2} + \Delta_a\Gamma_2)}{2(\Delta_e^2+\Gamma_2^2)(\Delta_a^2+\frac{\kappa_a^2}{4})},\ \beta_1 = \frac{J^2(\Delta_c\Delta_a - \frac{\kappa_c\kappa_a}{4})}{(\Delta_c^2+\frac{\kappa_c^2}{4})(\Delta_a^2+\frac{\kappa_a^2}{4})},$

$\beta_2 = \frac{J^2(\frac{\Delta_c\kappa_a}{2} + \frac{\Delta_a\kappa_c}{2})}{(\Delta_c^2+\frac{\kappa_c^2}{4})(\Delta_a^2+\frac{\kappa_a^2}{4})}, \gamma_1 = \frac{2g_{om}^2\omega_b\Delta_a}{(\omega_b^2+\frac{\kappa_b^2}{4})(\Delta_a^2+\frac{\kappa_a^2}{4})},\ \gamma_2 = \frac{g_{om}^2\omega_b\kappa_a}{(\omega_b^2+\frac{\kappa_b^2}{4})(\Delta_a^2+\frac{\kappa_a^2}{4})}.$

In order to justify our results, we consider realistic experimental values [1, 56, 64] . Note that all parameters used in our numerical study have been made dimensionless with respect to the primary cavity photon decay rate κ_a.

One of the essential pre-requisite to design and fabricate tunable all-optical switching devices is the existence of optical bistability / multistability [65]. A high degree of nonlinearity prevails in our proposed system due to the optomechanical interaction and this may result in the possibility of optical multistability to exist if the system parameters are tuned properly. Fig 3.2(a) illustrates the optical bistability curve obtained by solving equation (3.16) numerically. It is a plot of intracavity

photon number $|a_s|^2$ as a function of incident pumping rate E_p. It shows a typical hysteresis loop that the intracavity photon number follows as the incident pumping rate is increased or decreased. Transition from the off-state to the on-state takes place at the lower transition point (LIP) while transition from the on-state to off-state takes place at the upper transition point(UTP). Both the off-state and on-state are the stable solutions of equation (3.16).

Fig 3.2(b), illustrates the optical switching behaviour for two different values of the optomechanical coupling g_{om} . A sharp transition from the off-state to the on-state is observed for $g_{om} = 1.0$ (thick solid line) compared to a smooth transition seen for $g_{om} = 1.2$ (thin solid line). A sharp transition is desirable for optical switching. The ratio of the maximum (at the transition point) to minimum value of $|a_s|^2$ is defined as the switching ratio. As evident the switching ratio for $g_{om} = 1.0\kappa_a$ is higher compared to that for $g_{om} = 1.2\kappa_a$. A higher switching ratio is essential since a less sensitive detector is also able to distinguish between the OFF and ON state.

Fig 3.3(a) and 3.3(c) demonstrate two different tristabilities that can be generated in our hybrid system. In Fig.3(a), the system can jump from the lower stable region (LSR) to the meta-stable region (MSR) at lower transition point 1 (LTP1) as we increase E_p. On further increasing E_p, it continues on the MSR till it reaches LTP2 to make a further transition to USR. On decreasing E_p , the system first makes a transition to MSR at upper transition point (UTP), continues on MSR as E_p is decreased further and finally it jumps to LSR at UTP1. Thus a switching behaviour of the form, $LSR \longleftrightarrow MSR \longleftrightarrow USR$ has been observed. Fig 3.3(b) clearly shows the LSR of Fig.3(a).

A different tristable switching behaviour is observed in Fig 3.3(c). On increasing E_p, the system directly jumps from LSR to USR at LTP1 and continuous on USR on further increasing E_p. Decreasing E_p now leads the system to jump from USR to MSR at UTP1. Hence we have the following two observations : At this point if E_p is again increased, a transition from MSR to USR occurs at LTP2. Decreasing E_p when the system is in MSR , takes the system to LSR at UTP2. The switching behaviour in this case is of the form $LSR \rightarrow USR \rightleftharpoons MSR \rightarrow LSR$.

This interesting tristability behaviour demonstrated by our proposed hybrid system opens new

possibilities to develop advanced quantum devices for multi-valued logic circuits.

3.4 Optomechanically induced transparency (OMIT)-Fano Resonances

Optomechanically induced transparency exhibited in optomechanical systems is similar to the phenomena of electromagnetically induced transparency(EIT) observed in atomic systems. Destructive interference between photon excited through different pathways is responsible for the transparency window in the transmitted field. In this section, we analyze the generation of Fano resonance/OMIT in the probe absorption spectra. In particular we investigate the tunability of the OMIT/Fano resonance and the effect of various system parameters on it. Since the probe field is weaker than the pump field, the Heisenberg operators of the system can be rewritten as $O = O_s + \delta O$ $(O = a, b, c, \sigma^z, \sigma^-)$, where O_s is the steady state mean value of O and δO is the corresponding small fluctuation with zero mean value, that is $< \delta O >= 0$. In order to explore the dynamics of quantum fluctuations, we neglect the small nonlinear fluctuation terms and make the ansatz $< \delta O >= O_+ e^{-i\delta t} + O_- e^{i\delta t}$[27]. The procedure for obtaining the fluctuation equations is outlined in Appendix A.

Solving analytically the set of ten equations A1-A10 and working to the lowest order in E_s , we obtain from eqn. A11, the linear susceptibility as,

$$\chi^{(1)}_{eff}(\omega_s) = \frac{N_1 + iN_2}{D_1 + iD_2}, \tag{3.17}$$

where,

$N_1 = g\sigma_s^z(\Gamma\kappa_3 - \delta\kappa_1),\ N_2 = g\sigma_s^z(\Gamma\kappa_1 + \delta\kappa_3),$

$D_1 = (\kappa_1^2 + \kappa_3^2)(\delta^2 + \Gamma^2) + g|a_s|^2(\kappa_1^2 + \kappa_3^2)(\Gamma\sigma_I - \delta\sigma_R) + g^2\sigma_s^z(\kappa_3\Gamma - \delta\kappa_1),$

$$D_2 = g|a_s|^2(\kappa_1^2+\kappa_3^2)(\Gamma\sigma_R+\delta\sigma_I)+g^2\sigma_s^z(\kappa_3\delta+\Gamma\kappa_1),$$

$$\kappa_1 = \tfrac{\kappa_a}{2}+\epsilon_{2+},\ \kappa_2 = \delta - g_{om}R_{bo} - A|a_s|^2,\ \kappa_3 = \epsilon_{2-}-\delta-g_{om}R_{bo}-A|a_s|^2,$$

$$R_{bo} = \tfrac{2g_{om}\omega_b|a_s|^2}{\omega_b^2+\frac{\kappa_b^2}{4}},\ A = \tfrac{2g_{om}^2(\omega_b^2+\frac{\kappa_b^2}{4}-\delta^2)}{[(\omega_b-\delta)^2+\frac{\kappa_b^2}{4}][(\omega_b+\delta)^2+\frac{\kappa_b^2}{4}]},\ \epsilon_{2+} = \tfrac{J^2\frac{\kappa_c}{2}}{\delta^2+\frac{\kappa_c^2}{4}}, \epsilon_{2-} = \tfrac{J^2\delta}{\delta^2+\frac{\kappa_c^2}{4}},$$

$$\sigma_R = \tfrac{2g(1-|a_s|^2\epsilon_\sigma)\delta}{\Gamma^2+\delta^2},\ \sigma_I = \tfrac{2g(1-|a_s|^2\epsilon_\sigma)\Gamma}{\Gamma^2+\delta^2},\ \epsilon_\sigma = \tfrac{2g^2}{\delta^2+\Gamma^2+2g^2|a_s|^2}.$$

Here, we have taken $\Gamma_1 = \Gamma_2 = \Gamma$ for simplicity. Also, we have taken the resonance condition $\Delta_a = \Delta_c = \Delta_e = 0$.

The real and imaginary part of $\chi_{eff}^{(1)}(\omega_s)$ give the absorption and dispersion of the system respectively. In order to analyze OMIT in our system, we choose realistic experimental values obtained by other researchers [1, 56]. In particular, our parameter values will be based on InAs/GaAs QD embedded in a photonic crystal optomechanical nanocavity. Typical experimental values of the system [66] are $\kappa_a = \kappa_c = 8MHz,\ \Gamma_1 = 5.2MHz,\ \Gamma_2 = 2.6MHz$, J ranges between 1.0 - 2.0 MHz, (depending on the distance between the two cavities), g is tuned between weak(20 MHz) to strong(15 MHz) coupling strength. The other parameters like the mechanical frequency ω_b can vary between 10-600 MHz, κ_b and the single photon optomechanical strength have the ranges between 10-600 MHz, 0.01-0.06 MHz and 1-8 MHz, respectively. We work in the resolved side band regime (RBS) where, $\kappa_a < \omega_b$. In this regime, the intracavity photons on average remains in the cavity for longer duration compared to the mechanical period. Thus, the photons interact equally with all the quadratures of the mechanical motion.

In fig 3.4, we show the variation of absorption spectra (Im $\chi_{eff}^{(1)}(\omega_s)$) as a function of probe detuning δ . A typical Mollow tripet along with Fano resonance modified by OMIT (OMIT-Fano resoance) is observed. A Mollow triplet is observed only in the strong coupling regime [67] . The central peak is slightly shifted from $\delta = 0$ which may be attributed to an the optomechanical effect. In fig 3.4(a), $\omega_b = 0.25\kappa$ while that in fig 3.4(b), is $\omega_b = 0.30\kappa$. Clearly, an asymmetric transparency window is observed exactly at $\delta = 0, \pm\omega_b$. The inset in the figures show the magnified

view of the Fano resonance at $\delta = \omega_b$. The occurrence of Fano resonance/OMIT can be understood as follows. The beat of the control pump and the probe field creates a time-dependent radiation pressure force with beat frequency $\delta = \omega_p - \omega_s$. As the mechanical resonator is driven resonantly at $\delta = \pm\omega_b$, a coherent oscillation is initiated resulting in optical sidebands on the auxiliary cavity field. The optical sidebands are generated at frequencies $\omega_p \pm n\omega_b$ with n being an integer, denoting the order of the sideband. In the presence of a strong pump field and recalling that we were in the RSB regime, the first order sideband ($n = 1$) dominates having the same frequency. Comparing Fig 3.4(a) and 3.4(b), we note that the transparency window in fig 3.4(a) occurs at $\delta = \pm\omega_b (= 0.25\kappa)$ while in fig 3.4(b), it occurs at $\delta = \pm 0.30\kappa$.

We can see that optomechanical interaction has generated dressed photon-phonon states analogous to atom-photon dressed states generated through Autler-Townes (AC Stark) effect in EIT [65]. The physical origin of the asymmetric transparency windows may be argued in the following ways. In the dressed state picture, OMIT is a result of destructive interference between the two excitation pathways due to the probability amplitude of the indirect excitation pathway having a π phase shift compared with the direct excitation pathway [68, 69]. If the phase difference between the two excitation pathways is not exactly π, an asymmetric Fano resonance profile is generated in the probe transmission [69] . Fig 3.4(c), illustrates the absorption profile for a lower value of the optomechanical coupling ($g_{om} = 0.2\kappa$) compared to that of plots 3.4(a), (b) ($g_{om} = 0.6\kappa$). It is evident that by lowering g_{om} , the transparency window almost disappears, which clearly implies that observed Fano profile is a result of optomechanical interaction. It is important to note that both Fano resonance and OMIT show transparency window. The absorption profile for a lower value of $J = 0.4\kappa$ (weak coupling between the primary and auxiliary cavity) shows that the asymmetric Fano profile gradually makes a transition towards a symmetric OMIT profile. This indicates that the intercavity coupling leads to a phase shift between the two pathways different from π. Double cavities coupled by a single optomechanical mirror is known to show splitting of the Fano resonance and has a zero at $\omega = \pm\omega_m$ [70]. However in our proposed system, the tunabilty is more due to the presence of QD and the auxiliary cavity. In addition, our results also show a combination of

Mollow triplet and a clear OMIT superimposed on the Fano profile.

3.5 Conclusions

In summary, we have theoretically designed and investigated the optical response properties of a novel hybrid C-QED system consisting of a QD implemented in an optomechanical photonic crystal cavity that is optically coupled to an auxiliary cavity. The steady state mean-field analysis shows the existence of tunable optical bistability, double-bistability and tristability, paving the way for novel multi-switching photonic devices. The probe absorption spectra of the fluctuations, reveals a Mollow triplet along with an OMIT modified asymmetric Fano resonances. We identify the parameters which can coherently tune the OMIT-Fano line shapes. In particular the auxiliary cavity, the QD and the mechanically compliant DBR offers three different quantum channels to influence and control the optical response of the system. This study provides a novel platform for further research on chip-scale nano quantum photonic devices.

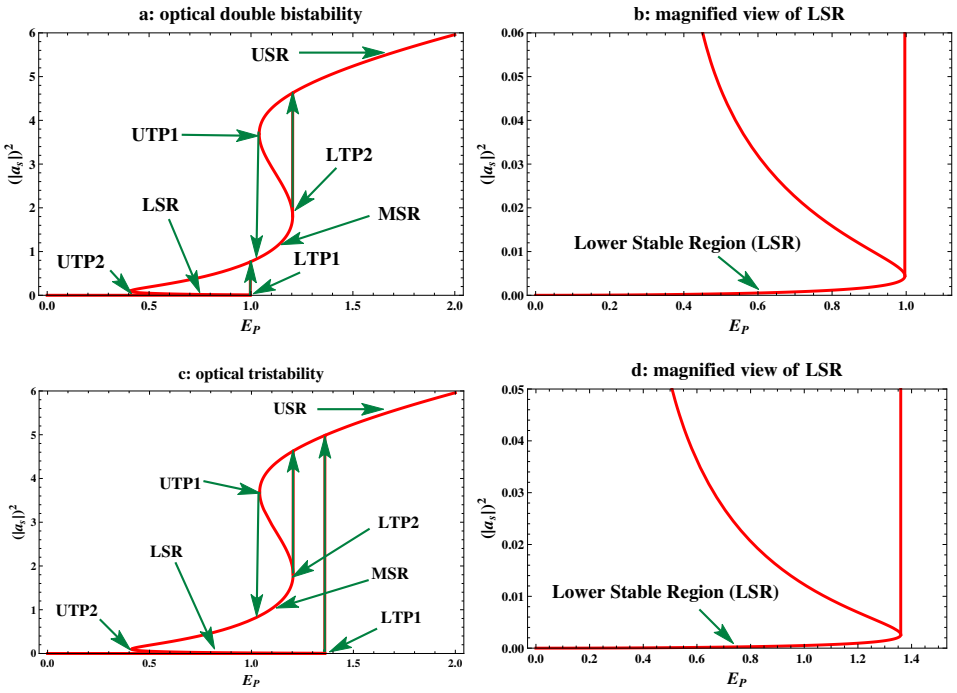

Figure 3.3: (a): Plot illustrating two connected bistable behavior (optical double bistability). Three stable roots are clearly visible. (b): Magnified plot showing the lower stable root of plot (a). (c): Optical tristability obtained from eqn. (16). (d): Magnified plot showing the lower stable region of plot (c). The tristable behavior of plot (a) differs from that shown in plot (c). Parameters used are, (a): $\Delta_e = 0.5\kappa_a$, $\Delta_a = 1.5\kappa_a$, $\Delta_c = 8.0\kappa_a$, $\kappa_c = \kappa_a$, $\Gamma_1 = 0.65\kappa_a$, $\Gamma_2 = 0.33\kappa_a$, $g = 6.0\kappa_a$, $g_{om} = 0.5\kappa_a$, $\omega_b = 1.5\kappa_a$, $J = 1.0\kappa_a$, $\kappa_b = 0.0001\kappa_a$. (c): $g = 8.0\kappa_a$, all other parameters are same as that in plot (a). MSR: Middle Stable Region, LTP1: Lower Transition Point 1, UTP1: Upper Transition Point 1, LTP2: Lower Transition Point 2, UTP2: Upper Transition Point 2.

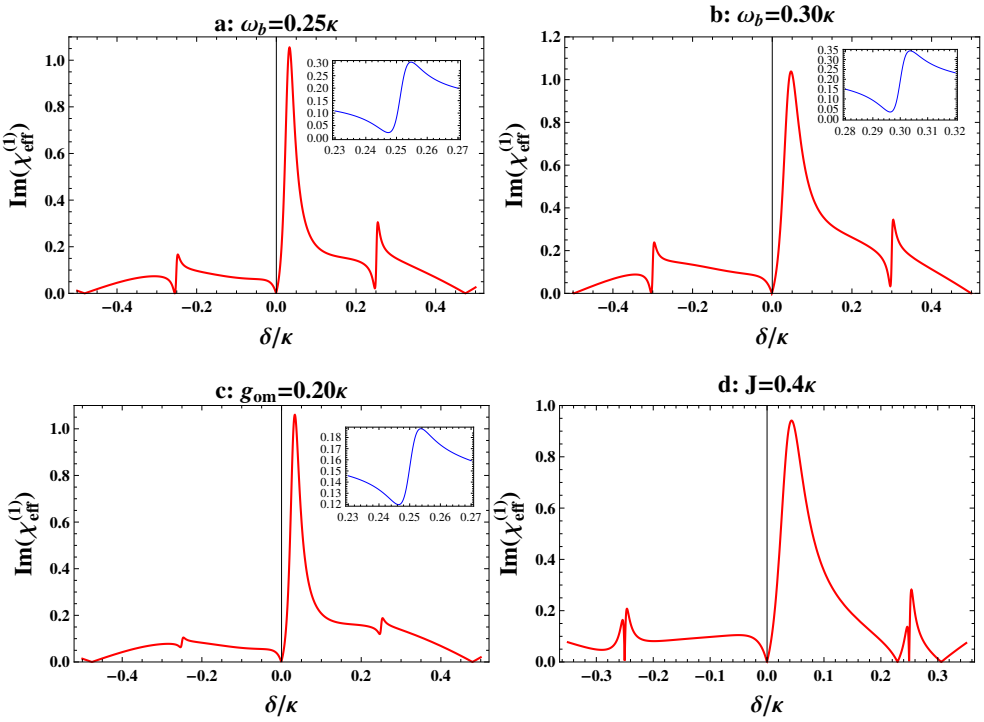

Figure 3.4: Absorption spectra of the probe field as a function of probe detuning δ. Plots (a) and (b) at $\omega_b = 0.25\kappa$ and $\omega_b = 0.30\kappa$ respectively. The inset depicts the magnified shape of the curve near the transparency window $\delta = \omega_b$. Plot (c) shows the Fano profile for $g_{om} = 0.20\kappa$ while plot (d) illustrates the absorption spectra at $J = 0.4\kappa$. The parameters used are: $\kappa_a = \kappa_c = \kappa = 1.0, J = 0.6\kappa$, $\kappa_b = 0.0075\kappa$, $g_{om} = 0.4\kappa$, $g = 1.3\kappa$, $\Gamma_1 = \Gamma_2 = 0.08\kappa$.

CHAPTER 4

Optical bistability and four-wave mixing response of a quantum dot coupled to a photonic crystal optomechanical nanocavity

We theoretically investigate the hybrid cavity quantum electrodynamic (C-QED) system's nonlinear optical response, including optical bistability and the four-wave mixing (FWM) process. The hybrid C-QED system comprises of a quantum dot (QD) placed in an optomechanical photonic crystal (PhC) nanocavity and coherently controlled by two-tone laser beams. Our theoretical analysis shows optical bistability, where the steady-state photon number follows a steady increase in the switch's gain by regulating a strong pump field that drives the QD. The dressed state may be typically modified successfully by creating a strong coupling between matter and quantized fields, and the dressed state of QDs can also be modulated by changing the field parameters. We also detail the effects of exciton-nanocavity coupling strength, Rabi coupling strength, and off-resonant

detuning in our proposed system, which produces a controlled FWM signal in the system's output probe field. When strong coupling and high pump power are present simultaneously, the intensity of the FWM is considerably altered, which causes the establishment of an OMIT window and slow light. The analysis of the proposed system may be useful for on-chip QD-based nanophotonic devices.

4.1 Introduction

Studying the physics behind the coherent interaction between a quantum emitter and a single radiation field mode inside various types of optical cavities [58] has significantly advanced the field of cavity quantum electrodynamics (C-QED) systems and may have applications in quantum information science [1, 41, 42]. Numerous fascinating quantum phenomena, such as laser oscillation [71], spontaneous emission control [72], and multi-emitter quantum optics [73], have been seen in the investigation of such hybrid QD-based photonic crystal systems. The radiation pressure induced coherent photon-phonon interaction offers a platform for manipulating mechanical resonators and electromagnetic fields, in an optomechanical system (OMS) which has drawn a lot of attention. This opens the door for potential applications in optomechanical devices, such as phonon lasers [74, 75], sensing [76], phonon squeezing [77], the realization of squeezed light [78, 79], ground-state cooling [80, 81], and optomechanically induced transparency (OMIT) [35, 82] - induced store light in solid-state devices [83, 84]. The light-matter interaction becomes reversible in the strong coupling domain when photons and the quantum emitter become entangled which leads to an important phenomena called Vacuum Rabi splitting (VRS) [1, 44, 54, 85].

The interaction of light and matter in an optomechanical system (OMS) results in a wide range of nonlinear effects that can be thoroughly studied. Among other nonlinear effects, optical bistability (OB) and four-wave mixing (FWM) are the typical optical responses that have drawn attention. The bistable behaviour of the mean intracavity photon number inside various systems, including atom-cavity systems [86, 87, 88, 89, 90, 91], metal–semiconductor hybrid nanostruc-

tures [92, 93, 94, 95, 96, 97, 98], hybrid optomechanical systems [99, 100, 101, 102], etc., has always been thoroughly studied. It is now known that a typical system, consisting of an optical cavity and a two-level system, can achieve optical bistability [103]. It is interesting to note that a system with optical bistability could display all optical switching behaviour, opening the door for the development of devices like optical switches, logic gates, and memory components [28, 104, 105, 106].

The four-wave mixing (FWM) phenomenon, on the other hand, is a different nonlinear phenomenon that occurs in a variety of optical and optomechanical systems. The nonlinear four-wave mixing phenomena results from the interaction of a two-level system exposed to a strong pump field and a weak probe field at off-resonant frequencies that creates index gratings generating multi-sidebands [107]. In addition to wavelength conversion [108, 109] , parametric amplification [110, 111], and sampling, FWM is an extremely fast process with many potential applications. Due to their adaptable atom-like characteristics, quantum dot (QD) nanostructures have been proposed for a variety of quantum mechanical applications. For the use of quantum information processing, the emitters of controllable quantum states are essential. An InAs QD can store quantum information which can be totally controlled with fast light pulses by developing the information in the electron or hole spin [112]. Due to their extremely small optical mode volumes, photonic crystal cavities are advantageous for integration with optical waveguides and on-chip electronics [113]. Therefore, the incorporation of such QD-based structures into PhC cavities leads to a variety of applications, including optical switching and quantum networks for processing quantum information [47]. Potential applications that could result from the creation of quantum dots inside a photonic crystal cavity have undergone major analysis[41, 114, 115, 116] . The bistable four-wave mixing response in a semiconductor quantum dot (SQD) in the simultaneous presence of a strong pump field and a weak probe field coupled to a PhC nanocavity was recently studied theoretically by Li et al. [103]. But prior to this, no systematic analysis of the bistable four-wave mixing (FWM) behaviour of a quantum dot (QD) coupled to an optomechanical photonic crystal (PhC) nanocavity had been taken into consideration. In contrast to Li et al. [103], we have taken

into account an optomechanical radiation pressure kind of interaction in our PhC nanocavity. Even though the radiation pressure type of optomechanical coupling is weaker than QD-cavity coupling, our studies reveal that this weak coupling exhibits enhanced optical bistability.

In this study, we theoretically examined the optical response properties of a quantum dot (QD) embedded in an optomechanical photonic crystal (PhC) nanocavity which is driven by two optical fields. Here, we have explicitly investigated the optical bistability, switching ratio, and gain of the optical switch along with various FWM signals regulated by the exciton-nanocavity coupling regime, the strength of the Rabi coupling, and the pump power. The FWM signal is significantly altered by the off-resonant coupling between the exciton and the PhC nanocavity, which has been comprehensively explored. It has been extensively discussed how the FWM signal could change significantly as a result of the off-resonant coupling between the exciton and the PhC nanocavity.

4.2 Theoretical model and formalism

Our theoretical model is based on a single quantum dot embedded in an optomechanical photonic crystal nanocavity as shown in figure 4.1(a). The experimental approach for designing and fabricating a photonic crystal (PhC) cavity in an optomechanical system has recently been reviewed [56, 117]. Using well developed experimental techniques [47, 59, 118, 119], the semiconductor heterostructure involving a InAs quantum dot embedded in a GaAs photonic crystal structure can be fabricated easily. Here, a quantum dot with two distinct energy levels and an electric dipole moment μ, has been driven simultaneously to both a strong pump field and a weak probe field. So the Hamiltonian of the QD coupled to the two-tone fields is given by, $H_{Q-F} = -\mu E_p(\sigma_{10}e^{-i\omega_{pu}t} + \sigma_{01}e^{i\omega_{pu}t}) - \mu E_{pr}(\sigma_{10}e^{-i\omega_{pr}t} + \sigma_{01}e^{i\omega_{pr}t})$, where μ is the dipole moment and $\omega_{pu}(\omega_{pr})$ are the frequency of the pump (probe) field respectively and the slowly varying envelope of the pump (probe) field is written as $E_p(E_{pr})$.

The optomechanical interaction between the cavity mode and the mechanical mode via radiation pressure is described by the Hamiltonian $H_{om} = \hbar g_0 a^\dagger a(b + b^\dagger)$, where $a^\dagger(a)$ and $b^\dagger(b)$ are

the creation (annihilation) operators of the cavity mode and the mechanical mode respectively with optomechanical coupling strength g_0.

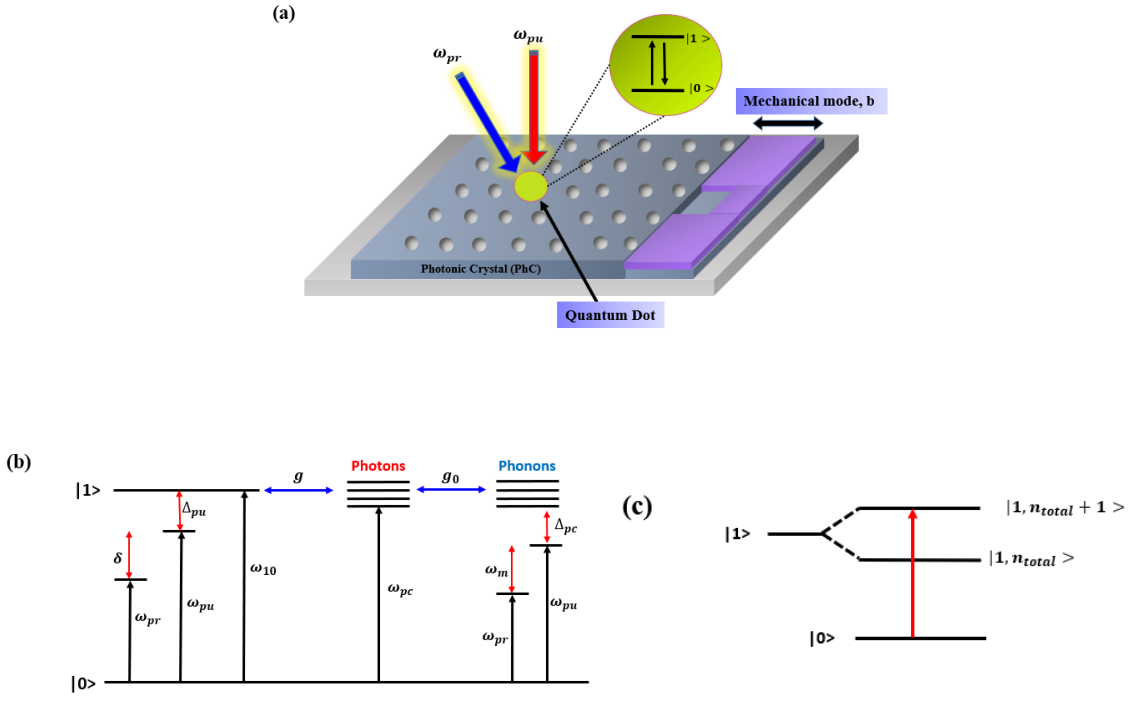

Figure 4.1: (a) Schematic diagram of a QD embedded in an optomechanical PhC nanocavity. The QD is driven by a strong pump field (ω_{pu}) and probed by a weak field (ω_{pr}) (b) Energy level diagram of exciton interacting with photons in the PhC optomechanical nanocavity and (c) Energy level transition with entangled state $|n_{total}>$ formed upon coupling exciton and photon.

In a frame rotating at the pump frequency ω_{pu}, the Hamiltonian of the proposed optomechanical system is written as,

$$H = \hbar\Delta_{pu}\sigma_z + \hbar\Delta_{pc}a^\dagger a + \hbar\omega_m b^\dagger b + \hbar g_0 a^\dagger a(b + b^\dagger) + \hbar g(\sigma_{10}a + \sigma_{01}a^\dagger) - \hbar\Omega(\sigma_{10} + \sigma_{01}) - \mu E_{pr}(\sigma_{10}e^{-i\delta t} + \sigma_{01}e^{i\delta t}), \tag{4.1}$$

where, $\Delta_{pu} = \omega_{10} - \omega_{pu}$ is the exciton-pump field detuning, $\Delta_{pc} = \omega_{pc} - \omega_{pu}$ is the cavity-pump

field detuning and $\delta = \omega_{pr} - \omega_{pu}$ is the probe-pump detuning. The two-level QD is approximated as an artificial two-level atom consisting of the ground state $|0>$ and the single exciton (first excited) state $|1>$ and characterized by three pseudospin Pauli operators σ_{01}, σ_{10} and σ_z. Here, g denotes the coupling strength between the exciton in the QD and photons in the PhC cavity, ω_m is the resonance frequency of the mechanical resonator and $\Omega = \mu E_p/\hbar$ is the effective Rabi frequency of the control (pump) field.

The quantum dynamics of the operators of our proposed system are described by the following quantum Langevin equations, while considering the relevant quantum or thermal noise and dissipation terms, we have

$$\dot{\sigma_{01}} = -(i\Delta_{pu} + \Gamma_2)\sigma_{01} + 2ig\sigma_z a - 2i\Omega\sigma_z - 2i\mu E_{pr}\sigma_z e^{-i\delta t} + \sqrt{\Gamma_2}\sigma_{01_{in}}, \tag{4.2}$$

$$\dot{\sigma_z} = -\Gamma_1(\sigma_z + \frac{1}{2}) - ig[\sigma_{10}a - \sigma_{01}a^\dagger] + i\Omega[\sigma_{10} - \sigma_{01}] + i\mu E_{pr}[\sigma_{10}e^{-i\delta t} - \sigma_{01}e^{i\delta t}] + \sqrt{\Gamma_1}\sigma_{z_{in}}, \tag{4.3}$$

$$\dot{b} = -(i\omega_m + \frac{\gamma_m}{2})b - ig_0 a^\dagger a + \sqrt{\gamma_m}b_{in}, \tag{4.4}$$

$$\dot{a} = -(i\Delta_{pc} + \frac{\kappa}{2})a - ig\sigma_{01} - ig_0 a(b + b^\dagger) + \sqrt{\kappa}a_{in}. \tag{4.5}$$

Here, κ and γ_m are the decay rates of cavity and mechanical mode respectively. Also, $\Gamma_2(\Gamma_1)$ denotes the exciton dephasing rate (relaxation rate). $\sigma_{01_{in}}, \sigma_{z_{in}}, b_{in}$ and a_{in} are the quantum input noises that are initially dependent on the bath operators. The time derivatives of the mean values of the system operators and the average values of these input noises disappear in the steady state approximation i.e, $< \sigma_{01_{in}} >=< \sigma_{z_{in}} >=< b_{in} >=< a_{in} >= 0$. Since, we are examining the system's average response to the signal field, quantum fluctuations are not taken into consideration. Furthermore, we neglect quantum correlations and entanglement between different subsystems. Therefore, we can re-write the system operators in terms of mean classical values as follows,

$$< \dot{\sigma_{01}} >= -(i\Delta_{pu} + \Gamma_2) < \sigma_{01} > +2ig < \sigma_z >< a > -2i\Omega < \sigma_z > -2i\mu E_{pr} < \sigma_z > e^{-i\delta t}, \tag{4.6}$$

$$< \dot{\sigma_z} > = -\Gamma_1(< \sigma_z > + \frac{1}{2}) - ig(< \sigma_{10} >< a > - < \sigma_{01} >< a^\dagger >) + i\Omega(< \sigma_{10} > - < \sigma_{01} >) + i\mu E_{pr}(< \sigma_{10} > e^{-i\delta t} - < \sigma_{01} > e^{i\delta t}), \tag{4.7}$$

$$< \dot{b} >= -(i\omega_m + \frac{\gamma_m}{2}) < b > -ig_0 < a^\dagger >< a >, \tag{4.8}$$

$$< \dot{a} >= -(i\Delta_{pc} + \frac{\kappa}{2}) < a > -ig < \sigma_{01} > -ig_0 < a > (< b > + < b^\dagger >). \tag{4.9}$$

In the next section we will further solve the equations(4.6)-(4.9) for analysing the optical switching behaviour of our system.

4.3 Optical Bistability

Optical bistability is a common phenomenon found in various non-linear systems. This optical response has been demonstrated in many optomechanical systems which are identified by a high degree of nonlinearity arising due to the dynamical backaction induced by radiation pressure. The mechanical oscillator of an optomechanical cavity gets displaced from its original position due to the radiation pressure force that changes the resonance frequency of the optical cavity and thereby changing the intracavity intensity. This results in optical bistability, where a given incident light intensity can yield two different stable states in the mechanical position as well as the intracavity photon number. Moreover, in an optomechanical system, the displacement of the mechanical oscillator caused by the mean effect of the optical field depends on the strength of the optomechanical coupling which is different from a bare optical cavity [26]. Optical bistability is an important optical response for designing and fabricating tunable all-optical switching devices. The fundamental benefit of optical switching is that it enables the routing of optical data streams without transforming them into electrical signals. Therefore, it is not constrained by data protocol or rate [120]. In this section we will investigate the bistable behaviour of the steady-state photon number $|a_0|^2$ of the cavity field. For simplicity, we set $< \sigma_{01} >= P$ and $2 < \sigma_z >= w$, and use the following ansatz [27] to analyse the steady-state solutions of Equations (4.6)-(4.9),

$$\begin{aligned} P &= P_0 + P_1 e^{-i\delta t} + P_{-1} e^{i\delta t}; \\ w &= w_0 + w_1 e^{-i\delta t} + w_{-1} e^{i\delta t}; \\ a &= a_0 + a_1 e^{-i\delta t} + a_{-1} e^{i\delta t}; \\ b &= b_0 + b_1 e^{-i\delta t} + b_{-1} e^{i\delta t}. \end{aligned} \tag{4.10}$$

Here, the steady state amplitudes of the parameters follows: $|P_0| >> |P_1|, |P_{-1}|$; $|w_0| >> |w_1|, |w_{-1}|$; $|a_0| >> |a_1|, |a_{-1}|$; $|b_0| >> |b_1|, |b_{-1}|$.

Now, by substituting the above mentioned ansatz and further solving for the steady-state solution of the equations (4.6)-(4.9), we obtain the mean intracavity photon number as,

$$|a_0|^2 = \frac{g^2\Omega^2 w_0^2}{[\Gamma_2\frac{k}{2} - \Delta_{pu}\Delta_{pc} - \Delta_{pu}B_1|a_0|^2 - g^2 w_0]^2 + [\Delta_{pu}\frac{k}{2} + \Gamma_2\Delta_{pc} + \Gamma_2 B_1|a_0|^2]^2}, \tag{4.11}$$

where, $B_1 = \frac{-2g_0^2\omega_m}{\omega_m^2 + \frac{\gamma_m^2}{4}}$.

The results illustrated in Fig 4. 2 shows optical bistability obtained by numerically solving Eq. (4.11). For illustration, we have considered a realistic system of InAs QD embedded in a GaAs photonic crystal optomechanical nanocavity. Here, we have considered realistic experimental values [1, 56] to justify our results. All the parameters used for the numerical analysis have been made dimensionless with respect to the photon decay rate κ of the PhC cavity. Fig 4.2(a) is a plot of steady-state photon number $|a_0|^2$ as a function of incident pumping rate E_p , for different values of optomechanical frequency $\omega_m = 2.5\kappa$ (solid purple line), $\omega_m = 2\kappa$ (dot-dashed black line) and $\omega_m = 1.5\kappa$ (dashed blue line), when $g_0 = 0.02\kappa$. Here, when ω_m increases from 1.5κ through 2κ to 2.5κ then the threshold value of the incident pumping rate to observe the optical bistability gradually increases giving rise to a broader bistable regime. The transition from Off-State to On-State takes place at the Lower Transition Point (LTP) where the transition occurs from a low photon number to a higher photon number while increasing E_p . On the other hand, the transition from On-State to Off-State takes place at the Upper Transition Point (UTP) where the transition occurs from a higher photon number to a lower photon number while decreasing E_p . The plot shows a typical hysteresis loop which the intracavity photon number follows with the increase or decrease of the pumping rate. Thus, the switching from the Off-State to On-State takes place at a

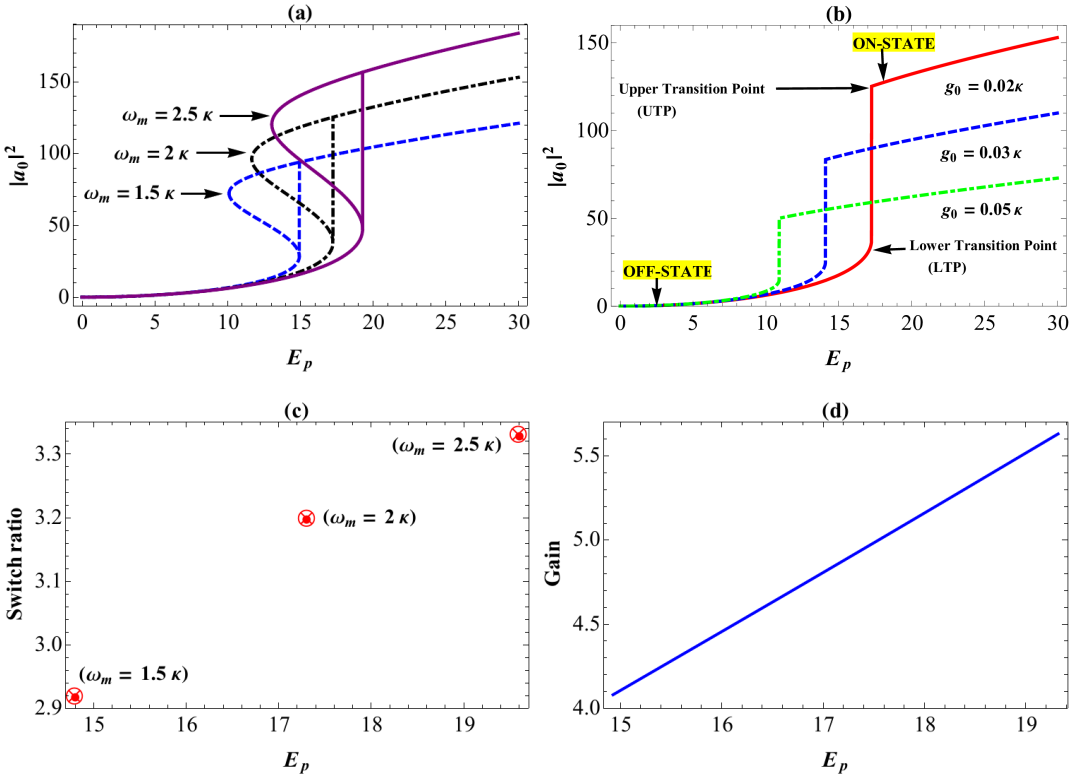

Figure 4.2: Plot of intracavity photon number $|a_0|^2$ as a funtion of pumping rate E_p

lower value of E_p when ω_m is small. A lower value of E_p for optical switching indicates a power efficient device.

Fig. 4.2(b) illustrates the optical switching behaviour for three different values of the optomechanical coupling, $g_0 = 0.02\kappa$ (solid Red line), $g_0 = 0.03\kappa$ (dashed Blue line) and $g_0 = 0.05\kappa$ (dot-dashed green line), when $\omega_m = 2\kappa$. At $g_0 = 0.02\kappa$ (thick solid Red line), we observe a large transition from Off-State to On-State for a lower value of coupling. However, for $g_0 = 0.03\kappa$ (dashed Blue line) and $g_0 = 0.05\kappa$ (dot-dashed Green line), we demonstrate the possibility of a smooth transition in the strong opto-mechanical coupling regime. A large transition indicates a higher switching ratio which is defined as the ratio of the maximum to minimum cavity emission in the steady-state driving curve and is obtained by the following equation,

$$SwitchRatio(SR) = \frac{(P_{out})_{max.}}{(P_{out})_{min.}}$$

Here, $P_{out} =< {a_0}^{\dagger} a_0 >$. Here, all the values of g_0 allows optical switching where the steady-state photon number jumps from Off-State to On-State at a given pump rate. But, for application in efficient optical switching, a large transition from Off-State to On-State is desirable. Hence, it is clear that the switching ratio for $g_0 = 0.02\kappa$ is higher compared to that of $g_0 = 0.03\kappa$ and $g_0 = 0.05\kappa$. Since, a less sensitive detector can also easily differentiate between the Off-State and On-State, so a higher switching ratio is very much important. But at the same time it is to be noted that for $g_0 = 0.02\kappa$, switching occurs at a relatively higher value of E_P. Thus, one has to optimize the low switching power and high switching ratio. Based on this, we extend our analysis into the switching ratio (SR) and gain of the switch.

In figure 4.2(c), we show the switching ratio versus the input pump amplitude. We observe that the switch operates in analogous to a high pass filter and the ratio increases as the value of E_p increases. The greater ratio shows that the switch has more exact control over the light signal that is propagating. We also analyze the gain of the switch versus pump amplitude, which is defined as follows:

$$Gain = \frac{(P_{out})_{max.} - (P_{out})_{min.}}{P_{in}}$$

Figure 4.2(d) shows that a constant gain in the population ($n_a = |a_0|^2$) of the photon number is observed as we increase the pumping amplitude. It should be emphasised that a high gain is necessary for an effective optical switch. This implies that the input amplitude and coupling parameters have a major impact on the switch performance, and a large E_p and g are necessary for an efficient switch.

All the other parameters used in figure 4.2 are: $g = 1\kappa$, $\Gamma_2 = 0.33\kappa$, $\gamma_m = 0.01\kappa$, $\Delta_{pu} = 2\kappa$,$\Delta_{pc} = 2.5\kappa$.

4.4 Four-wave mixing process

In this section we investigate a typical optical nonlinear phenomenon which is the four-wave mixing (FWM) process in our proposed QD based PhC optomechanical cavity. FWM describes the generation of new waves where the annihilation of a signal wave with two incident pump photons generates an idler wave [121]. In order to study the FWM process of the output field, we can use the input-output relation, [26]

$\sigma_{out}(t) = \sigma_{in}(t) - \sqrt{2\Gamma_2}\sigma_{01}(t)$

where, σ_{in} and σ_{out} are the input and output operators respectively.

In this system, we use the previously mentioned ansatz from Eq.(4.10) and obtain the expectation value of the output field as,

$$\begin{aligned} < \sigma_{out}(t) > = (E_p/\sqrt{2\Gamma_2} - \sqrt{2\Gamma_2}P_0)e^{-i\omega_{pu}t} + (E_{pr}/\sqrt{2\Gamma_2} - \sqrt{2\Gamma_2}P_1)e^{-i(\omega_{pu}+\delta)t} \\ - \sqrt{2\Gamma_2}P_{-1}e^{-i(\omega_{pu}-\delta)t} \end{aligned} \tag{4.12}$$

We now write $< \sigma_{out}(t) >$ as,

$$< \sigma_{out}(t) >= \sigma_{out_0}e^{-i\omega_{pu}t} + \sigma_{out_+}e^{-i(\omega_{pu}+\delta)t} + \sigma_{out_-}e^{-i(\omega_{pu}-\delta)t} \tag{4.13}$$

and by comparing Eqs. (4.12) and (4.13), we obtain the output field amplitude of the FWM as,

$$\sigma_{out-} = -\sqrt{2\Gamma_2}P_{-1} \tag{4.14}$$

To describe the FWM briefly, a dimensionless FWM intensity in terms of the probe field is defined as,

$$\begin{aligned} I_{FWM} &= |\frac{\sigma_{out-}}{E_{pr}/\sqrt{2\Gamma_2}}|^2 = |\frac{P_{-1}2\Gamma_2}{E_{pr}}|^2 \\ &= |\frac{(\gamma_1\tau_2^*X_2^* + \gamma_1\tau_3^*w_0^* + \gamma_2X_4X_2^* + \gamma_2X_5)\Gamma_2}{1 - \gamma_1\tau_1^* - \gamma_1\tau_2^*X_1^* - \gamma_2X_3 - \gamma_2X_4X_1^*}|^2 \end{aligned} \tag{4.15}$$

All the unknown variables of the above equation is given in Appendix B. The FWM component mentioned above is produced at frequency $2\omega_{10} - \omega_{pr}$ and the transmission of the output probe field is defined as

$$t_m(\omega_{pr}) = \frac{2\Gamma_2 < P_{+1} >}{E_{pr}} + 1. \tag{4.16}$$

The transmission of the probe signal can be changed with respect to the input pump field, causing a quick phase shift, $\phi_t(\omega_{pr}) = arg[t_m(\omega_{pr})]$ over the transparency window as well as an obvious group delay as [35],

$$\tau_g = \frac{d\phi_t(\omega_{pr})}{d\omega_{pr}} = \frac{d(arg[t_m(\omega_{pr})])}{d\omega_{pr}}. \tag{4.17}$$

Our technique is built around an InAs/GaAs quantum dot embedded in a silicon photonic crystal cavity that couples exciton-photon confinement with flexural mechanical motion, as depicted in figure 4.1. We are all aware that the exciton-photon interaction is crucial in changing the optical characteristics of the QD system [122, 123, 124]. In order to demonstrate how the exciton-photon interaction affects the FWM response in a coupled SQD-PhC nanocavity system, we illustrate how $|\frac{P_{-1}\hbar\Gamma_2}{\mu E_{pr}}|$ described in Eq.(4.15) changes with the probe-pump detuning in four different scenarios, including off coupling (g=0), the weak coupling regime ($g < \kappa$), the intermediate regime ($g \approx \kappa$), and the strong coupling regime ($g > \kappa$), is shown in figure 4.3. The outcome in figure 4.3(a) demonstrate that the peak at $\omega_{pr} = \omega_{pu}$ can be attributed to a typical optical absorptive behaviour [125]. In actuality, the SQD-PhC nanocavity system in the absence of QD-cavity coupling can be treated as a pure SQD system. Additionally, single InAs quantum dots have been found to have single-peaked FWM spectra [126]. As we switch the exciton-nanocavity coupling from off ($g = 0$) to on ($g = 0.5\kappa$), as illustrated in Fig. 4.3(b), the situation becomes very clear. Two Fano profiles emerge as the FWM spectrum's shape changes from single-peaked to asymmetric double-peaked in this weak coupling regime. The amplitude of the central absorption peak in the FWM spectrum is decreased for weak coupling regime, and the Fano peaks appears at two Rabi sidebands.

The situation varies somewhat in the intermediate regime ($g = 1\kappa$), shown in figure 4.3(c). Despite the rise in g, the FWM spectrum has two peaks similar to figure 4.3(b) but as g rises, so does the peak value of the FWM signal. The vacuum Rabi splitting (VRS) is thought to be the cause of these two Rabi sideband peaks [1, 127]. Individual InAs QDs placed in an asymmetrical low-Q GaAs/AlGaAs microcavity have also been found to exhibit such double-peaked FWM

spectra experimentally [128]. It is possible to quantify the SQD-nanocavity coupling strength and determine the VRS using the measured zero-detuning ($\Delta_{pu} = 0$) vacuum Rabi splitting in this case, which is $\frac{2g}{\omega_m} = 2$. Figure 4.3(d) illustrates the peak splitting in the FWM spectra in the strong coupling regime ($g = 4\kappa$), which is a total vacuum Rabi splitting based on C-QED. Here, we take into account the role of photon-phonon mode when the VRS varies significantly to produce distinct FWM spectra at $\delta = \pm\omega_m$ and two additional important peaks at $\delta = \pm 4$, which emerges around the Rabi splitting ($\approx \frac{2g}{\omega_m}$). A dressed-state picture can be used to explain the occurrence. When the QD is coupled to the mechanical PhC cavity, the excited state of the exciton $|1>$ is dressed by an entangled state $|n_{tot}>$ that satisfies the total population of the photon-phonon mode $n_{tot} = n_a + n_b$(note that n_a and n_b stand for the number states of the photon mode a and phonon mode b). Then, two dressed states are created by altering the original eigenstates $|1>$ i.e,$|1, n_{tot}>$ and $|1, n_{tot} + 1 >$, as shown in figure 4.1(c) . The transition from $|0 >$ to $|1, n_{tot} + 1 >$ is shown by the sharp peak on the left, while the transition from $|0 >$ to $|1, n_{tot} >$ is shown by the sharp peak on the right. Thus, the interaction of the QD with the strong pump and weak probe field leads to the generation of two new sidebands for two different frequencies at $\delta = \pm\omega_m$ due to the four-wave mixing(FWM) process. The separation of the two side peaks is more evident when the coupling strength is increased. The propagation of FWM signals is strongly dependent on the combined effects of the vacuum Rabi splitting and the exciton-nanocavity coupling, as we may infer from the description above. All the other system parameters used in figure 4.3 are: $g_0 = 0.005\kappa, \gamma_m = 0.002\kappa, \Gamma_1 = 0.6\kappa, \Gamma_2 = 0.3\kappa, \omega_m = 1\kappa, \Delta_{pu} = 0, \Delta_{pc} = 0, \Omega = 0.1\kappa$.

The FWM signal as a function of pump-probe detuning δ is shown in Figure 4 for various Rabi coupling strength Ω in order to determine the effect of the coupling on the FWM response. As seen in figure 4.4(a), the peak intensity of the FWM signal increase with the increase in the pump power from $E_p = 0.1$ (figure 3d) to $E_p = 0.5$ (figure 4.4a) at $g = 4\kappa$, and $\Omega = 1\kappa$. Figure 4.4(b), which demonstrates the dependence of the peak values on the Rabi coupling strength Ω, also shows the increase at peak intensity of the FWM spectrum in the higher order sidebands at $\delta \approx \frac{2g}{\omega_m} = \pm 4$, along with the peaks appears at $\delta = \pm\omega_m$. As it can be seen that, the pump power is tuned from

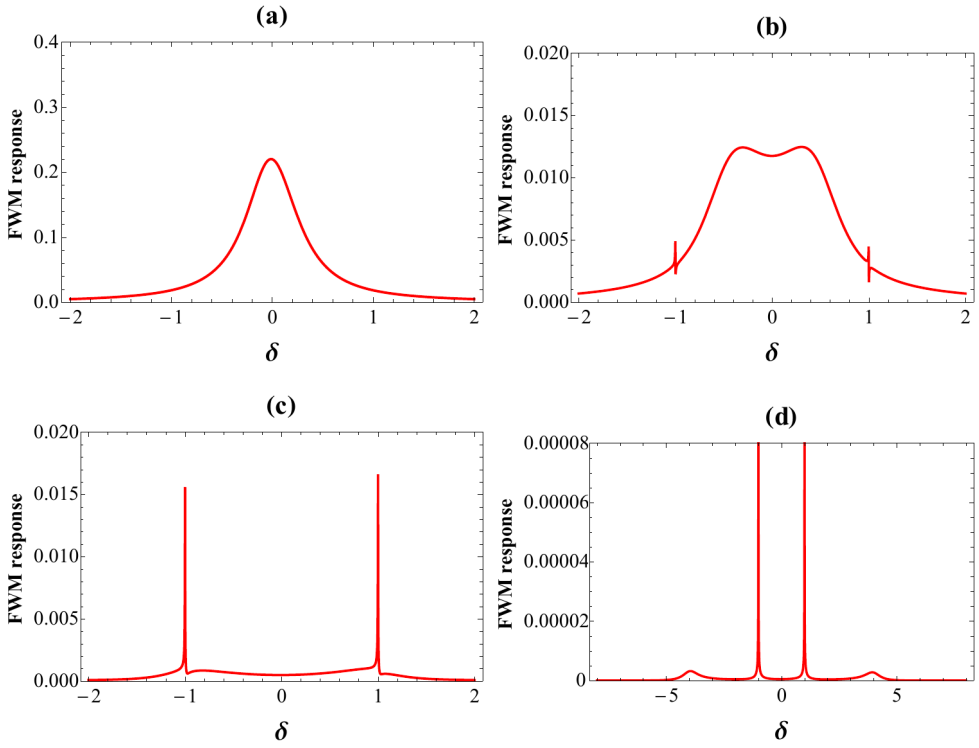

Figure 4.3: FWM response as a function of probe-pump detuning δ for different QD-cavity coupling at (a) $g = 0$. (b) $g = 0.5\kappa$. (c) $g = 1\kappa$. and (d) $g = 4\kappa$.

$E_p = 3$(figure 4.4b) to $E_p = 5$(figure 4.4c), clearly increases the peak intensities of the FWM signal when $g = 6\kappa$, and $\Omega = 10\kappa$. Additionally, it appears that there are more peaks showing OMIT phenomena with a narrow transparency window at $\delta = \pm\omega_m$ (figure 4.4(b) and (c) inset). The homodyne traces were employed in experimental observation to demonstrate the similar transparency window, where the formation of optomechanically induced nonreciprocity in the system occurs as a result of the copropagating signal used to obtain the OMIT spectrum [129]. The physical mechanism of the above mentioned can be seen from two different perspectives. First off, the coupled hybrid COS exhibits quantum interference effects and correlation when various physical modes interact and compete with one another [130, 131]. Moreover, the optomechanical coupling and exciton-photon coupling induces a frequency shift $(2{g_0}^2|a_0|^2 + g^2\omega_0)$ in the amplitude a_0 of

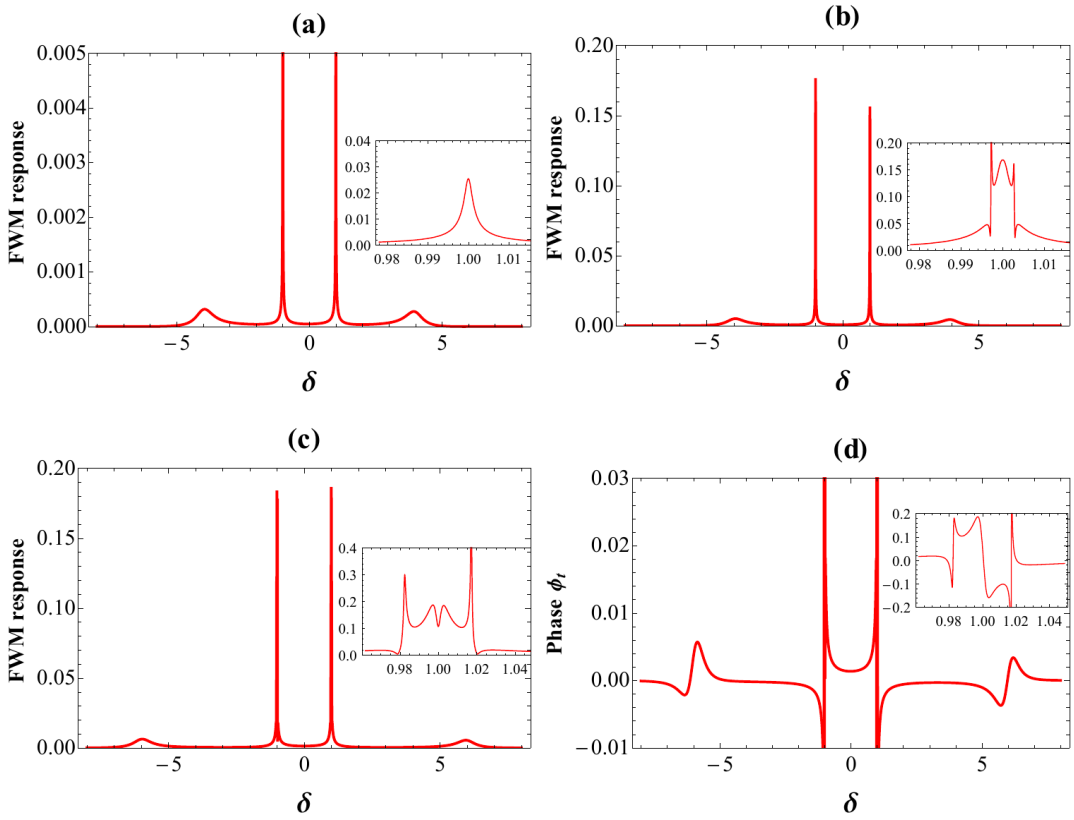

Figure 4.4: The FWM response as a function of probe-pump detuning δ for various Rabi coupling strength.

the cavity field which leads to the decrease in the intracavity photon number and simultaneously effects the mean displacement b_0 of the system. As a result of cavity-QDs and photon-phonon coupling, this produces bipartite dressed excitations (optomechanical interference between various dressed states). We may therefore draw the conclusion that in this hybrid QD-COS, a robust FWM signal can be generated when the pump power is optimally controlled.

We show the phase (ϕ_t) of the output probe field as a function of δ in the range of the FWM signals for $g = 6\kappa$, and $\Omega = 10\kappa$ are illustrated in figure 4.4(d). It demonstrates that in the range of the FWM signals, the output probe field exhibits rapid phase dispersion spectra. The rapid normal-phase dispersion at $\delta = \pm\omega_m$ and $\delta = \pm\frac{g}{\omega_m}$ which is thought to represent the slow light, can occur in a positive group delay. Each of the Fano-type transparency windows is enabled

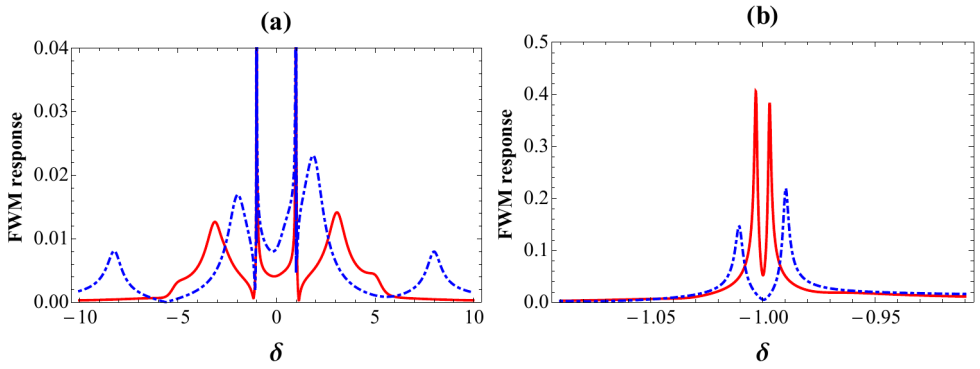

Figure 4.5: FWM response as a function of probe-pump detuning δ for off-resonant values of the exciton-pump detuning at (a) $\Delta_{pu} = 2\kappa$ (Red solid line) and $\Delta_{pu} = 6\kappa$ (Blue dot-dashed line) and (b) Same plot as figure (a) near $\delta = 0$.

by rapid phase dispersion, as shown in figure 4.4(d) (inset). Additionally, it can be helpful to see the propagation of slow and stop lights. The position of the output spectrum will shift as a result of better control over the pump power and exciton-photon interaction of the system, allowing for more precise tuning of the output probe field's total group delay dispersion over a wider frequency range. We may therefore draw the conclusion that in this hybrid QD-COS, a robust FWM signal can be generated when the pump power is optimally controlled. All the other parameters used in figure 4.4 are: $g_0 = 0.005\kappa, \gamma_m = 0.002\kappa, \Gamma_1 = 0.6\kappa, \Gamma_2 = 0.3\kappa, \omega_m = 1\kappa, \Delta_{pu} = 0, \Delta_{pc} = 0$. Figure 4.5 illustrates how the FWM spectrum changes with the exciton-pump field detuning Δ_{pu} at $\Omega = 5\kappa$ and $g = 4\kappa$. The FWM spectrum shows an asymmetric single-peak structure at $\delta = \pm 3$ whose symmetry axis is provided by the line $\delta = 0$. This occurs in the strong coupling regime when the pump field is off resonant with the exciton in the SQD, i.e, at $\Delta_{pu} = 2\kappa$(Red solid line). The situation completely changes when the pump field is set further detuned from the exciton transition (at $\Delta_{pu} = 6\kappa$). The FWM spectrum will shift from being double-peaked to quadrupole-peaked when Δ_{pu} rises, with two new peaks occurring inside of two sideband peaks. In a coupled system of a single QD and a nanobeam PC cavity, such an off-resonant coupling behavior has been observed [132]. Additionally, when Δ_{pu} increases, the magnitudes of the sideband peaks appears

larger while those of the other peaks get smaller. Evidently, the off-resonant coupling between the SQD and the PC nanocavity allows for efficient modification of the FWM spectrum. All the other parameters used in figure 4.5 are: $g = 4\kappa, g_0 = 0.005\kappa, \gamma_m = 0.002\kappa, \Gamma_1 = 0.6\kappa, \Gamma_2 = 0.3\kappa, \omega_m = 1\kappa, \Delta_{pc} = 0, \Omega = 5\kappa$.

4.5 Conclusions

Optical bistability and four-wave mixing have been theoretically studied in a C-QED system made up of an optomechanical photonic crystal nanocavity connected to a QD that is driven by two-tone fields. All optical switching can be achieved via tunable optical bistability, which is demonstrated by the study of the steady-state mean field. A tunable four-wave mixing (FWM) spectrum is produced by the interaction of the exciton-nanocavity coupling strength, Rabi coupling strength, and pump power. For a strong coupling regime, the FWM displays a stronger signal. The size of the sideband peaks is controlled by the exciton-pump field detuning, while the distance between the two peaks of the vacuum Rabi splitting is best controlled by the off-resonant QD-cavity coupling strength. In regions of the four-wave mixing spectrum where a transparency window exists, the two-level system considerably changes the output probe fields at high pump power, creating a mechanism to further improve the system's group delay and slow light. As a result, the obtained results demonstrate that a QD-based optomechanical photonic crystal nanocavity system is suitable for the development of optical switches as well as for the processing of quantum information.

CHAPTER 5

Coupling of QD-based PhC nanocavity with double mechanical modes: An approach to tunable optical switching and sensing applications

We theoretically study the dynamical change in the amplification of the output probe field spectra of a hybrid optomechanical system consisting of double mechanical membrane coupled to a photonic crystal (PhC) nanocavity. The PhC cavity is also embedded with a quantum dot (two-level system) and simultaneously driven by an external pump and a probe field. We show that multiple number of transparency windows that appear can be controlled by the QD-cavity coupling strength and also the Fano profiles are directly measured by the resonant frequency of the mechanical mode. We also show the optical transition from bistability to tristability/multistability by adjusting the

switching threshold of the system parameters. These results can also be used to study frequency optical nonreciprocity and all-optical switches in multi-resonator photonic devices.

5.1 Introduction

Cavity quantum electrodynamics (QED) has recently emerged as one of the key physical systems for integrating quantum information processing, structural quantum computing, and quantum modeling because of the rapid growth of micro- and nano-processing technologies. Qubits possess discrete energy levels that can be controlled by external fields and the coherence time of qubits has also been considerably enhanced up to the order of 0.2 to $0.6\mu s$ [133, 134] by applying advanced technologies. On the other hand, the damping term in the hybrid state is described by the non-Markovian regime since its lifetime is still many times shorter than the time required for vibrational damping, i.e., in the range of tens of femtoseconds. To be precise, nonresonant excitation conditions were used for many experiments. One of the best candidates for studying the strong coupling regime is semiconductor nanocrystals [135, 136, 137], also referred to as quantum dots (QDs). Also, additional experiments conducted under resonant conditions would offer more details of the hybrid cavity-QD states coupled to multiple vibrational modes.

Cavity optomechanics is used in engineering metrology for precision measurement of nanophotonic optomechanical devices for sensing applications [138, 139] as well as for understanding the dynamics of radiation force-driven interaction beyond the conventional quantum limit [140]. For photonic intregated circuits, current on-chip nano-/micro-electromechanical systems provide a number of competitive advantages, including a compact footprint, an easy fabrication method, and compatibility with photonic integrated circuits integration [141] . Mechanically tunable photonic crystal (PhC) cavities have evolved into a variety of sensors for use in sensing applications, including magnetic [142, 143] and electric field [144] sensors, displacement [145, 146] and stress sensing [147, 148]. These sensors benefit from tunable mechanical combinations and integration with nano-/micro-electromechanical systems. The strict requirements for testing in experiments

have improved as a result, though; for instance, the majority of optomechanical measurements call for a vacuum atmosphere and a low adiabatic temperature.

The emerging field of cavity optomechanical systems (COMS), which studies the radiation pressure interaction between optical and mechanical degrees of freedom, has made significant advancements in recent years, including the realization of non-classical or squeezed light [149, 150, 151, 152, 153], phonon cooling [154, 155, 156, 157], ultrasensitive sensing [158], phonon squeezing [159], phonon laser [160, 161], and slow light [162, 163, 164]. When multi-mechanical resonators are constructed inside an optical cavity, cooperative response, switching properties, improved interactions, and nontrivial characteristics emerge [165, 166, 167, 168, 169, 170, 171, 172]. In particular, one can create and manipulate the coherent exchange of excitations [173, 174, 175, 176] or analyze self-oscillations and synchrony via dynamical interactions in the context of two or more mechanical resonators [177, 178, 179]. This article focuses on an optomechanical system consisting of two nanomechanical resonators(NR) in a high-Q photonic crystal cavity. The linear interactions of such hybrid systems are previously investigated in the red sideband regime by controlling the pump power of the optical cavity. The optomechanical interaction can be spatially modified along the cavity axis to change the interaction as needed in two-membrane-in-the-middle cavity optomechanical system [180]. Also, multiple modulators can be cooled asynchronously [181], or used for heat transfer and photon-mediated coherent coupling between different resonators [175, 176].

Moreover, optomechanically induced transparency(OMIT)[182, 183] becomes a fundamental absorption phenomenon that is associated with the present work. This is analogous to an Electromagnetically induced transparency-type phenomenon found in natural atomic systems in C-OMS [184], which offers an alternate method for coherent control of light using a solid state device, including precision measurement of charge number [185] and quantum memory [186]. In order to achieve OMIT, two optical lasers fields known as a pump field and a probe field produce an anti-Stokes field that interacts with the excitation of an intracavity probe field and, when a two-photon resonance condition is satisfied, it creates a transparency window in the transmission spectrum of

the output probe field. The study of the OMIT phenomena has advanced to include the double OMIT and Multi-OMIT in the aspect of multiple electromechanical induced transparency [187] of a charged two-mechanical-mode system [188] and two coupled optomechanical resonators [189]. This was similar to how the EIT was done. Additionally, some hybrid optomechanical systems have been shown to exhibit Fano lineshapes transparency windows to produce slow light in the output probe spectra [190].

In this study, we are focused on the controllable and efficient output probe response, particularly the multiple OMIT and Fano resonance in contrast to the above-mentioned hybrid systems in Ref[187,188,189,190]. Inspired by the various C-OMS systems discussed above, we introduce a coupled QD-PhC optomechanical system, in which the cavity is driven by a strong pump and a weak probe field consisting of two mechanical modes as shown in figure 1(a). J is the coupling strength between two mechanical modes, that could be achieved in a C-OMS using either Coulomb interaction [191] or phononic crystal waveguides in an optomechanical cavity [192]. This hybrid C-OMS enables controllable switching between a single OMIT (single Fano resonance) and multiple OMIT (two or more Fano resonances) by manipulating and modifying the system parameters. We also study the frequency switching between the ON and OFF states to show the optical switching characteristic.

5.2 Theoretical framework

As schematically illustrated in Figure 5.1, we consider a theoretical model consisting of a single quantum dot embedded in an optomechanical photonic crystal(PhC) nanocavity where the PhC cavity is coupled to two mechanical modes with the interaction strength J. The quantum dot(QD) is approximated as a two-level system with a ground state $|1>$ and a single excited state $|2>$ and can be characterized by the pseudospin operators $\sigma^{\pm}$ and σ^{z}. A proper approximate representation of the mentioned two-level system is analogous to a QD molecule [193], which when coupled to a hybrid system affects both the output optical probe field and the displacement spectrum of the

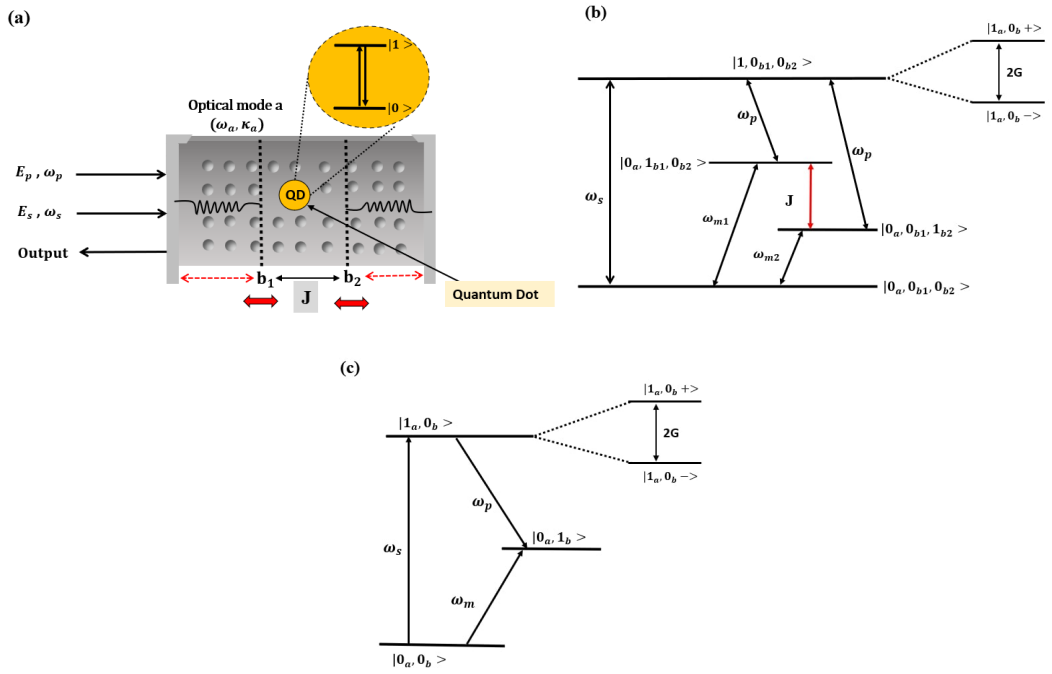

Figure 5.1: (a) Schematic diagram of the proposed system where a QD is embedded in the PhC optomechanical nanocavity. (b) Energy level diagram of the optomechanical system interacting with the two-level system (QD) where $|0_a>, |0_{b1}>$ and $|0_{b2}>$ denotes the zero number states of the cavity photons and the two phonons respectively and (c) Energy level diagram of the hybrid system when the two mechanical modes are identical (with the same frequency and mass) and the interaction is not considered (i.e., at $J = 0$).

mechanical modes. Here, the optical mode of the PhC cavity is coherently driven by a strong pump field with frequency ω_p and a weak probe field with frequency ω_s. So the total Hamiltonian of the proposed system is written as,

$$H = H_0 + H_I + H_d, \tag{5.1}$$

where

$$H_0 = \hbar\omega_a a^\dagger a + \hbar\omega_{m1} b_1^\dagger b_1 + \hbar\omega_{m2} b_2^\dagger b_2 + \frac{\hbar}{2}\omega_q \sigma^z \tag{5.2}$$

$$H_I = \hbar g_1 a^\dagger a(b_1 + b_1^\dagger) + \hbar g_2 a^\dagger a(b_2 + b_2^\dagger) - \hbar J(b_1^\dagger b_2 + b_1 b_2^\dagger) + \hbar G(\sigma^\dagger a + a^\dagger \sigma^-) \tag{5.3}$$

$$H_d = i\hbar E_p(a^\dagger e^{-i\omega_p t} - a e^{i\omega_p t}) + i\hbar E_s(a^\dagger e^{-i\omega_s t} - a^{i\omega_s t}) \tag{5.4}$$

Here, the first term of the bare Hamiltonian H_0 is the energy of the optical cavity mode with resonant frequency ω_a and $a(a^\dagger)$ are the respective annihilation (creation) operator of the cavity mode. The second and third term describes the energy of the two mechanical modes with frequencies ω_{m1} and ω_{m2} respectively and $b_1(b_1^\dagger)$ and $b_2(b_2^\dagger)$ are the annihilation(creation) operators of the two different mechanical modes respectively. The last term represents the energy of the two-level system (QD) with frequency ω_q. The first and second term of the interaction Hamiltonian H_I denotes the optomechanical interaction between the cavity mode and the two different mechanical modes with optomechanical coupling strengths g_1 and g_2 respectively. A 'defect' in a planar, one or two-dimensional, periodic dielectric structure of PhC cavity can confine both photons and phonons simultaneously inside a relatively small volume which exhibits strong optomechanical coupling [194, 195]. The cavity photons cause the mechanical modes to move slightly, modulating the resonance frequency of the optical cavity $\omega_a(x)$ up to the 1st order of Taylor's expansion as $\omega_a(x) = \omega_a(0) + x.\frac{d\omega_c}{dx}|_{x=0}$, where x is the displacement of the NR which forms the linear interaction of the optomechanical coupling. The third term of Eq. (5.3) denotes the energy exchange between both the mechanical modes of the system with the interaction strength J. The coupling strength between the two mechanical modes J can be accomplished by tuning the frequencies ω_{m1} and ω_{m2}, when the system was pumped at $2\omega_{m1}$ or $2\omega_{m2}$ (a process known as parametric pumping) or at $\omega_{m1} + \omega_{m2}$ (a process known as mechanical pumping) [196]. The last term denotes the QD-cavity interaction with coupling strength G. The Hamiltonian of the coherent pump and probe field is given by H_d where the first term denotes the driving of the cavity field at pumping amplitude E_p and the second term denotes the probe with amplitude E_s. The relationship between the amplitude of the control field (E_p) and the probe field (E_s) can be expressed as, $E_p = \sqrt{\frac{2\kappa_a P_p}{\hbar\omega_p}}$ and $E_s = \sqrt{\frac{2\kappa_a P_s}{\hbar\omega_s}}$, where $P_p(P_s)$ are the relevant field powers of the control(probe) field.

In a frame rotating with the pump field frequency ω_p, the Hamiltonian of the proposed system

is rewritten as,

$$\begin{aligned} H =&\hbar\Delta_a a^\dagger a + \hbar\omega_{m1} b_1^\dagger b_1 + \hbar\omega_{m2} b_2^\dagger b_2 + \frac{\hbar}{2}\Delta_q \sigma^z + \hbar g_1 a^\dagger a(b_1 + b_1^\dagger) + \hbar g_2 a^\dagger a(b_2 + b_2^\dagger) \\ &- \hbar J(b_1^\dagger b_2 + b_1 b_2^\dagger) + \hbar G(\sigma^\dagger a + a^\dagger \sigma^-) + i\hbar E_p(a^\dagger - a) + i\hbar E_s(a^\dagger e^{-i\delta t} - a^{i\delta t}) \end{aligned} \tag{5.5}$$

where $\Delta_a = \omega_a - \omega_p$ is the cavity-pump field detuning, $\Delta_q = \omega_q - \omega_p$ is the exciton-pump field detuning and $\delta = \omega_s - \omega_p$ is the probe-pump detuning.

Now, using $i\hbar\dot{O} = [O, H]$ (O is any operator), we obtain the following Heisenberg-Langevin equations of motion for the various degrees of freedom for our proposed system as,

$$\dot{a} = -(i\Delta_a + \frac{\kappa_a}{2})a - iG\sigma^- - ig_1 a(b_1 + b_1^\dagger) - ig_2 a(b_2 + b_2^\dagger) + E_p + E_s e^{-i\delta t} \tag{5.6}$$

$$\dot{b_1} = -(i\omega_{m1} + \frac{\kappa_{b1}}{2})b_1 - ig_1 a^\dagger a + iJb_2 \tag{5.7}$$

$$\dot{b_2} = -(i\omega_{m2} + \frac{\kappa_{b2}}{2})b_2 - ig_2 a^\dagger a + iJb_1 \tag{5.8}$$

$$\dot{\sigma^z} = -\Gamma_1(\sigma^z + \frac{1}{2}) + 2iG(\sigma^- a^\dagger - \sigma^\dagger a) \tag{5.9}$$

$$\dot{\sigma^-} = -(i\Delta_q + \Gamma_2)\sigma^- + iG\sigma^z a \tag{5.10}$$

Here, κ_a is the decay rate of cavity mode and κ_{b1} and κ_{b2} are the decay rates of the two different mechanical modes, respectively. $\Gamma_1(\Gamma_2)$ is the exciton relaxation (dephasing) rate.

5.3 Optical Multistability

In this section we investigate the steady state solution of equations (5.6)-(5.10), to understand the conditions during which the system experiences multistable (bistable and tristable) behaviour. Under the condition of strong pump field and weak probe field ($E_p >> E_s$), the Heisenberg operators a, b_1, b_2, σ^- and σ^z can be rewritten as the sum of its average steady-state values O_s and small fluctuation δO having a zero average value i.e. $O = O_s + \delta O$ ($O = a, b_1, b_2, \sigma^-, \sigma^z$). Thus the steady-state solutions of (5.6)-(5.10) can be obtained as,

$$\sigma_s^- = \frac{iG\sigma_s^z a_s}{(i\Delta_q + \Gamma_2)} \tag{5.11}$$

$$b_{1s} = \frac{-ig_1|a_s|^2 + iJb_{2s}}{(i\omega_{m1} + \frac{\kappa_{b1}}{2})} \tag{5.12}$$

$$b_{2s} = \frac{-ig_2|a_s|^2 + iJb_{1s}}{(i\omega_{m2} + \frac{\kappa_{b2}}{2})} \tag{5.13}$$

$$a_s = \frac{E_p}{i\Delta_1 + \frac{\kappa_a}{2} - \frac{G^2\sigma_s^z}{i\Delta_q + \Gamma_2}} \tag{5.14}$$

$$\sigma_s^z = -\frac{1}{2}(\frac{A_1}{A_1 + A_2|a_s|^2}) \tag{5.15}$$

where, $A_1 = \Gamma_1(\Gamma_2^2 + \Delta_q^2)$, $A_2 = 4G^2\Gamma_2$ and $\Delta_1 = \Delta_a + g_1(b_{1s} + b_{1s}^*) + g_2(b_{2s} + b_{2s}^*)$ is the effective detuning.

Further solving the above steady-state solutions we obtain the mean number of intracavity photons $n_a = |a_s|^2$, given by

$$|a_s|^2 = \frac{E_p^2}{(\frac{\kappa_a}{2} - \frac{G^2A_1C}{C^2+D^2})^2 + (\Delta_a + \frac{G^2A_1D}{C^2+D^2} + (g_1w_1 + g_2w_2)|a_s|^2)^2} \tag{5.16}$$

where $C = 2\Gamma_2(A_1 + A_2|a_s|^2)$, $D = 2\Delta_q(A_1 + A_2|a_s|^2)$, $w_1 = \frac{g_2J - ig_1}{M_1M_2 + J^2} + \frac{g_2J + ig_1}{M_1^*M_2^* + J^2}$, $w_2 = \frac{Jg_1 + ig_2(J^2-1)}{M_1M_2^2 + J^2M_2} + \frac{Jg_1 - ig_2(J^2-1)}{M_1^*M_2^{*2} + J^2M_2^*}$, $M_1 = \frac{\kappa_{b1}}{2} + i\omega_{m1}$ and $M_2 = \frac{\kappa_{b2}}{2} + i\omega_{m2}$.

Mean intracavity photon number (n_a) is important in measuring the optical nonreciprocity in the transmission of the light field in a typical bistable region [197]. In our case, we use realistic experimental values from [198, 199, 200] to support our findings and all the parameters used for the numerical study have been made dimensionless with respect to the mechanical frequency ω_{m1}. The optomechanical interaction of the two mechanical modes in our proposed system generates a higher rate of nonlinearity, which results in the possibility of optical multistability provided the system parameters are tuned properly.

Figure 5.2(a) illustrates the optical bistability curve, which is achieved by numerically solving Eq.(5.16), where the mean intracavity photon number is plotted as a function of incident pumping amplitude E_p. Here, the mean intracavity photon number shows a typical hysteresis type behaviour that changes with the increase or decrease of the pump power. Figure 5.2(a) demonstrates that

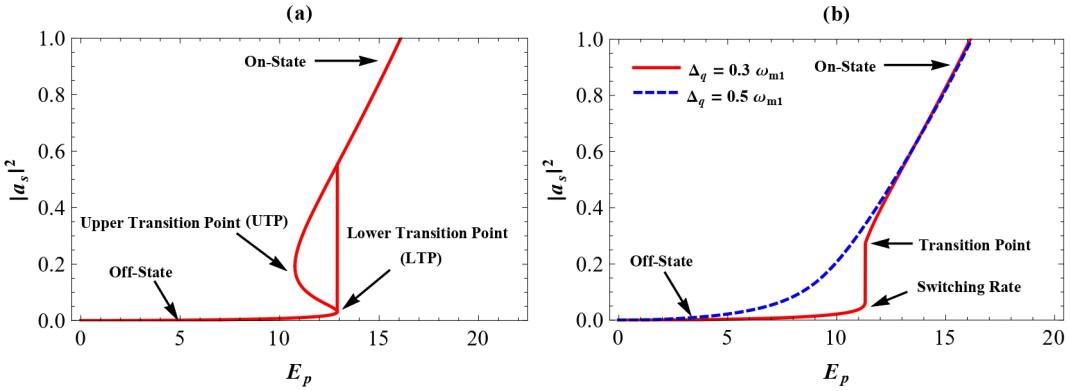

Figure 5.2: (a)Plot of intracavity photon number n_a as a function of E_p which illustrates an optical bistability curve for the value of exciton-pump detuning $\Delta_q = 0.2\omega_{m1}$. (b)Optical Switching behaviour for two different values of the exciton-pump detuning $\Delta_q = 0.3\omega_{m1}$ (Red solid line) and $\Delta_q = 0.5\omega_{m1}$ (Blue dashed line).

initially, the mean intracavity photon number (n_a) remains in the lower transition point (LTP, which corresponds to the smallest root), in which the photon number transitions from the Off-state to the On-state takes place, while the upper transition point (UTP) is where the photon number transition jumps from the On-state to the Off-state on reversing the pump field. As a result, increasing the input pump power will result in more intracavity photons. Thus, both the Off-state and On-state of the photon number can be considered as the stable solutions of Eq.(5.16). Figure 2(b) illustrates the typical optical switching behaviour for two different exciton-pump detuning values, where the intracavity photon value switches from a lower to a higher value at a certain rate of the incident pump power. Here, a smooth transition from the Off-state to the On-state can be seen for $\Delta_q = 0.5\omega_{m1}$ (Blue dashed line). However, for a lower value of exciton-pump detuning $\Delta_q = 0.3\omega_{m1}$ (Red solid line), a sharp transition from Off-state to On-state can be seen which indicates a higher gain and is favourable for optical switching [201, 202]. A sharp transition indicates a greater switching ratio, which is calculated as the ratio of maximum to minimum cavity emission in the steady-state driving curve using the equation, $SwicthingRatio = \frac{(P_{out})_{max}}{(P_{out})_{min}}$; where $P_{out} =< a_0^{\dagger} a_0 >$. When the steady-state photon number jumps from the Off-state to the On-state

at a certain pump rate, E_p, optical switching is possible for both the values of $\Delta_q = 0.3\omega_{m1}$ and $\Delta_q = 0.5\omega_{m1}$. It is obvious that the switching ratio for $\Delta_q = 0.3\omega_{m1}$ is greater compared to $\Delta_q = 0.5\omega_{m1}$. Since a less sensitive detector may also distinguish between the Off-state and On-state, a higher switching ratio is essential. Optomechanical interactions are known to be nonlinear, hence our proposed system becomes highly nonlinear when two coupled mechanical modes are introduced to it. This approach overcomes the limits that a single mechanical mode will have by significantly enhancing both the power density and speed. For example, in figure 5.2(b), switching between off-state to on-state occurs at the driving laser strength $E_p = 11MHz$. Correspondingly, the power level of the driving laser is equal to several nW ($\sim 22nW$ for $\kappa_a = 1kHz$). The field strength E_p is measured in the units of MHz which is directly related to the optical pump power by, $P_p = \frac{\hbar\omega_p E_p^2}{2\kappa_a}$. It is also known that coupling the two mechanical modes allows the transfer of information between the two modes which is useful for quantum networks. All other parameters used in figure 5.2 are : $\Delta_a = 15, G = 1, g_1 = g_2 = 0.02, \kappa_a = 1, \kappa_{b1} = \kappa_{b2} = 0.000001, \Gamma_1 = 0.65, \Gamma_2 = 0.33, \omega_{m1} = \omega_{m2} = 1, J = 0.01$.

Now, further adjusting the system parameters of our proposed system, optical double-bistability and tristability can be attained, as illustrated in figure 5.3. Figure 5.3(a) shows two connecting bistable behaviour for the value of QD-cavity coupling strength at $G = 8$, which has three distinct stable roots. At Lower Transition Point 1 (LTP 1), the system switches from Lower Stable Region (LSR) to the Meta-stable Region (MSR) with the increasing pump power. The system continues to be at MSR until it reaches the Lower Transition Point 2 (LTP 2) in response to a higher E_p before making a transition to the Upper Stable Region (USR). At this point, when E_p is lowered, the system first switches to the MSR at UTP 1, stays on MSR while E_p is being lowered further and then abruptly switches to LSR at LTP 1. The Lower Stable Region (LSR) of the Fig. 5.3(a) is clearly shown in a magnified form in Fig. 5.3(b). Thus the observed transition indicates an optical switching threshold behaviour of the form $LSR \rightleftharpoons MSR \rightleftharpoons USR$. The chemical potential in optical materials or superconductors can easily be used to adjust the switching thresholds of all-optical switching via optical bistability where the bistability's upper threshold denotes logic 1 and

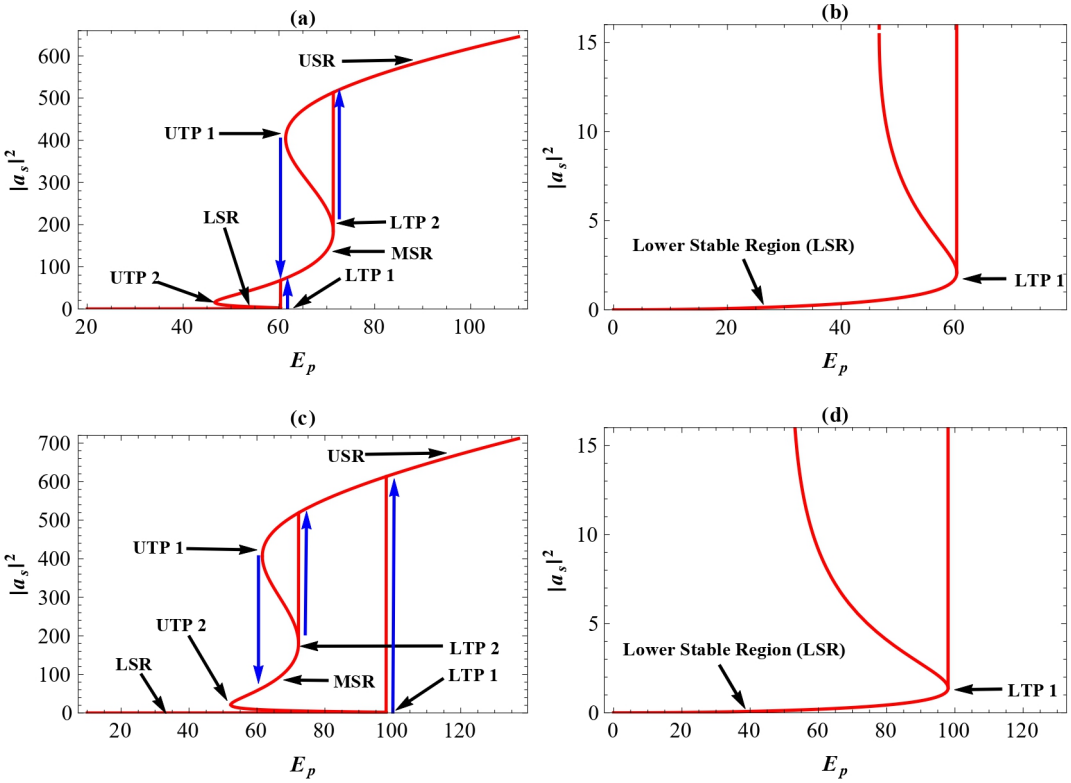

Figure 5.3: (a)and(c) Plot of intracavity photon number as a function of E_p. (b) Magnified view of the double-bistability, showing the Lower Stable Region (LSR) of the plot and (d) Magnified view of the optical tristability, showing the Lower Stable Region (LSR) of the plot.

writing, while its lower threshold denotes logic 0 and erasing [203]. As a result, logical processes and data access activities can be fully realized within the optical domain or dynamically controlled by the external parameters.

On the other hand Figure 5.3(c) illustrates a different tristable switching behaviour for the value of QD-cavity coupling strength at $G = 9$. Here, the system makes a direct transition from the LSR to USR at LTP 1, when the pump field is switched on at a higher rate and continues to stay on USR until the pumping rate E_p starts decreasing. Due to the reduced pumping rate another transition is made which brings the system down from USR to the MSR at UTP 1. At this stage, we may consider two different possibilities. Firstly, if the pumping rate is further increased then

the system will again switch to the USR by making a transition from the MSR at LTP 2. And secondly, if the system experiences a low pumping rate then it makes a transition from the MSR to the LSR at UTP 2. Thus, this type of tristable switching behaviour introduces new opportunities for developing advanced photonic devices. Note that the figure 5.3(d) illustrates the magnified view of the LSR of figure 5.3(c). A higher intracavity photon number in the USR of the hysteresis results from simultaneous presence of stronger pump field effect as well as strong QD-cavity coupling as shown in figure 5.3(a) and 5.3(c). Also, the ground state cooling of an optically levitated high-Q mechanical system has been shown in the aspect of bistability and multistability [204]. All other parameters used in figure 5.3 are: $\Delta_a = 7, \Delta_q = 6, g_1 = g_2 = 0.1, \kappa_a = 6, \kappa_{b1} = \kappa_{b2} = 0.000001, \Gamma_1 = 0.65, \Gamma_2 = 0.33, \omega_{m1} = \omega_{m2} = 1, J = 0.2$.

5.4 Tunable Multi-OMIT and Fano resonance in Transmission field

Optomechanically Induced Transparency(OMIT)[205] is a nonlinear phenomena which occurs due to an optomechanical(OM) interaction where a strong pump (control) field drives the OM system on the red sideband. Such OM interaction generates photons at second and higher-order sidebands as a result of the nonlinearity. In this section we will discuss the possibility of multiple OMIT and other nonlinear effects by controlling and tuning different system parameters of our proposed model. The quadrature of the phase and amplitude are defined by the operators

$X_1 = (a^* + a),\ X_2 = i(a^* - a),\ Y_1 = (b_1^* + b_1),\ Y_2 = i(b_1^* - b_1),\ Z_1 = (b_2^* + b_2),$

$Z_2 = i(b_2^* - b_2),\ U_1 = (\sigma^{-*} + \sigma^-),\ U_2 = i(\sigma^{-*} - \sigma^-),\ V_1 = (\sigma^{z*} + \sigma^z),\ V_2 = i(\sigma^{z*} - \sigma^z).$

However, each of the above mentioned operators can be rewritten as sum of its average steady-state value and small fluctuations as, $C = C_s + \delta C$ (where, $C = X_1, X_2, Y_1, Y_2, Z_1, Z_2, U_1, U_2, V_1$, and V_2). Now, to solve the linearized Quantum Langevin equations we remove the oscillatory terms and define the fluctuations of the system quadratures by using the following ansatz,

$$\delta X_1 = X_{1+}e^{-i\delta t} + X_{1-}e^{i\delta t} \tag{5.17}$$

$$\delta X_2 = X_{2+}e^{-i\delta t} + X_{2-}e^{i\delta t} \tag{5.18}$$

$$\delta Y_1 = Y_{1+}e^{-i\delta t} + Y_{1-}e^{i\delta t} \tag{5.19}$$

$$\delta Y_2 = Y_{2+}e^{-i\delta t} + Y_{2-}e^{i\delta t} \tag{5.20}$$

$$\delta Z_1 = Z_{1+}e^{-i\delta t} + Z_{1-}e^{i\delta t} \tag{5.21}$$

$$\delta Z_2 = Z_{2+}e^{-i\delta t} + Z_{2-}e^{i\delta t} \tag{5.22}$$

$$\delta U_1 = U_{1+}e^{-i\delta t} + U_{1-}e^{i\delta t} \tag{5.23}$$

$$\delta U_2 = U_{2+}e^{-i\delta t} + U_{2-}e^{i\delta t} \tag{5.24}$$

$$\delta V_1 = V_{1+}e^{-i\delta t} + V_{1-}e^{i\delta t} \tag{5.25}$$

$$\delta V_2 = V_{2+}e^{-i\delta t} + V_{2-}e^{i\delta t} \tag{5.26}$$

After the relevant substitutions, we used the standard input-output relation [206] to investigate the optical response of the output field of the optomechanical cavity as,

$$\begin{aligned} < X_{out}(t) > &= (E_p - \sqrt{\kappa_a}X_s)e^{-i\omega_p t} + (E_s - \sqrt{\kappa_a}X_{1+})e^{-i(\delta+\omega_p)t} - \sqrt{\kappa_a}X_{1-}e^{-i(\delta-\omega_p)t} \\ &= (E_p - \sqrt{\kappa_a}X_s)e^{-i\omega_p t} + (E_s - \sqrt{\kappa_a}X_{1+})e^{-i\omega_s t} - \sqrt{\kappa_a}X_{1-}e^{-i(2\omega_p-\omega_s)t} \end{aligned} \tag{5.27}$$

The phase dispersion can create a transmission group delay given as,

$$\tau_{Gd} = \frac{d\psi_t}{d\omega_s} = \frac{d(arg[t(\omega_s)])}{d\omega_s} \tag{5.28}$$

The transmission coefficient of the output probe field at the probe frequency is given as

$$t(\omega_s) = 1 - \frac{2\kappa_a < X_{1+} >}{E_s} \tag{5.29}$$

The transmission of the probe field over the OMIT window can change in response to the incident pump field resulting in phase dispersion given as,

$$\psi(t) = arg[t(\omega_s)] \tag{5.30}$$

In the case of positive group delay ($\tau_{Gd} > 0$), there will be faster transmission of light compared to negative group delay ($\tau_{Gd} < 0$) which corresponds to slow light. Thus, for both slow and fast light propagation the change of phase plays a significant role.

After rescaling the total transmission field, we get the transmission rate as,

$$|t|^2 = |1 - \frac{2\kappa_a < X_{1+} >}{E_s}|^2 \tag{5.31}$$

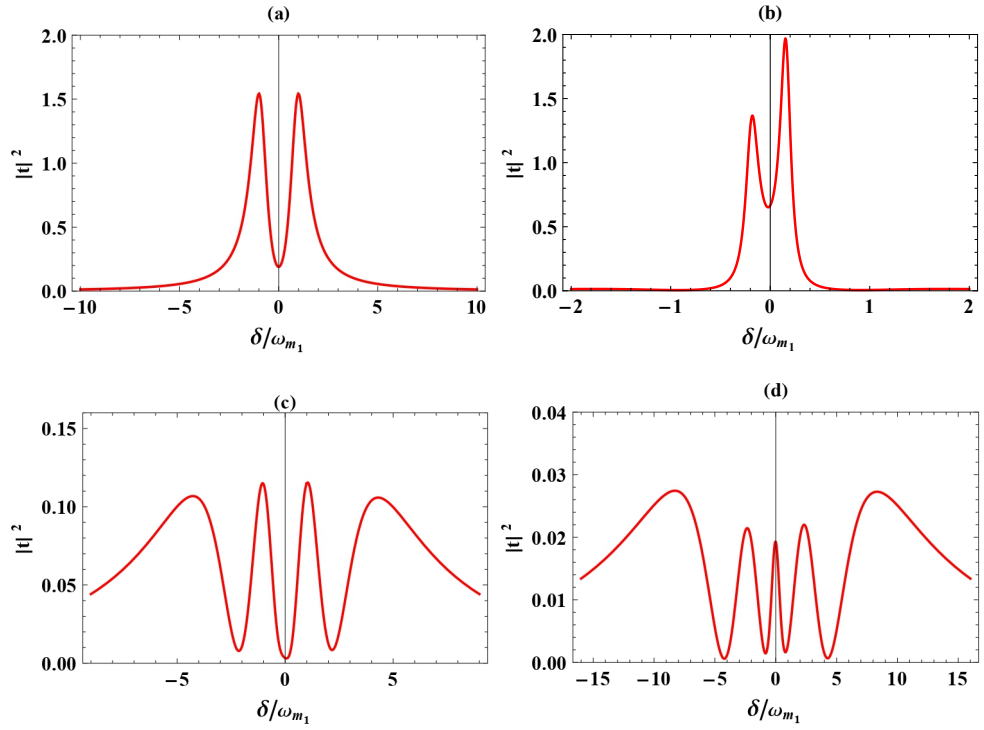

Figure 5.4: Plot of output probe field transmission $|t|^2$ as a function of normalised probe-pump detuning δ/ω_{m1} for different values of QD-cavity coupling strength (a) at $G = 0$ (b) at $G = 1$ (c) at $G = 3$, and (d) at $G = 6$. All other parameters used are: $\Delta_a = 0.9$, $\Delta_q = 0.5$, $g_1 = g_2 = 0.01$, $\kappa_a = 1$, $\kappa_{b1} = \kappa_{b2} = 0.00001$, $\Gamma_1 = 0.65$, $\Gamma_2 = 0.33$, $\omega_{m1} = \omega_{m2} = 1$, and $J = 0.01$.

In figure 5.4, the probe transmission $|t|^2$ is plotted as a function of normalised probe-pump detuning δ/ω_{m1} for different QD-cavity coupling strength G. In the absence of QD-cavity coupling i.e., at $G = 0$, the output probe field transmission as illustrated in figure 5.4(a) has the standard

absorption shape at $\delta/\omega_{m1} = 0$ along with the narrow transmission peaks which describes the transmission field behaviour as a single OMIT-phenomena [182]. Figure 5.4(b) illustrates the transmission spectrum of the output probe field which is observed in the presence of the two-level system (QD) i.e., at $G = 1$. Here, also a single dip can be seen evolving at $\delta = 0$, when the coupling between the QD and the cavity is in the intermediate regime ($G \sim \kappa_a/\omega_{m1}$). Now, further increasing the QD-cavity coupling strength to $G = 3$, it can be observed that the transmission spectra has three dips as illustrated in figure 5.4(c). These three dips occurs as a result of strong QD-cavity coupling ($G > \kappa_a/\omega_{m1}$) and the observed behaviour of the transmission field can be attributed as triple-OMIT, which is analogous to a $N + 1$ transparency window in a multiple cavity OM system [207].

Figure 4(d) illustrates the transmission spectrum with four dips occurs at off-resonant i.e, at $\delta/\omega_{m1} \neq 0$. Such transmission spectrum with four dips and five transmission peaks occurs due to coupled multi-mechanical mode system, when the QD-cavity coupling is in the ultra-strong regime i.e., at ($G >> \kappa_a/\omega_{m1}$). So this behaviour of the optical response can be attributed as four-OMIT phenomena. The results mentioned above can be achieved due to the destructive interference between the optical sidebands and the probe field when the beat frequency of the input fields matches multiple no of times with the frequency space of the mechanical motion which leads to multiple-OMIT in the tranmission spectrum.

Next, we investigate the influence of cavity detuning on the output probe transmission field of the system. In figure 5.5, the probe transmission $|t|^2$ is plotted as a function of normalised probe-pump detuning δ/ω_{m1} for different values of cavity detuning Δ_a. In Figure 5.5(a), a broad peak can be observed along with a narrow Fano profile for the value of detuning at $\Delta_a = \omega_{m1} - 0.5\kappa = 0.5$. The Fano line shape on the broad peak appears at $\delta/\omega_{m1} = 1$ for resonant frequency of the NR i.e., at $\omega_{m1} = \omega_{m2}$. For a larger value of detuning close to the red-sideband regime at $\Delta_a = \omega_{m1} - 0.1\kappa = 0.9$, as shown in figure 5.5(b), the output field generates a standard OMIT profile with narrow transparency window at $\delta/\omega_{m1} = 1$ which results due to the destructive interference between the first-order sideband and the input probe field of the system. For the value of detuning

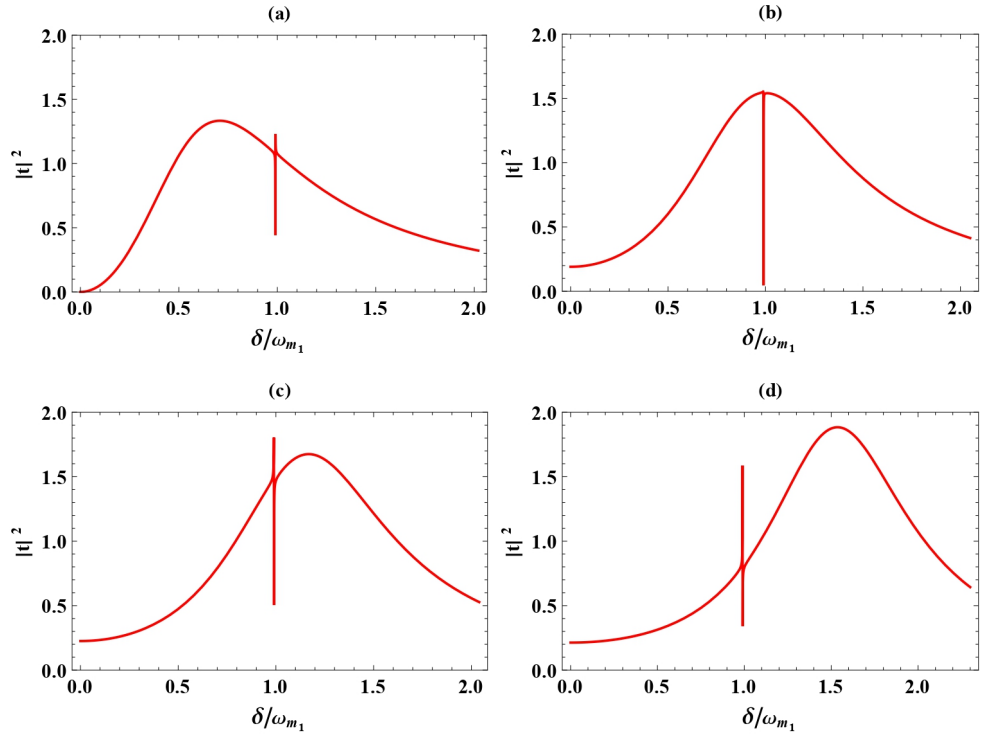

Figure 5.5: Plot of output probe field transmission $|t|^2$ as a function of normalised probe-pump detuning δ/ω_{m1} in the absence of the two-level system i.e, at $G = 0$ for different values of cavity detuning (a) at $\Delta_a = 0.5$ (b) at $\Delta_a = 0.9$. (c) at $\Delta_a = 1.1$ and (d) at $\Delta_a = 1.5$. All other parameters used are: $\Delta_q = 0.5$, $g_1 = g_2 = 0.1$, $\kappa_a = 1$, $\kappa_{b1} = \kappa_{b2} = 0.00001$, $\Gamma_1 = 0.65$, $\Gamma_2 = 0.33$, $\omega_{m1} = \omega_{m2} = 1$, and $J = 0.01$.

at $\Delta_a = \omega_{m1} + 0.1\kappa = 1.1$, as shown in figure 5.5(c), illustrates a broad peak that can be observed towards right of the Fano line shape. The Fano profile in the transmission spectrum can be seen located at the same coordinate (at $\delta/\omega_{m1} = 1$) as already shown in Figure 5(a). Similarly, for the value of detuning at $\Delta_a = \omega_{m1} + 0.5\kappa = 1.5$, a similar Fano profile is observed at $\delta/\omega_{m1} = 1$ along with a broad peak, as shown in Figure 5.5(d). Here, the broad peak of the transmission spectra makes a further shift towards far-right of the Fano line shape. From the above mentioned results we can conclude that the narrow dip of the Fano line shape appears exactly at $\delta/\omega_{m1} = 1$, when Δ_a is either larger or smaller than $\omega_{m1} = \omega_{m2} = 1$ and the shifting of the transparency peak

occurs due to the different sideband detuning.

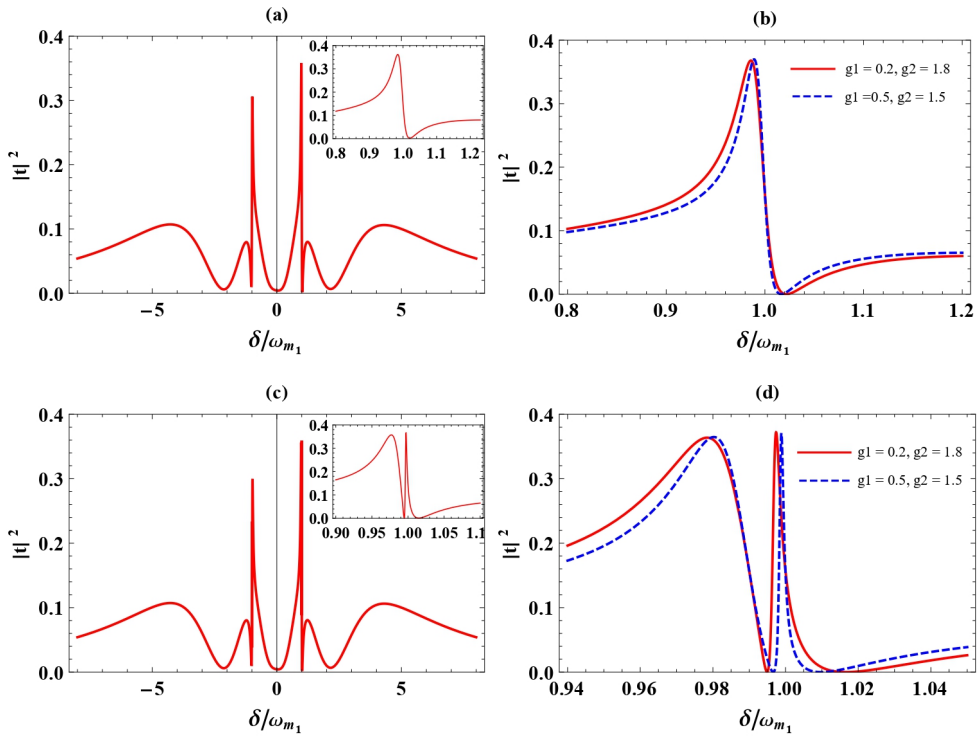

Figure 5.6: Plot of output probe field transmission $|t|^2$ as a function of normalised probe-pump detuning δ/ω_{m1}, when $g_1 \neq g_2$ (a) for the value of $J = 0$. (b)Magnified view of the single Fano profile for two different values of $g_1 = 0.2$ and $g_2 = 1.8$(Red solid line) and $g_1 = 0.5$ and $g_2 = 1.5$(Blue dashed line) for the value of $J = 0$. (c) for the value of $J = 0.01$, and (d)Magnified view of the double-Fano profile for two different values of $g_1 = 0.2$ and $g_2 = 1.8$(Red solid line) and $g_1 = 0.5$ and $g_2 = 1.5$(Blue dashed line) for the value of $J = 0.01$.

In our proposed system, the PhC cavity is coupled to two NRs with optomechanical coupling strengths g_1 and g_2 respectively. We analyse the effects of these two optomechanical-coupling strengths under strong QD-cavity coupling regime to show its influence on OMIT phenomena. Figure 5.6(a) illustrates the probe transmission plotted as function of normalised probe-pump detuning δ/ω_{m1}, for different values of both the optomechanical coupling strengths g_1 and g_2 in the

absence of the NRs interaction i.e $J = 0$. Here, we can observe four transmission peaks along with a single asymmetric splitting at $\delta/\omega_{m1} = \pm 1$ in the transmission spectrum of the output probe field when $g_1 \neq g_2$ (at $g_1 = 0.2$ and $g_2 = 1.8$), under the condition $J = 0$. Figure 6(b) illustrates the magnified view of the asymmetric single-Fano lineshape near $\delta/\omega_{m1} = 1$, in the transmission spectrum for two different values of g_1 and g_2 under the condition $J = 0$.In figure 5.6(b), we observed an identical single-Fano type structure at $\delta/\omega_{m1} = \pm 1$ for each different value of coupling (i.e, for increasing value of g_1 and decreasing value of g_2 or vice versa). The transmission spectra in Electromagnetically induced transparency (which is analogous to OMIT phenomena) or Fano lineshapes, were important to study while investigating structural asymmetry in quasi-bound states in the continuum [208].

On the other hand, when the interaction between the two mechanical modes is considered, the transmission spectrum of the output field demonstrates four transmission peaks (similar to the peaks appearing in figure 5.6(a)) but experiences a change from a single asymmetric splitting to double asymmetric splitting at $\delta/\omega_{m1} = \pm 1$, as shown in Figure 6(c). Here, for two different values of $g_1 = 0.2$ and $g_2 = 1.8$ we observe double-Fano profile under the condition of $J = 0.01$. Moreover, when we investigate for either increasing value of g_1 (decreasing value of g_2) or vice versa, then for each different values of optomechanical coupling, we observe double-Fano profile at $\delta/\omega_{m1} = \pm 1$. Figure 5.6(d) illustrates the magnified view of the double-Fano line shape in the transmission spectrum for two different values of g_1 and g_2 ($g_1 \neq g_2$) under the condition $J = 0.01$. The asymmetric Fano profile appears in the transmission spectrum for both the values of $J = 0$ and $J = 0.01$, because the scattering of field amplitude does not satisfy the criteria for OMIT phenomena. All other parameters used in figure 5.6 are: $\Delta_a = 0.9$, $\Delta_q = 0.5$, $\kappa_a = 1$, $\kappa_{b1} = \kappa_{b2} = 0.00001$, $\Gamma_1 = 0.65$, $\Gamma_2 = 0.33$, $\omega_{m1} = \omega_{m2} = 1$, and $G = 3$.

The output probe field contains information on the mechanical position because the mechanical movement induced by radiation pressure force (also known as optical force) can tune the optical cavity field due to the optomechanical coupling. In addition to the amplitude fluctuation of the optical mode, the cavity field is again coupled back to the mechanical modes via optical field

detuning that results in a backaction. In an optomechanical system, the dynamical backaction is represented by an interaction Hamiltonian, H_I where both the optical and the mechanical modes are coupled to each other and the radiation pressure force induced in the system can be derived as, $F_{rad} = -\frac{\partial H_I}{\partial x}$ [208]. Therefore, the optical force dependency on optomechanical interaction can be exploited for the application of optomechanical sensing to develop sensors that have inherent advantages over mechanically tunable methods in terms of bandwidth, speed, and efficiency [198, 209].

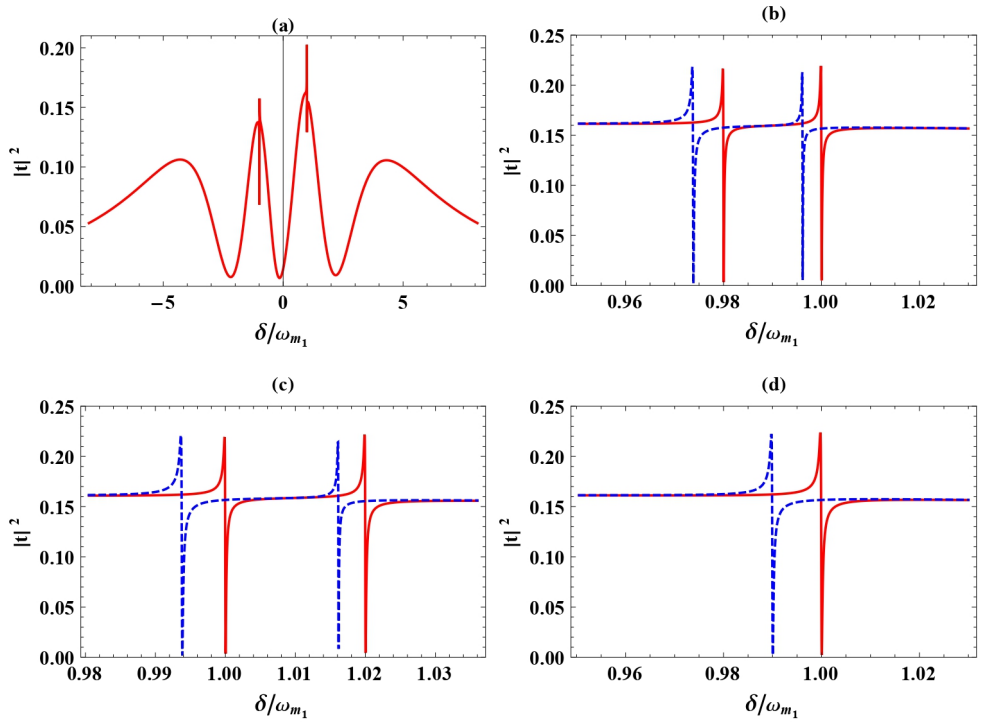

Figure 5.7: Plot of output probe field transmission $|t|^2$ as a function of normalised probe-pump detuning δ/ω_{m1} for two different cases at $J = 0$ (Red Solid line) and $J = 0.01$ (Blue dashed line). (a), (b), and (c) under the condition $\omega_{m1} \neq \omega_{m2}$ and (d) under the condition $\omega_{m1} = \omega_{m2}$.

We now investigate the possible results of the output transmission spectrum if we treat the two mechanical modes of our proposed system as independent oscillators with off-resonant mechanical frequencies ($\omega_{m1} \neq \omega_{m2}$) for two different cases at $J = 0$ and $J = 0.01$. Figure 5.7(a) shows the

probe transmission as a function of normalised probe-pump detuning δ/ω_{m1} under strong QD-cavity coupling regime. It shows four transmission peaks that appear with three transparency windows in the output probe field transmission of the system. Here, we observe an emerging Fano profile appearing in the Lorentzian absorption peak located at $\delta/\omega_{m1} = \pm 1$. We further investigate the Fano profile of the transmission spectrum for two different cases (at $J = 0$ and $J = 0.01$). It is observed that, in absence of the interaction between the two mechanical modes i.e, at $J = 0$, for different value of mechanical frequencies $\omega_{m1} = 1$ and $\omega_{m2} = 0.98$, we get two Fano lineshape at $\delta/\omega_{m1} = 1$ and 0.98 (Red solid line) respectively, as shown in figure 5.7(b). On the other hand, if the interaction between the two mechanical modes are considered i.e at $J = 0.01$, then two Fano lineshapes are generated again but here with a slight phase shift from right to left at $\delta/\omega_{m1} = 0.99$ and 0.97 (Blue dashed line) as shown in figure 5.7(b). Similarly, figure 5.7(c) illustrates two Fano lineshapes for $\omega_{m1} = 1$ and $\omega_{m2} = 1.02$ under the two different cases at $J = 0$ and $J = 0.01$. For $J = 0$, the Fano lineshape can be seen located at $\delta/\omega_{m1} = 1$ and 1.02 (Red solid line) and for $J = 0.01$, the Fano lineshape makes a phase shift from right to left at $\delta/\omega_{m1} = 0.99$ and 1.01 (Blue dashed line). But, in case of identical frequencies ($\omega_{m1} = \omega_{m2} = 1$), a single-fano lineshape can be observed under both the conditions $J = 0$ and $J = 0.01$ as shown in figure 5.7(d). For $J = 0$, the single Fano profile can be seen located at $\delta/\omega_{m1} = 1$ (Red solid line) and for $J = 0.01$, the single-Fano profile is located at $\delta/\omega_{m1} = 0.99$ (Blue dashed line), as illustrated in figure 5.7(d). Hence, the result obtained from our proposed model can be used to realize double-channel optical communication [210], high resolution spectroscopy [211], tunable cross-phase modulation [212], and high-speed optical switches [213]. All other parameters used in figure 5.7 are: $\Delta_a = 0.9, \Delta_q = 0.5, \kappa_a = 1, \kappa_{b1} = \kappa_{b2} = 0.00001, \Gamma_1 = 0.65, \Gamma_2 = 0.33, g_1 = g_2 = 0.2, G = 3$. Typically, linear or nonlinear optomechanical coupling is used to transmit the optical signal's output probe field, which also transmits data based on the displacement of the mechanical oscillator. By using displacement sensing based on an optomechanical system, it is possible to determine the displacement $x(\omega_{m1})$or $x(\omega_{m2})$ in the frequency domain of the mechanical oscillator. Also, the force acting on the mechanical oscillator may be measured with

high precision by the optomechanical system. The displacement of the mechanical mode and the external force has a relationship that follows $F(\omega) = x(\omega)/\chi(\omega)$, which can be used to derive the force signal via displacement detection. It is obvious that the only variable that distinguishes the sensitivity of force detection from that of displacement detection is a response factor that depends on mechanical frequency of the system [214].

5.5 Conclusion

In conclusion we have shown the possibilities of different optical response properties of our proposed system consisting of a QD embedded in a PhC cavity with two mechanical modes. The hybrid system attains tunable optical bistability, double-bistability and tristability by analysing the steady-state mean field approximation of the system. The presence of the two-level system in the hybrid optomechanical cavity shows single and multiple OMIT windows for strong QD-cavity coupling regime. The probe transmission spectrum also shows the occurrence of tunable Fano resonance by adjusting the system parameters for different sideband regimes. The enhancement of the radiation pressure interaction caused by the mechanical displacement results in a cavity frequency shift equivalent to or greater than the optical linewidth, which produces a nontrivial change in the cavity response. This provides another way to explain the nonlinear optomechanical interactions in this multi-mechanical parametric coupling regime. Using multiple mechanical modes in a hybrid PhC cavity to control both optical switching and light transmission will be a convenient method to explore in all-optical switching and sensing applications.

CHAPTER 6

Conclusions

6.1 Brief summary of work

In this thesis, I have presented a detailed theoretical study of a few novel hybrid cavity-QED systems consisting of optomechanical photonic crystal (PhC) cavities that are experimentally feasible for applications in all-optical switching, quantum information processing and sensing. We have demonstrated that a very high optical and optomechanical nonlinearity may be attained at the single photon level for each of our proposed systems. Photonic crystal(PhC) cavities based on optomechanical interaction have a promising future in the field of nanophotonics for further manipulating light propagation and have a lot of potential for developing lab-on-a-chip devices. In the emerging field of cavity optomechanics, coherent coupling between the optical modes of the cavity and the mechanical modes of the mechanical resonator is achieved by using the radiation

pressure of the confined cavity photon. Strong light-matter coupling in a hybrid cavity-QED system is evident due to the occurrence of vacuum Rabi splitting (VRS). To create quantum dot-based on-chip devices, any hybrid mesoscopic system that displays VRS can be employed. In order to do this, non-linearities in hybrid mesoscopic semiconductor cavities could potentially be important for coherently manipulating VRS and producing novel and intriguing physics that can be used to realise novel quantum devices. We have thoroughly investigated the optomechanical nonlinearities due to the radiation pressure of light on a mechanical resonator, which was earlier not explored in the context of vacuum Rabi splitting(VRS). We proposed a theoretical model that consists of a hybrid quantum electrodynamics (C-QED) system where a quantum dot(QD)-based photonic crystal optomechanical microcavity is coupled to an auxiliary cavity with a single mode waveguide. The auxiliary cavity plays an important role to study the quantum dynamics of the system. The steady-state mean-field analysis of our proposed system demonstrates the presence of tunable optical bistability, double-bistability, and tristability, paving the way for innovative multi-switching photonic devices. The probe absorption spectra of the fluctuations show a Mollow triplet including an asymmetric Fano resonance that has undergone optomechanically induced transparency (OMIT) modification. We identify the parameters that can coherently tune the OMIT-Fano line shapes. Particularly, three distinct quantum channels are offered by the auxiliary cavity, the QD, and the mechanically compliant DBR, to influence and control the system's optical response. This finding offers a novel foundation for further research into chip-scale nano-quantum photonic devices.

In a variety of optical and optomechanical systems,a nonlinear phenomenon known as four-wave mixing (FWM) has been observed which results from the creation of index grating that generates multiple sidebands when a two-level system interacts with a strong pump field and a weak probe field at off-resonant frequencies. Cavity-QED was an unexplored area to study four-wave mixing process along with optomechanical nolinearities induced due to radiation pressure force. Therefore, we have done a systematic study on the four-wave mixing (FWM) response of a cavity-QED system with optomechanical nonlinearity. In our proposed system all optical switching can be achieved through tunable optical bistability, which is demonstrated by the investigation of the

steady-state mean field. A controllable four-wave mixing (FWM) spectrum is generated due to the QD-cavity coupling strength, Rabi coupling strength, and pump power. For a strong coupling regime, the FWM displays a stronger signal. The off-resonant QD-cavity coupling strength controls the separation between the two peaks of the vacuum Rabi splitting, and the exciton-pump field detuning regulates the size of the sideband peaks. When the pump power is high, the two-level system significantly modifies the output probe fields where a transparency window appears in the four-wave mixing spectrum, allowing an approach to further improve the group delay and slow light of the system. Therefore, the results that were obtained show that a QD-based optomechanical photonic crystal nanocavity system is suitable for the development of optical switches as well as for the processing of quantum information.

When multi-mechanical resonators are built inside an optical cavity, cooperative response, switching features, better interactions, and nontrivial characteristics appear. For instance, using dynamical interactions between two or more mechanical resonators, one can engineer and control the coherent exchange of excitations or examine self-oscillations and synchronization. Optomechanical interactions are known to be nonlinear and hence including two coupled mechanical modes inside a cavity-QED system makes the system highly nonlinear. This approach overcomes the limitations that a single mechanical mode will have by considerably enhancing both power density and speed. Furthermore, it is known that coupling two mechanical modes can allow rapid transfer of information between them, which is useful for quantum networks. We have theoretically proposed a design where two nano-mechanical resonators are coupled to a cavity-QED system. The presence of two mechanical modes in our hybrid system will provide a strong control system for fast optical switching application than a single microcavity.

6.2 Future scope of work

For recent quantum technologies like quantum precision measurement and quantum information processing, quantum squeezing is a significant asset. In the field of cavity optomechanics, the creation of squeezed states of mechanical modes is an essential challenge. The increasing interest in the topic of multi-mode optomechanics inspires the development of quadrature squeezing in several mechanical resonators. However, the dark-mode effect highly overpowers the quantum effects in multiple-degenerate-mechanical modes of an optomechanical system. The creation of mechanical squeezing in a multi-mechanical-mode hybrid optomechanical system can be investigated by eliminating the dark-mode effect using the synthetic-gauge field method. Therefore, investigating optomechanical cooling and squeezing in a non-Hermitian system that consists of a photonic crystal cavity coupled to multiple intercoupled lossy mechanical resonators, that includes a closed-loop interaction, will be fascinating.

Some of the important cooling restrictions in Hermitian optomechanics are optical decoherence, mechanical damping, optomechanical backaction, heating due to optical excitations, strong coupling and thermal noise. The investigation of non-Hermitian optomechanics will be interesting for future approaches as it is a promising platform to overcome certain cooling limitations and develop novel cooling techniques with asymmetric damping.

Quantum optomechanical systems can be explored further by using non-Gaussian states which might be a non-Gaussian resource to study quantum optomechanical phenomena and to cool mechanical oscillators to reach the quantum ground state.

Bibliography

[1] T. Yoshie, A. Scherer, J. Hendrickson, G. Khitrova, H.M. Gibbs, G. Rupper, C. Ell, O.B. Shchekin and D.G. Deppe, Vacuum Rabi splitting with a single quantum dot in a photonic crystal nanocavity, Nature, **432** 200-203 (2004).

[2] H. J. Kimble. in Cavity Quantum Electrodynamics, edited by P. Berman. Academic Press, San Diego, (1994).

[3] M. O. Scully, and M. S. Zubairy, Quantum Optics, Cambridge University Press UK (1997).

[4] G. Gabrielse and J. Tan, Cavity Quantum Electrodynamics, P. Berman (Ed.), Academic Press, San Diego, 267 (1994).

[5] J. McKeever, A. Boca, A. D. Boozer, J. R. Buck and H. J. Kimble, Experimental realization of a one-atom laser in the regime of strong coupling, Nature, **425** 268-271 (2003).

[6] J. Y. Marzin, J. M. Gérard, A. Izraël, D. Barrier and G. Bastard, Photoluminescence of single InAs quantum dots obtained by self-organized growth on GaAs, Physical review letters, **73** 716 (1994).

[7] K. Brunner, G. Abstreiter, G. Böhm, G. Tränkle and G. Weimann, Sharp-line photoluminescence and two-photon absorption of zero-dimensional biexcitons in a GaAs/AlGaAs structure, Physical review letters, **73** 1138 (1994).

[8] A. J. Nozik, Exciton multiplication and relaxation dynamics in quantum dots: applications to ultrahigh-efficiency solar photon conversion, Inorg. Chem. **44** 6893–6899 (2005).

[9] P. Prabhakaran, W.J. Kim, K. S. Lee, and P. N. Prasad, Quantum dots (QDs) for photonic applications, Optical Materials Express, **2** 578-593 (2012).

[10] A. D. Yoffe, Low-dimensional systems: quantum size effects and electronic properties of semiconductor microcrystallites (zero-dimensional systems) and some quasi-two dimensional systems, Adv. Phys. **42** 173-266 (1993).

[11] A. D. Yoffe, Semiconductor quantum dots and related systems: electronic, optical, luminescence and related properties of low dimensional systems, Adv. in Phys. **50** 1-208 (2001).

[12] Y. Wang, and N. Herron, Nanometer-sized semiconductor clusters: materials synthesis, quantum size effects, and photophysical properties, J. Phys. Chem **95** 525-532(1991).

[13] D. Bera, L. Qian, T. K. Tseng and P. H. Holloway, Quantum dots and their multimodal applications: a review, Materials, **3** 2260 (2010).

[14] D. Fattal, Single Photons for Quantum Information Processing, Ph.D. thesis, Stanford University (2005).

[15] P. Prabhakaran, W. J. Kim, K. S. Lee, and P. N. Prasad, Quantum dots (QDs) for photonic applications, Optical Materials Express, **2** 578-593 (2012).

[16] J. Vu ˇckovic, Quantum optics and cavity QED with quantum dots in photonic crystals, Quantum Optics and Nanophotonics, 365-406 (2017).

[17] E. M. Purcell, H. C. Torrey, and R. V. Pound, Resonance absorption by nuclear magnetic moments in a solid, Physical review, **69** 37 (1946).

[18] E. M. Purcell, Spontaneous emission probabilities at radio frequencies. Confined Electrons and Photons: New Physics and Applications, 839-839 (1995).

[19] S. John, Strong localization of photons in certain disordered dielectric superlattices, Physical review letters, **58** 2486 (1987).

[20] E. Yablonovitch, Inhibited spontaneous emission in solid-state physics and electronics, Physical review letters, **58** 2059 (1987).

[21] R. G. Jackson, Novel sensors and sensing. CRC Press (2019).

[22] J. Xiang, and K. Hu, Limitation of multi-resolution methods in community detection, Physica A: Statistical Mechanics and its Applications, **391** 4995-5003 (2012).

[23] E. F. Nichols, and G. F. Hull, A preliminary communication on the pressure of heat and light radiation, Physical Review (Series I) **13**, 307 (1901).

[24] A. Xuereb, R. Schnabel, and K. Hammerer, Dissipative Optomechanics in a Michelson Sagnac Interferometer, Phys. Rev. Lett. **107** 213604 (2011).

[25] A. Sawadsky et al, Observation of Generalized Optomechanical Coupling and Cooling on Cavity Resonance, Phys. Rev. Lett. **114** 043601 (2015).

[26] W. P. Bowen, and G. J. Milburn, Quantum optomechanics, CRC press (2015).

[27] R. W. Boyd, Nonlinear optics, Academic press (2020).

[28] H. M. Gibbs, S. L. McCall, and T. N. C. Venkatesan, Differential gain and bistability using a sodium-filled Fabry-Perot interferometer, Phys. Rev. Lett. **36** 1135 (1976).

[29] G. I. Stegeman and A. Miller, Physics of All-Optical Chapter 5 Switching Devices, In Photonics in switching (p. 81) Academic Press (2012, December).

[30] D. E. McClelland, N. Mavalvala, Y. Chen and R. Schnabel, Advanced interferometry, quantum optics and optomechanics in gravitational wave detectors, Laser and Photonics Reviews, **5** 677-696 (2011).

[31] C. F. Ockeloen-Korppi, E. Damskägg, J. M. Pirkkalainen, M. Asjad, A. A. Clerk, F. Massel, M. J. Woolley and M. A. Sillanpää, Stabilized entanglement of massive mechanical oscillators, Nature, **556** 478-482 (2018).

[32] G. A. Brawley, M. R. Vanner, P. E. Larsen, S. Schmid, A. Boisen and W. P. Bowen, Nonlinear optomechanical measurement of mechanical motion, Nature communications, **7** 10988 (2016).

[33] W. D. Phillips, Nobel Lecture: Laser cooling and trapping of neutral atoms, Reviews of Modern Physics, **70** 721 (1998).

[34] G. S. Agarwal and S. Huang, Electromagnetically induced transparency in mechanical effects of light, Physical Review A,**81** 041803 (2010).

[35] S. Weis, R. Rivière, S. Deléglise, E. Gavartin, O. Arcizet, A. Schliesser, and T. J. Kippenberg, Optomechanically induced transparency, Science, **330** 1520-1523 (2010).

[36] M. Aspelmeyer, T. J. Kippenberg, and F. Marquardt, Cavity optomechanics, Reviews of Modern Physics, **86** 1391 (2014).

[37] C. K. Law, Interaction between a moving mirror and radiation pressure: A Hamiltonian formulation, Physical Review A, **51** 2537 (1995).

[38] I Carusotto and C Ciuti, Quantum fluids of light, Rev. Mod. Phys. **85** 299 (2013).

[39] I. Carusotto, Nonlinear atomic Fabry-Perot interferometer: From the mean-field theory to the atom blockade effect, Phys. Rev. A **63** 023610 (2001).

[40] A. Imamoglu, H. Schmidt, G. Woods, and M. Deutsch, Strongly interacting photons in a nonlinear cavity, Phys. Rev. Lett. **79** 1467 (1997).

[41] H.Mabuchi and A. C. Doherty, Cavity quantum electrodynamics: coherence in context, Science, **298** 1372-1377 (2002).

[42] S. Haroche and D. Kleppner, Cavity quantum electrodynamics, Phys. Today, **42** 24-30 (1989).

[43] A. M. Fox and M. Fox, Quantum optics: an introduction (Vol. 15), Oxford university press (2006).

[44] S. Strauf, Lasing under strong coupling, Nature Physics, **6** 244-245 (2010).

[45] H. J. Kimble, Strong interactions of single atoms and photons in cavity QED, Physica Scripta, **1998** 127 (1998).

[46] H. J. Chen, Auxiliary-cavity-assisted vacuum Rabi splitting of a semiconductor quantum dot in a photonic crystal nanocavity, Photonics Research, **6** 1171-1176 (2018).

[47] A. Faraon, A. Majumdar, D. Englund, E. Kim, M. Bajcsy, and J. Vučković, Integrated quantum optical networks based on quantum dots and photonic crystals, New Journal of Physics, **13** 055025 (2011).

[48] A. Majumdar, N. Manquest, A.Faraon, and J. Vučković, Theory of electro-optic modulation via a quantum dot coupled to a nano-resonator, Optics Express, **18** 3974-3984 (2010).

[49] J. J. Li, and K. D. Zhu, A quantum optical transistor with a single quantum dot in a photonic crystal nanocavity, Nanotechnology, **22** 055202 (2010).

[50] T. K. Fryett, C. M. Dodson, and A. Majumdar, Cavity enhanced nonlinear optics for few photon optical bistability, Optics express, **23** 16246-16255 (2015).

[51] P. D. Drummond and D. F. Walls, Quantum theory of optical bistability. I. Nonlinear polarisability model, Journal of Physics A: Mathematical and General, **13** 725 (1980).

[52] Y. C. Liu, Y. F. Xiao, X. Luan, Q. Gong, and C. W. Wong, Coupled cavities for motional ground-state cooling and strong optomechanical coupling, Physical Review A, **91** 033818 (2015).

[53] V. Fiore, Y. Yang, M. C. Kuzyk, R. Barbour, L. Tian and H. Wang, Storing optical information as a mechanical excitation in a silica optomechanical resonator, Physical review letters, **107** 133601 (2011).

[54] G. Khitrova, H. M. Gibbs, M. Kira, S. W. Koch, and A. Scherer, Vacuum Rabi splitting in semiconductors, Nature physics, **2** 81-90 (2006).

[55] K.Santhosh, O. Bitton, L. Chuntonov, and G. Haran, Vacuum Rabi splitting in a plasmonic cavity at the single quantum emitter limit, Nature communications, **7** , ncomms11823 (2016).

[56] J. Xia, Q. Qiao, G. Zhou, F. S. Chau, and G. Zhou, Opto-mechanical photonic crystal cavities for sensing application, Applied Sciences, **10** 7080 (2020).

[57] K.Asakawa et al., Photonic crystal and quantum dot technologies for all-optical switch and logic device, New Journal of Physics, **8** 208 (2006).

[58] K. Hennessy et al., Quantum nature of a strongly coupled single quantum dot–cavity system, Nature, **445** 896-899 (2007).

[59] D. Englund, A. Faraon, A. Majumdar, N. Stoltz, P. Petroff, and J. Vučković, An optical modulator based on a single strongly coupled quantum dot-cavity system in a pin junction, Optics Express, **17** 18651-18658 (2009).

[60] R. Bose, T. Cai, G.S. Solomon and E. Waks, All-optical tuning of a quantum dot in a coupled cavity system, Applied Physics Letters, **100** 231107 (2012).

[61] B. Peng et al., Parity–time-symmetric whispering-gallery microcavities, Nature Physics, **10** 394-398 (2014).

[62] S. Stufler, P. Ester, A. Zrenner and M. Bichler, Quantum optical properties of a single quantum dot two-level system, Physical Review B, **72** 121301 (2005).

[63] A. Zrenner, E. Beham, S. Stufler, F. Findeis, M. Bichler and G. Abstreiter, Coherent properties of a two-level system based on a quantum-dot photodiode, Nature, **418** 612-614 (2002).

[64] L Chang et al., Parity–time symmetry and variable optical isolation in active–passive-coupled microresonators, Nature photonics, **8** 524-529 (2014).

[65] V. N. Prakash, and A. B. Bhattacherjee, Negative effective mass, optical multistability and Fano line-shape control via mode tunnelling in double cavity optomechanical system, Journal of Modern Optics, **66** 1611-1621 (2019).

[66] L. M. Duan and H. J. Kimble, Scalable photonic quantum computation through cavity-assisted interactions, Physical review letters, **92** 127902 (2004).

[67] E. Del Valle and F. P. Laussy, Mollow triplet under incoherent pumping, Physical review letters, **105** 233601 (2010).

[68] H. Xiong and Y. Wu, Fundamentals and applications of optomechanically induced transparency, Applied physics reviews, **5** 031305 (2018).

[69] Y. C. Liu, B. B. Li, and Y. F. Xiao, Electromagnetically induced transparency in optical microcavities, Nanophotonics, **6** 789-811(2017).

[70] K. Qu, and G. S. Agarwal, Fano resonances and their control in optomechanics, Physical Review A, **87** 063813 (2013).

[71] M. Nomura, N. Kumagai, S. Iwamoto, Y. Ota, and Y. Arakawa, Laser oscillation in a strongly coupled single-quantum-dot-nanocavity system, Nat. Phys., **6** 279–283 (2010).

[72] S. Noda, M. Fujita, and T. Asano, Spontaneous-emission control by photonic crystals and nanocavities, Nat. Photonics, **1** 449–458 (2007).

[73] J. Q. Grim, I. Welland, S. G. Carter, A. S. Bracker, A. Yeats, C. S. Kim, M. Kim, K. Tran, I. Vurgaftman, and T. L. Reinecke, Scattering laser light from two resonant quantum dots in a photonic crystal waveguide, Physical Review B, **106** L081403 (2022).

[74] I.S. Grudinin, H. Lee, O. Painter, and K.J. Vahala, Phonon laser action in a tunable two-level system, Physical review letters,**104** 083901 (2010).

[75] H. Jing, S.K. Özdemir, X.Y. Lü, J. Zhang, L. Yang, and F. Nori, PT-symmetric phonon laser, Physical review letters, **113** 053604 (2014)

[76] J.J. Li, and K.D. Zhu, All-optical mass sensing with coupled mechanical resonator systems, Physics Reports **525** 223-254 (2013).

[77] E. E. Wollman, C. U. Lei, A. J. Weinstein, J. Suh, A. Kronwald, F. Marquardt, A. A. Clerk, and K. C. Schwab, Quantum squeezing of motion in a mechanical resonator, Science **349** 952-955 (2015).

[78] D. W.C. Brooks, T. Botter, S. Schreppler, T. P. Purdy, N. Brahms, and D. M. Stamper-Kurn, Non-classical light generated by quantum-noise-driven cavity optomechanics, Nature **488** 476-480 (2012).

[79] A. H. S. Naeini, S. Gröblacher, J. T. Hill, J. Chan, M. Aspelmeyer, and O. Painter, Squeezed light from a silicon micromechanical resonator, Nature **500** 185-189 (2013).

[80] A. D. O'Connell, M. Hofheinz, M. Ansmann, R. C. Bialczak, M. Lenander, E. Lucero, M. Neeley et al, Quantum ground state and single-phonon control of a mechanical resonator, Nature **464** 697-703 (2010).

[81] J. Chan, T. P. Alegre, A. H. S. Naeini, J. T. Hill, A. Krause, S. Gröblacher, M. Aspelmeyer, and O. Painter, Laser cooling of a nanomechanical oscillator into its quantum ground state, Nature **478** 89-92 (2011).

[82] A. H. S. Naeini, T. P. Alegre, J. Chan, M. Eichenfield, M. Winger, Q. Lin, J. T. Hill, D. E. Chang, and O. Painter, Electromagnetically induced transparency and slow light with optomechanics, Nature **472** 69-73 (2011).

[83] X. Zhou, F. Hocke, A. Schliesser, A. Marx, H. Huebl, R. Gross, and T. J. Kippenberg, Slowing, advancing and switching of microwave signals using circuit nanoelectromechanics, Nature Physics **9** 179-184 (2013).

[84] L. Fan, K. Y. Fong, M. Poot, and H. X. Tang, Cascaded optical transparency in multimode-cavity optomechanical systems, Nature communications **6** 1-6 (2015).

[85] J. Yang, and H. Chen, Vacuum Rabi Splitting of a Single Nitrogen-Vacancy Center Coupled to a Photonic Crystal Nanocavity, International Journal of Theoretical Physics **60** 3188-3196 (2021).

[86] H. Wang, D. J. Goorskey, and M. Xiao, Bistability and instability of three-level atoms inside an optical cavity, Physical Review A **65** 011801 (2001).

[87] H. Chang, H. Wu, C. Xie, and H. Wang, Controlled shift of optical bistability hysteresis curve and storage of optical signals in a four-level atomic system, Physical review letters **93** 213901 (2004).

[88] T. Elsässer, B. Nagorny, and A. Hemmerich, Optical bistability and collective behavior of atoms trapped in a high-Q ring cavity, Physical Review A **69** 033403 (2004).

[89] A. Joshi, W. Yang, and M. Xiao, Dynamical hysteresis in a three-level atomic system, Optics letters **30** 905-907 (2005).

[90] S. Gupta, K. L. Moore, K. W. Murch, and D. M. S. Kurn, Cavity nonlinear optics at low photon numbers from collective atomic motion, Physical review letters **99** 213601 (2007).

[91] A. Mitra, and R. Vyas, Entanglement and bistability in coupled quantum dots inside a driven cavity, Physical Review A **81** 012329 (2010).

[92] A. Mitra, and R. Vyas, Entanglement and bistability in coupled quantum dots inside a driven cavity, Physical Review A **81** 012329 (2010).

[93] R. D. Artuso, and G. W. Bryant, Optical Response of Strongly Coupled Quantum Dot-Metal Nanoparticle Systems: Double Peaked Fano Structure and Bistability, Nano letters **8** 2106-2111 (2008).

[94] A. V. Malyshev, Condition for resonant optical bistability, Physical Review A **86** 065804 (2012).

[95] J. B. Li, N. C. Kim, M. T. Cheng, L. Zhou, Z. H. Hao, and Q. Q. Wang, Optical bistability and nonlinearity of coherently coupled exciton-plasmon systems, Optics express **20** 1856-1861 (2012).

[96] J. B. Li, S. Liang, S. Xiao, M. D. He, N. C. Kim, L. Q. Chen, G. H. Wu, Y. X. Peng, X. Y. Luo, and Z. P. Guo, Four-wave mixing signal enhancement and optical bistability of a hybrid metal nanoparticle-quantum dot molecule in a nanomechanical resonator, Optics express **24** 2360-2369 (2016).

[97] B. S. Nugroho, A. A. Iskandar, V. A. Malyshev, and J. Knoester, Instabilities in the optical response of a semiconductor quantum dot—Metal nanoparticle heterodimer: Self-oscillations and chaos, Journal of Optics **19** 015004 (2016).

[98] S. H. Asadpour, and H. R. Soleimani, Phase dependence of optical bistability and multistability in a four-level quantum system near a plasmonic nanostructure, Journal of Applied Physics **119** 023102 (2016).

[99] B. Sarma, and A. K. Sarma, Controllable optical bistability in a hybrid optomechanical system, JOSA B **33** 1335-340 (2016).

[100] S. H. Kazemi, S. Ghanbari, and M. Mahmoudi, Controllable optical bistability in a cavity optomechanical system with a Bose–Einstein condensate, Laser Physics **26** 055502 (2016).

[101] S. A. Barbhuiya, and A. B. Bhattacherjee, Quantum optical response of a hybrid optomechanical device embedded with a qubit, Journal of Optics **22** 115401 (2020).

[102] S. Yeasmin, S. Yadav, A. B. Bhattacherjee, and S. Banerjee, Multistability and Fano resonances in a hybrid optomechanical photonic crystal microcavity, Journal of Modern Optics **68** 975-983 (2021).

[103] J. B. Li, S. Xiao, S. Liang, M. D. He, J. H. Luo, N. C. Kim, and L. Q. Chen, Bistable four-wave mixing response in a semiconductor quantum dot coupled to a photonic crystal nanocavity, Optics Express **25** 25663-25673 (2017).

[104] D. E. Grant and H. J. Kimble, Optical bistability for two-level atoms in a standing-wave cavity, Optics Letters **7** 353-355 (1982).

[105] B. Nagorny, Th. Elsässer and A. Hemmerich, Collective atomic motion in an optical lattice formed inside a high finesse cavity, Physical review letters **91** 153003 (2003).

[106] Z. Wang, S. Zhen, and B. Yu, Controlling optical bistability of acceptor and donor quantum dots embedded in a nonlinear photonic crystal, Laser Physics Letters **12** 046004 (2015).

[107] P. Meystre, and M. Sargent, Elements of quantum optics, Springer Science and Business Media, (2007).

[108] X. Liu, B. Kuyken, G. Roelkens, R. Baets, R. M. Osgood, and W. M. J. Green, Bridging the mid-infrared-to-telecom gap with silicon nanophotonic spectral translation, Nature Photonics **6** 667-671 (2012).

[109] Y. Ding, J. Xu, H. Ou, and C. Peucheret, Mode-selective wavelength conversion based on four-wave mixing in a multimode silicon waveguide, Optics express **22** 127-135 (2014).

[110] M. A. Foster, A. C. Turner, J. E. Sharping, B. S. Schmidt, M. Lipson, and A. L. Gaeta, Broad-band optical parametric gain on a silicon photonic chip, Nature **441** 960-963 (2006).

[111] J. S. Levy, A. Gondarenko, M. A. Foster, A. C. T. Foster, A. L. Gaeta, and M. Lipson, CMOS-compatible multiple-wavelength oscillator for on-chip optical interconnects, Nature photonics **4** 37-40 (2010).

[112] D. Press, T.D. Ladd, B. Zhang, and Y. Yamamoto, Complete quantum control of a single quantum dot spin using ultrafast optical pulses, Nature **456** 218-221 (2008).

[113] S. Noda, A. Chutinan, and M. Imada, Trapping and emission of photons by a single defect in a photonic bandgap structure, Nature **407** 608-610 (2000).

[114] Y. Gong, B. Ellis, G. Shambat, T. Sarmiento, J. S. Harris, and J. Vučković, Nanobeam photonic crystal cavity quantum dot laser, Optics express **18** 8781-8789 (2010).

[115] D. Englund, A. Faraon, I. Fushman, N. Stoltz, P. Petroff, and J. Vučković, Controlling cavity reflectivity with a single quantum dot, Nature **450** 857-861 (2007).

[116] J. Li, R. Yu, C. Ding, and Y. Wu, Optical bistability and four-wave mixing with a single nitrogen-vacancy center coupled to a photonic crystal nanocavity in the weak-coupling regime, Optics Express **22** 15024-15038 (2014).

[117] H. Yamaguchi, GaAs-based micro/nanomechanical resonators, Semiconductor Science and Technology **32** 103003 (2017).

[118] S. M. Thon, M. T. Rakher, H. Kim, J. Gudat, W. T. M Irvine, P. M. Petroff, and D. Bouwmeester, Strong coupling through optical positioning of a quantum dot in a photonic crystal cavity, Applied Physics Letters **94** 111115 (2009).

[119] R. Bose, T. Cai, G. S. Solomon, and E. Waks, All-optical tuning of a quantum dot in a coupled cavity system, Applied Physics Letters **100** 231107 (2012).

[120] G. I. Papadimitriou, C. Papazoglou, and A. S. Pomportsis, Optical switching: switch fabrics, techniques, and architectures, Journal of lightwave technology **21** 384-405 (2003).

[121] M. Borghi, C. Castellan, S. Signorini, A. Trenti, and L. Pavesi, Nonlinear silicon photonics, Journal of Optics **19** 093002 (2017).

[122] V. M. Rao, and S. Hughes, Single quantum-dot Purcell factor and β factor in a photonic crystal waveguide, Physical Review B **75** 205437 (2007).

[123] D. E. Reiter, T. Kuhn, M. Glässl, and V. M. Axt, The role of phonons for exciton and biexciton generation in an optically driven quantum dot, Journal of Physics: Condensed Matter **26** 423203 (2014).

[124] A. M. Barth, S. Lüker, A. Vagov, D. E. Reiter, T. Kuhn, and V. M. Axt, Fast and selective phonon-assisted state preparation of a quantum dot by adiabatic undressing, Physical Review B **94** 045306 (2016).

[125] R. W. Boyd, M. G. Raymer, P. Narum, and D. J. Harter, Four-wave parametric interactions in a strongly driven two-level system, Physical Review A **24** 411 (1981).

[126] J. Kasprzak, and W. Langbein, Four-wave mixing from individual excitons: Intensity dependence and imaging, physica status solidi (b) **246** 820-823 (2009).

[127] Y. C. Yu, J. F. Liu, X. L. Zhuo, G. Chen, C. J. Jin, and X. H. Wang, Vacuum Rabi splitting in a coupled system of single quantum dot and photonic crystal cavity: effect of local and propagation Green's functions, Optics Express **21** 23486-23497 (2013).

[128] Q. Mermillod, D. Wigger, V. Delmonte, D. E. Reiter, C. Schneider et al, Dynamics of excitons in individual InAs quantum dots revealed in four-wave mixing spectroscopy, Optica **3** 377-384 (2016).

[129] Z. Shen, Y. Zhang, Y. Chen, C. L. Zou, Y. F. Xiao, X. B. Zou, F. W. Sun, G. C. Guo, and C. H. Dong, Experimental realization of optomechanically induced non-reciprocity, Nature Photonics **10** 657-661 (2016).

[130] J. Restrepo, C. Ciuti, and I. Favero, Single-polariton optomechanics, Physical review letters **112** 013601 (2014).

[131] J. Restrepo, I. Favero, and C. Ciuti, Fully coupled hybrid cavity optomechanics: Quantum interferences and correlations, Physical Review A **95** 023832 (2017).

[132] A. Rundquist, A. Majumdar, and J. Vučković, Off-resonant coupling between a single quantum dot and a nanobeam photonic crystal cavity, Applied Physics Letters **99** 251907 (2011).

[133] X. Zhou, G. Koolstra, X. Zhang, et. al., Single electrons on solid neon as a solid-state qubit platform, Nature **605**, 46–50 (2022).

[134] M. Zanner, T. Orell, C. M. F. Schneider, et. al., Coherent control of a multi-qubit dark state in waveguide quantum electrodynamics, Nat. Phys. **18**, 538–543 (2022).

[135] O. Bitton, S. N. Guptaa, and G. Haran, Quantum dot plasmonics: from weak to strong coupling, Nanophotonics **8**, 559–575 (2019).

[136] P. Xie, Z. Liang, T. Jia, et. al., Strong coupling between excitons in a two-dimensional atomic crystal and quasibound states in the continuum in a two-dimensional all-dielectric asymmetric metasurface, Phys. Rev. B **104**, 125446 (2021).

[137] N. V. Leppenen, L. Lanco, and D. S. Smirnov, Quantum Zeno effect and quantum nondemolition spin measurement in a quantum dot–micropillar cavity in the strong coupling regime, Phys. Rev. B **103**, 045413 (2021).

[138] M. Metcalfe, Applications of cavity optomechanics, Applied Physics Reviews **1**, (2014).

[139] Yi-Wen Hu, Y-F Xiao, Y-C Liu, and Q. Gong, Optomechanical sensing with on-chip microcavities, Frontiers of Physics **8** 475-490 (2013).

[140] John D. Teufel, T. Donner, M. A. Castellanos-Beltran, J. W. Harlow, and K. W. Lehnert, Nanomechanical motion measured with an imprecision below that at the standard quantum limit, Nature nanotechnology **4** 820-823 (2009).

[141] M. Aspelmeyer, T. J. Kippenberg, and F. Marquardt, Cavity optomechanics, Reviews of Modern Physics, **86** 1391 (2014).

[142] D.J. Rogers, S.J. Papadakis, L.R. Churchill and C.W. Wong, Chip-scale optomechanical magnetometer, U.S. Patent 9,897,666 (2018).

[143] H. Du, G. Zhou, Y. Zhao, G. Chen, and F. S. Chau, Magnetic field sensor based on coupled photonic crystal nanobeam cavities, Applied Physics Letters **110** 061110 (2017).

[144] S. Sun, H. Kim, G. S. Solomon, and E. Waks, Strain tuning of a quantum dot strongly coupled to a photonic crystal cavity, Applied Physics Letters **103** 151102 (2013).

[145] X. Chew, G. Zhou, H. Yu, F. S. Chau, J. Deng, Y. C. Loke, and X. Tang, An in-plane nanomechanics approach to achieve reversible resonance control of photonic crystal nanocavities, Optics express **18** 22232-22244 (2010).

[146] F. Galeotti, I. S. Vollenbroek, M. Petruzzella, F. Pagliano, F. WM van Otten, Ž. Zobenica, A. Mohtashami, H. S. Marnani, R. W. van der Heijden, and A. Fiore, On-chip waveguide-coupled opto-electro-mechanical system for nanoscale displacement sensing, APL Photonics **5** 026103 (2020).

[147] B. Li, and C. Lee, NEMS diaphragm sensors integrated with triple-nano-ring resonator, Sensors and Actuators A: Physical **172** 61-68 (2011).

[148] T.W. Lu, and P-T Lee, Ultra-high sensitivity optical stress sensor based on double-layered photonic crystal microcavity, Optics express **17** 1518-1526 (2009).

[149] Y. Zhang, M. Menotti, K. Tan, et. al., Squeezed light from a nanophotonic molecule, Nat. Commun. **12**, 2233 (2021).

[150] G. Li, and Z. Q. Yin, Squeezing Light via Levitated Cavity Optomechanics, Photonics, **9**, 57 (2022).

[151] D. W. C. Brooks, T. Botter, S. Schreppler, T. P. Purdy, N. Brahms, and D. M. Stamper-Kurn, Non-classical light generated by quantum-noise-driven cavity optomechanics, Nature **488**, 476 (2012).

[152] A. H. Safavi-Naeini, S. Groblacher, J. T. Hill, J. Chan, M. Aspelmeyer, and O. Painter, Squeezed light from a silicon micromechanical resonator, Nature **500**, 185 (2013).

[153] T. P. Purdy, P. L. Yu, R. W. Peterson, N. S. Kampel, and C. A. Regal, Strong optomechanical squeezing of light, Phys. Rev. X **3**, 031012 (2013).

[154] Y. Seis, T. Capelle, E. Langman, et. al., Ground state cooling of an ultracoherent electromechanical system, Nat. Commun. **13**, 1507 (2022).

[155] D. Bothner, I. C. Rodrigues, and G. A. Steele, Four-wave-cooling to the single phonon level in Kerr optomechanics, Commun. Phys. **5**, 33 (2022).

[156] J. Chan, T. P. M. Alegre, A. H. Safavi-Naeini, et. al., Laser cooling of a nanomechanical oscillator into its quantum ground state, Nature **478**, 89 (2011).

[157] J. D. Teufel, T. Donner, D. Li, et. al., Sideband cooling of micromechanical motion to the quantum ground state, Nature **475**, 359 (2011).

[158] J.J Li, and Ka-Di Zhu, All-optical mass sensing with coupled mechanical resonator systems, Physics Reports **525** 223-254 (2013).

[159] K. Kustura, Carlos Gonzalez-Ballestero, A de los Ríos Sommer, N. Meyer, R. Quidant, and O. Romero-Isart, Mechanical squeezing via unstable dynamics in a microcavity, Physical Review Letters **128** 143601 (2022).

[160] I. S. Grudinin, H. Lee, O. Painter, and K. J. Vahala, Phonon laser action in a tunable two-level system, Phys. Rev. Lett. **104**, 083901 (2010).

[161] H. Jing, S. K. Ozdemir, X. Y. Lu, J. Zhang, L. Yang, and F. Nori, PT-symmetric phonon laser, Phys. Rev. Lett. **113**, 053604 (2014).

[162] A. H. Safavi-Naeini, T. P. Mayer Alegre, J. Chan, et. al., Electromagnetically induced transparency and slow light with optomechanics, Nature **472**, 69 (2011).

[163] X. Zhou, F. Hocke, A. Schliesser, et. al., Slowing advancing and switching of microwave signals using circuit nanoelectromechanics, Nature Phys. **9**, 179 (2013).

[164] H. J. Chen, Multiple-Fano-resonance-induced fast and slow light in the hybrid nanomechanical-resonator system, Phys. Rev. A **104**, 013708 (2021).

[165] M. Bhattacharya, and P. Meystre, Multiple membrane cavity optomechanics, Phys. Rev. A **78**, 041801 (2008).

[166] M. J. Hartmann, and M. B. Plenio, Steady state entanglement in the mechanical vibrations of two dielectric membranes, Phys. Rev. Lett. **101**, 200503 (2008).

[167] Z. Zhang, J. Yang, X. He, et. al., All-optical multi-channel switching at telecommunication wavelengths based on tunable plasmon-induced transparency, Opt. Comm. **425**, 196 (2018).

[168] B. Nair, A. Xuereb, and A. Dantan, Cavity optomechanics with arrays of thick dielectric membranes, Phys. Rev. A **94**, 053812 (2016).

[169] J. Li, G. Li, S. Zippilli, D. Vitali, and T. Zhang, Enhanced entanglement of two different mechanical resonators via coherent feedback, Phys. Rev. A **95**, 043819 (2017).

[170] P. Piergentili, L. Catalini, M. Bawaj, et. al., Two–membrane cavity optomechanics, New J. Phys. **20**, 083024 (2018).

[171] C. Gärtner, J. P. Moura, W. Haaxman, R. A. Norte, and S. Gröblacher, Integrated optomechanical arrays of two high reflectivity SiN membranes, Nano Lett. **18**, 7171–7175 (2018).

[172] P. Piergentili, L. Catalini, M. Bawaj, et. al., Multimode cavity optomechanics, M. D. P. I. Proceedings **12**, 54 (2019).

[173] M. J. Weaver, F. Buters, F. Luna, et. al., Coherent optomechanical state transfer between disparate mechanical resonators, Nat. Commun. **8**, 824 (2017).

[174] M. Ludwig, and F. Marquardt, Quantum many–body dynamics in optomechanical arrays, Phys. Rev. Lett. **111**, 073603 (2013).

[175] C. Yang, X. Wei, J. Sheng, and H. Wu, Phonon heat transport in cavity-mediated optomechanical nanoresonators, Nat. Commun. **11**, 4656 (2020).

[176] M. H. J. de Jong, J. Li, C. Gärtner, R. A. Norte, and S. Gröblacher, Coherent mechanical noise cancellation and cooperativity competition in optomechanical arrays, Optica **9**, 170–176 (2022).

[177] G. Heinrich, M. Ludwig, J. Qian, B. Kubala, and F. Marquardt, Collective dynamics in optomechanical arrays, Phys. Rev. Lett. **107**, 043603 (2011).

[178] M. Bagheri, M. Poot, L. Fan, F. Marquardt, and H. X. Tang, Photonic cavity synchronization of nanomechanical oscillators, Phys. Rev. Lett. **111**, 213902 (2013).

[179] J. Sheng, X. Wei, C. Yang, and H. Wu, Self–organized synchronization of phonon lasers, Phys. Rev. Lett. **124**, 053604 (2020).

[180] X. Wei, J. Sheng, C. Yang, Y. Wu, and H. Wu, Controllable two-membrane–in–the–middle cavity optomechanical system, Phys. Rev. A **99**, 023851 (2019).

[181] C. Genes, D. Vitali, and P. Tombesi, Simultaneous cooling and entanglement of mechanical modes of a micromirror in an optical cavity, New J. Phys. **10**, 095009 (2008).

[182] H. Xiong and Y. Wu, Fundamentals and applications of optomechanically induced transparency, Appl. Phys. Rev. **5** , 031305 (2018).

[183] S. A. Barbhuiya, and A. B. Bhattacherjee, Quantum optical response of a hybrid optomechanical device embedded with a qubit, Journal of Optics **22** 115401 (2020).

[184] S. Shahidani, M. H. Naderi, and M. Soltanolkotabi, Control and manipulation of electromagnetically induced transparency in a nonlinear optomechanical system with two movable mirrors, Phys. Rev. A **88**, 053813 (2013).

[185] J. Q. Zhang, Y. Li, M. Feng, and Y. Xu, Precision measurement of electrical charge with optomechanically induced transparency, Phys. Rev. A **86**, 053806 (2012).

[186] C. Jiang, B. Chen, and K. D. Zhu, Tunable pulse delay and advancement device based on a cavity electromechanical system, Europhys. Lett. **94**, 38002 (2011).

[187] K. Ullah, H. Jing, and F. Saif, Multiple electromechanically-induced-transparency windows and Fano resonances in hybrid nano-electro-optomechanics, Phys. Rev. A **97**, 033812 (2018).

[188] Q. Yang, B. P. Hou, and D. G. Lai, Local modulation of double optomechanically induced transparency and amplification, Opt. Exp. **25**, 9697 (2017).

[189] P. C. Ma, J. Q. Zhang, Y. Xiao, M. Feng, and Z. M. Zhang, Tunable double optomechanically induced transparency in an optomechanical system, Phys. Rev. A **90**, 043825 (2014).

[190] C. Jiang, L. Jiang, H. Yu, Y. Cui, X. Li, and G. Chen, Fano resonance and slow light in hybrid optomechanics mediated by a two-level system, Phys. Rev. A **96**, 053821 (2017).

[191] L. Tian and P. Zoller, Coupled ion-nanomechanical systems, Phys. Rev. Lett. **93**, 266403 (2004).

[192] K. Fang, M. Matheny, X. Luan, and O. Painter, Optical transduction and routing of microwave phonons in cavity-optomechanical circuits, Nat. Photon. **10**, 489 (2016).

[193] V. Bhatt, S. Yadav, P. K. Jha, and A. B. Bhattacherjee, Optical response in a double quantum dot molecule inside a nonlinear photonic crystal cavity, Phot. and Nano. Fund. and App., **51** 101043 (2022).

[194] M. Eichenfield, J. Chan, R. M. Camacho, K. J. Vahala, and O. Painter, Optomechanical crystals, Nature, **462** 78-82(2009).

[195] E. Gavartin, R. Braive, I. Sagnes, O. Arcizet, A. Beveratos, T. J. Kippenberg, and I. Robert-Philip, Optomechanical coupling in a two-dimensional photonic crystal defect cavity, Physical review letters, **106** 203902 (2011).

[196] J. M. L. Miller, A. Ansari, D. B. Heinz, et al., Effective quality factor tuning mechanisms in micromechanical resonators, Appl. Phys. Rev. **5**, 041307 (2018).

[197] P. Yang, X. Xia, H. He, et. al., Realization of Nonlinear Optical Nonreciprocity on a Few-Photon Level Based on Atoms Strongly Coupled to an Asymmetric Cavity, Phys. Rev. Lett. **123**, 233604 (2019).

[198] J. Xia, Q. Qiao, G. Zhou, F. S. Chau, and G. Zhou, Opto-mechanical photonic crystal cavities for sensing application, Applied Sciences **10** 7080 (2020).

[199] T. Yoshie, A. Scherer, J. Hendrickson, G. Khitrova, H. M. Gibbs, G. Rupper, C. Ell, O. B. Shchekin, and D. G. Deppe, Vacuum Rabi splitting with a single quantum dot in a photonic crystal nanocavity, Nature **432** 200-203 (2004).

[200] L. Chang, X. Jiang, S. Hua, C. Yang, J. Wen, L. Jiang, G. Li, G. Wang, and M. Xiao, Parity–time symmetry and variable optical isolation in active–passive-coupled microresonators, Nature photonics **8** 524-529 (2014).

[201] V. Bhatt, S. A. Barbhuiya, P. K. Jha, and A. B. Bhattacherjee, Controllable bistable optical switch and normal mode splitting in hybrid optomechanical semiconductor microcavity containing single quantum dot driven by amplitude modulated field, J. Phys. B: At. Mol. Opt. Phys. **53**, 155402 (2020).

[202] S. Yeasmin, S. Yadav, A. B. Bhattacherjee, and S. Banerjee, Multistability and Fano resonances in a hybrid optomechanical photonic crystal microcavity, J. Mod. Opt. **68**, 975-983 (2021).

[203] J. Wang, F. Xu, F. Liu, and D. Zhao, Optical bistable and multistable phenomena in aperiodic multilayer structures with graphene, Opt. Mat. **119**, 111395 (2021).

[204] K. W. Xiao, A. Xiong, N. Zhao, and Z. Yin, Quantum ground state cooling of translational and librational modes of an optically trapped nanoparticle coupling cavity, Quan. Eng. **3**, e62 (2021).

[205] S. Weis, R. Rivière, S. Deléglise, E. Gavartin, O. Arcizet, A. Schliesser, and T. J. Kippenberg, Optomechanically induced transparency, Science **330** 1520-1523 (2010).

[206] C. W. Gardiner and P. Zoller, Quantum Noise, Springer, Berlin, (2000).

[207] R. J. Xiao, G. X. Pan, and Y. Liu, Tunable multicolor optomechanically induced transparency in multi-cavity optomechanical system, Int. J. Theo. Phys. **59**, 3256–3267 (2020).

[208] C. Ma, Q. Lin, L. Wang, and K. Huang, Highly tunable dual bound states in the continuum in bulk Dirac semimetal metasurface, Appl. Phys. Exp. **14**, 042002 (2021).

[209] J. Rosenberg, Q. Lin, and O. Painter, Static and dynamic wavelength routing via the gradient optical force, Nature Photonics, **3**, 478-483 (2009).

[210] Yang Chen, Zhiming Chen, and Guoxiang Huang, Storage and retrieval of vector optical solitons via double electromagnetically induced transparency, Phys. Rev. A **91**, 023820(2015).

[211] M. Mazelanik, A. Leszczyński, and M. Parniak, Optical-domain spectral super-resolution via a quantum-memory-based time-frequency processor, Nat. Commun. **13**, 1-12 (2022).

[212] Shujing Li, Xudong Yang, Xuemin Cao, Chunhong Zhang, Changde Xie, and Hai Wang, Enhanced Cross-Phase Modulation Based on a Double Electromagnetically Induced Transparency in a Four-Level Tripod Atomic System,Phys. Rev. Lett. **101**, 073602 (2008).

[213] Pardeep Kumar and Shubhrangshu Dasgupta, Optical switching and bistability in four-level atomic systems, Phys. Rev. A **94**, 023851 (2016).

[214] B-B Li, L. Ou, Y. Lei, and Y-C Liu, Cavity optomechanical sensing, Nanophotonics **10** 2799-2832 (2021).

[215] Edmund X. DeJesus, and C. Kaufman, Routh-Hurwitz criterion in the examination of eigenvalues of a system of nonlinear ordinary differential equations, Physical Review A **35** 5288 (1987).

[216] A. Patil, Routh-Hurwitz criterion for stability: an overview and its implementation on characteristic equation vectors using MATLAB, Emerging Technologies in Data Mining and Information Security: Proceedings of IEMIS 2020, Volume 1, Springer 319-329 (2021).

[217] Robert N Clark, The Routh-Hurwitz stability criterion, revisited, IEEE Control Systems Magazine **12** 119-120 (1992).

Appendix A

Substituting $< \delta O >= O_+ e^{-i\delta t} + O_- e^{i\delta t}$ (O = a,b,c,σ^z, σ^-) into equations (6)-(10) and comparing the terms containing $e^{\pm i\delta t}$ on both the sides of the equations, we obtain:

$$-i\delta a_+ = -(i\Delta_a + \frac{\kappa_a}{2})a_+ - ig\sigma_+^- - iJc_+ + ig_{om}[a_s(b_+ + b_-^*) + a_+(b_s + b_s^*)], \tag{6.1}$$

$$i\delta a_- = -(i\Delta_a + \frac{\kappa_a}{2})a_- - ig\sigma_-^- - iJc_- + ig_{om}[a_s(b_- + b_+^*) + a_-(b_s + b_s^*)] - iE_s, \tag{6.2}$$

$$-i\delta b_+ = -(i\omega_b + \frac{\kappa_b}{2})b_+ + ig_{om}(a_s^* a_+ + a_s a_-^*), \tag{6.3}$$

$$i\delta b_- = -(i\omega_b + \frac{\kappa_b}{2})b_- + ig_{om}(a_s^* a_- + a_s a_+^*), \tag{6.4}$$

$$-i\delta c_+ = -(i\Delta_c + \frac{\kappa_c}{2})c_+ - iJa_+, \tag{6.5}$$

$$i\delta c_- = -(i\Delta_c + \frac{\kappa_c}{2})c_- - iJa_-, \tag{6.6}$$

$$-i\delta\sigma_+^- = -(i\Delta_e + \Gamma_2)\sigma_+^- + ig(a_s\sigma_+^z + \sigma_s^z a_+), \tag{6.7}$$

$$i\delta\sigma_-^- = -(i\Delta_e + \Gamma_2)\sigma_-^- + ig(a_s\sigma_-^z + \sigma_s^z a_-), \tag{6.8}$$

$$-i\delta\sigma_+^z = -\Gamma_1\sigma_+^z + 2ig(a_s^*\sigma_+^- + \sigma_s^- a_-^* - \sigma_s^{-*}a_+ - a_s\sigma_-^{-*}), \tag{6.9}$$

$$i\delta\sigma_-^z = -\Gamma_1\sigma_-^z + 2ig(a_s^*\sigma_-^- + \sigma_s^- a_+^* - \sigma_s^{-*}a_- - a_s\sigma_+^{-*}. \tag{6.10}$$

Solving the above set of ten equations, we obtain the linear susceptibility as,

$$\chi_{eff}^{(1)}(\omega_s) = \frac{\sigma_+(\omega_s)}{E_s}. \tag{6.11}$$

Appendix B

All the additional variables used in Eq. (15) are mentioned below:

$b_0 = c_0|a_0|^2$,

$P_0 = \frac{igw_0a_0 - i\Omega w_0}{(i\Delta_{pu} + \Gamma_2)}$,

$a_0 = \frac{-g\Omega w_0}{\Gamma_2\frac{k}{2} - \Delta_{pu}\Delta_{pc} - \Delta_{pu}B_1|a_0|^2 - g^2w_0 + i[\Delta_{pu}\frac{k}{2} + \Gamma_2\Delta_{pc} + \Gamma_2B_1|a_0|^2}$,

$b_1 = c_1a_1 + c_2a_{-1}^*$,

$$b_{-1} = c_3 a_{-1} + c_4 a_1^* \,,$$
$$a_1 = \alpha P_1 + \beta P_{-1}^* \,,$$
$$a_{-1} = (D_3 + D_4\beta^*)P_{-1} + D_4\alpha^* P_1^* \,,$$
$$w_1 = X_1 P_1^* + X_2 \tfrac{\mu E_{pr}}{\hbar} \,,$$
$$w_{-1} = X_3 P_{-1} + X_4 w_1^* + X_5 \tfrac{\mu E_{pr}}{\hbar} \,,$$
$$P_1 = \tau_1 P_{-1}^* + \tau_2 w_1 + \tau_3 \tfrac{\mu E_{pr}}{\hbar} w_0 \,,$$
$$P_{-1} = \tfrac{(\gamma_1\tau_2^* X_2^* + \gamma_1\tau_3^* w_0^* + \gamma_2 X_4 X_2^* + \gamma_2 X_5)\Gamma_2}{1-\gamma_1\tau_1^* - \gamma_1\tau_2^* X_1^* - \gamma_2 X_3 - \gamma_2 X_4 X_1^*} (\tfrac{\mu E_{pr}}{\hbar}) \,,$$
$$c_0 = \tfrac{-ig_0}{i\omega_m + \frac{\gamma_m}{2}} \,,$$
$$c_1 = \tfrac{-ig_0 a_0^*}{i\omega_m + \frac{\gamma_m}{2} - i\delta} \;,\; c_2 = \tfrac{-ig_0 a_0}{i\omega_m + \frac{\gamma_m}{2} - i\delta} \;,\; c_3 = \tfrac{-ig_0 a_0^*}{i\omega_m + \frac{\gamma_m}{2} + i\delta} \quad c_4 = \tfrac{-ig_0 a_0}{i\omega_m + \frac{\gamma_m}{2} + i\delta} \,,$$
$$D_1 = \tfrac{-ig}{i\Delta_{pc} + \frac{k}{2} - i\delta + ig_0 a_0(c_1 + c_4^*) + ig_0(c_0 + c_0^*)|a_0|^2} \,,$$
$$D_2 = \tfrac{-ig_0 a_0(c_2 + c_3^*)}{i\Delta_{pc} + \frac{k}{2} - i\delta + ig_0 a_0(c_1 + c_4^*) + ig_0(c_0 + c_0^*)|a_0|^2} \,,$$
$$D_3 = \tfrac{-ig}{i\Delta_{pc} + \frac{k}{2} + i\delta + ig_0 a_0(c_3 + c_2^*) + ig_0(c_0 + c_0^*)|a_0|^2} \,,$$
$$D_4 = \tfrac{-ig_0 a_0(c_4 + c_1^*)}{i\Delta_{pc} + \frac{k}{2} + i\delta + ig_0 a_0(c_3 + c_2^*) + ig_0(c_0 + c_0^*)|a_0|^2} \,,$$
$$\alpha = \tfrac{D_1}{1 - D_2 D_4^*} \;,\; \beta = \tfrac{D_2 D_3^*}{1 - D_2 D_4^*} \,,$$
$$\tau_1 = \tfrac{igw_0\beta}{i\Delta_{pu} + \Gamma_2 - i\delta - igw_0\alpha} \;,\; \tau_2 = \tfrac{iga_0 - i\Omega}{i\Delta_{pu} + \Gamma_2 - i\delta - igw_0\alpha} \;,\; \tau_3 = \tfrac{-i}{i\Delta_{pu} + \Gamma_2 - i\delta - igw_0\alpha} \,,$$
$$\gamma_1 = \tfrac{igw_0 D_4\alpha^*}{i\Delta_{pu} + \Gamma_2 + i\delta - igw_0(D_3 + D_4\beta^*} \;,\; \gamma_2 = \tfrac{(iga_0 - i\Omega)}{i\Delta_{pu} + \Gamma_2 + i\delta - igw_0(D_3 + D_4\beta^*)} \,,$$
$$X_1 = \tfrac{-2ig[p_0^*\alpha\tau_1 + p_0^*\beta + a_0 - P_0(D_3^* + D_4^*\beta) - P_0 D_4^*\alpha\tau_1 - \tau_1 a_0^*] + 2i\Omega - 2i\Omega\tau_1}{\Gamma_1 - i\delta + 2igP_0^*\alpha\tau_2 - 2igP_0 D_4^*\alpha\tau_2 - 2ig\tau_2 a_0^* - 2i\Omega\tau_2} \,,$$
$$X_2 = \tfrac{-2ig[P_0^*\alpha\tau_3 w_0 - P_0 D_4^*\alpha\tau_3 w_0 - \tau_3 w_0 a_0^*] - 2i\Omega\tau_3 w_0 + 2iP_0^*}{\Gamma_1 - i\delta + 2igP_0^*\alpha\tau_2 - 2igP_0 D_4^*\alpha\tau_2 - 2ig\tau_2 a_0^* - 2i\Omega\tau_2} \,,$$
$$X_3 = \tfrac{-2igP_0^*(D_3 + D_4\beta^*) - 2igD_4\alpha^* P_0^*\tau_1^* - 2ig\tau_1^* a_0 + 2igP_0\alpha^*\tau_1^* + 2igP_0\beta^* + 2iga_0^* + 2i\Omega\tau_1^* - 2i\Omega}{(\Gamma_1 + i\delta)} \,,$$
$$X_4 = \tfrac{-2igD_4\alpha^* P_0^*\tau_2^* - 2ig\tau_2^* a_0 + 2igP_0\alpha^*\tau_2^* + 2i\Omega\tau_2^*}{(\Gamma_1 + i\delta)} \,,$$
$$X_5 = \tfrac{-2igD_4\alpha^* P_0^*\tau_3^* w_0^* - 2ig\tau_3^* w_0^* a_0 + 2igP_0\alpha^*\tau_3^* w_0^* + 2i\Omega\tau_3^* w_0^* - 2iP_0}{(\Gamma_1 + i\delta)} \,.$$

Appendix C

Using the Routh-Hurwitz Criterion [215], we discovered the stability requirements for our proposed system as follows:

By calculating Eq.(5.11-5.15), we obtained a characteristic equation of the form:

$$r_5\lambda^5 + r_4\lambda^4 + r_3\lambda^3 + r_2\lambda^2 + r_\lambda + r_0 = 0 \tag{6.12}$$

where,

$$r_5 = 1 \tag{6.13}$$

$$r_4 = A + iB - i\Delta_q - k_{b1}/2 - k_{b2}/2 + \Gamma_1 - \Gamma_2 - iw_{m1} - iw_{m2} \tag{6.14}$$

$$\begin{aligned} r_3 = {} & iA\Delta_q - B\Delta_q - G^2 - J^2 + (Ak_{b1})/2 + (iBk_{b1})/2 - (i\Delta_q k_{b1})/2 + (Ak_{b2})/2 + \\ & (iBk_{b2})/2 - (i\Delta_q k_{b2})/2 - (k_{b1}k_{b2})/4 - A\Gamma_1 - iB\Gamma_1 + i\Delta_q\Gamma_1 + (k_{b1}\Gamma_1)/2 + (k_{b2}\Gamma 1)/2 + \\ & A\Gamma_2 + iB\Gamma_2 - (k_{b1}\Gamma_2)/2 - (k_{b2}\Gamma_2)/2 + \Gamma_1\Gamma_2 + iAw_{m1} - Bw_{m1} + \Delta_q w_{m1} - (ik_{b2}w_{m1})/2 \\ & + i\Gamma_1 w_{m1} - i\Gamma_2 w_{m1} + iAw_{m2} - Bw_{m2} + \Delta_q w_{m2} - (ik_{b1}w_{m2})/2 + i\Gamma_1 w_{m2} - i\Gamma_2 w_{m2} + w_{m1}w_{m2} \end{aligned} \tag{6.15}$$

$$\begin{aligned} r_2 = {} & AJ^2 + iBJ^2 - i\Delta_q J^2 + 1/2iA\Delta_q k_{b1} - (B\Delta_q k_{b1})/2 - (G^2 k_{b1})/2 + 1/2iA\Delta_q k_{b2} \\ & - (B\Delta_q k_{b2})/2 - (G^2 k_{b2})/2 + (Ak_{b1}k_{b2})/4 + 1/4iBk_{b1}k_{b2} - 1/4i\Delta_q k_{b1}k_{b2} - iA\Delta_q\Gamma_1 \\ & + B\Delta_q\Gamma_1 + G^2\Gamma_1 + J^2\Gamma_1 - (Ak_{b1}\Gamma_1)/2 - 1/2iBk_{b1}\Gamma_1 + 1/2i\Delta_q k_{b1}\Gamma_1 - \\ & (Ak_{b2}\Gamma_1)/2 - 1/2iBk_{b2}\Gamma_1 + 1/2i\Delta_q k_{b2}\Gamma_1 + (k_{b1}k_{b2}\Gamma_1)/4 - J^2\Gamma_2 + (Ak_{b1}\Gamma_2)/2 + 1/2iBk_{b1}\Gamma_2 + \\ & (Ak_{b2}\Gamma_2)/2 + 1/2iBk_{b2}\Gamma_2 - (k_{b1}k_{b2}\Gamma_2)/4 - A\Gamma_1\Gamma_2 - iB\Gamma_1\Gamma_2 + (k_{b1}\Gamma_1\Gamma_2)/2 + (k_{b2}\Gamma_1\Gamma_2)/2 - A\Delta_q w_{m1} \\ & - iB\Delta_q w_{m1} - iG^2 w_{m1} + 1/2iAk_{b2}w_{m1} - (Bk_{b2}w_{m1})/2 + (\Delta_q k_{b2}w_{m1})/2 - iA\Gamma_1 w_{m1} \\ & + B\Gamma_1 w_{m1} - \Delta_q\Gamma_1 w_{m1} + 1/2ik_{b2}\Gamma_1 w_{m1} + iA\Gamma_2 w_{m1} - B\Gamma_2 w_{m1} - 1/2ik_{b2}\Gamma_2 w_{m1} + \\ & i\Gamma_1\Gamma_2 w_{m1} - A\Delta_q w_{m2} - iB\Delta_q w_{m2} - iG^2 w_{m2} + 1/2iAk_{b1}w_{m2} - (Bk_{b1}w_{m2})/2 \\ & + (\Delta_q k_{b1}w_{m2})/2 - iA\Gamma_1 w_{m2} + B\Gamma_1 w_{m2} - \Delta_q\Gamma_1 w_{m2} + 1/2ik_{b1}\Gamma_1 w_{m2} + iA\Gamma_2 w_{m2} - B\Gamma_2 w_{m2} \\ & - 1/2ik_{b1}\Gamma_2 w_{m2} + i\Gamma_1\Gamma_2 w_{m2} - Aw_{m1}w_{m2} - iBw_{m1}w_{m2} + i\Delta_q w_{m1}w_{m2} - \Gamma_1 w_{m1}w_{m2} + \Gamma_2 w_{m1}w_{m2} \end{aligned} \tag{6.16}$$

$$
\begin{aligned}
r_1 = {} & iA\Delta_q J^2 - B\Delta_q J^2 - G^2 J^2 + 1/4iA\Delta_q k_{b1} k_{b2} - 1/4B\Delta_q k_{b1} k_{b2} - 1/4G^2 k_{b1} k_{b2} \\
& - AJ^2\Gamma_1 - iBJ^2\Gamma_1 + i\Delta_q J^2\Gamma_1 \\
& - 1/2iA\Delta_q k_{b1}\Gamma_1 + 1/2B\Delta_q k_{b1}\Gamma_1 + 1/2G^2 k_{b1}\Gamma_1 - 1/2iA\Gamma_q k_{b2}\Gamma_1 + 1/2B\Delta_q k_{b2}\Gamma_1 \\
& + 1/2G^2 k_{b2}\Gamma_1 - 1/4Ak_{b1}k_{b2}\Gamma_1 - 1/4iBk_{b1}k_{b2}\Gamma_1 + 1/4i\Delta_q k_{b1}k_{b2}\Gamma_1 + AJ^2\Gamma_2 \\
& + iBJ^2\Gamma_2 + 1/4Ak_{b1}k_{b2}\Gamma_2 + 1/4iBk_{b1}k_{b2}\Gamma_2 + J^2\Gamma_1\Gamma_2 - 1/2Ak_{b1}\Gamma_1\Gamma_2 \\
& - 1/2iBk_{b1}\Gamma_1\Gamma_2 - 1/2Ak_{b2}\Gamma_1\Gamma_2 - 1/2iBk_{b2}\Gamma_1\Gamma_2 + 1/4k_{b1}k_{b2}\Gamma_1\Gamma_2 - 1/2A\Delta_q k_{b2} w_{m1} - \\
& 1/2iB\Delta_q k_{b2} w_{m1} - 1/2iG^2 k_{b2} w_{m1} + A\Delta_q\Gamma_1 w_{m1} + iB\Delta_q\Gamma_1 w_{m1} + iG^2\Gamma_1 w_{m1} - 1/2iAk_{b2}\Gamma_1 w_{m1} \\
& + 1/2Bk_{b2}\Gamma_1 w_{m1} - 1/2\Delta_q k_{b2}\Gamma_1 w_{m1} + 1/2iAk_{b2}\Gamma_2 wm1 - 1/2Bk_{b2}\Gamma_2 w_{m1} - iA\Gamma_1\Gamma_2 w_{m1} \\
& + B\Gamma_1\Gamma_2 w_{m1} + 1/2ik_{b2}\Gamma_1\Gamma_2 w_{m1} - 1/2A\Delta_q k_{b1} w_{m2} - 1/2iB\Delta_q k_{b1} w_{m2} - 1/2iG^2 k_{b1} w_{m2} \\
& + A\Delta_q\Delta_1 w_{m2} + iB\Delta_q\Gamma_1 w_{m2} + IG^2\Gamma_1 w_{m2} - 1/2iAk_{b1}\Gamma_1 w_{m2} + 1/2Bk_{b1}\Gamma_1 w_{m2} - \\
& 1/2\Delta_q k_{b1}\Gamma_1 w_{m2} + 1/2iAk_{b1}\Gamma_2 w_{m2} - 1/2Bk_{b1}\Gamma_2 w_{m2} - iA\Gamma_1\Gamma_2 w_{m2} + B\Gamma_1\Gamma_2 w_{m2} \\
& + 1/2ik_{b1}\Gamma_1\Gamma_2 w_{m2} - iA\Delta_q w_{m1} w_{m2} + B\Delta_q w_{m1} w_{m2} + G^2 w_{m1} w_{m2} + A\Gamma_1 w_{m1} w_{m2} \\
& + iB\Gamma_1 w_{m1} w_{m2} - i\Delta_q\Gamma_1 w_{m1} w_{m2} - A\Gamma_2 w_{m1} w_{m2} - iB\Gamma_2 w_{m1} w_{m2} - \Gamma_1\Gamma_2 w_{m1} w_{m2}
\end{aligned}
\tag{6.17}
$$

$$
\begin{aligned}
r_0 = {} & -iA\Delta_q J^2\Gamma_1 + B\Delta_q J^2\Gamma_1 + G^2 J^2\Gamma_1 - 1/4iA\Delta_q k_{b1} k_{b2}\Gamma_1 + 1/4B\Delta_q k_{b1} k_{b2}\Gamma_1 \\
& + 1/4G^2 k_{b1} k_{b2}\Gamma_1 - AJ^2\Gamma_1\Gamma_2 - iBJ^2\Gamma_1\Gamma_2 - 1/4Ak_{b1}k_{b2}\Gamma_1\Gamma_2 - 1/4iBk_{b1}k_{b2}\Gamma_1\Gamma_2 + \\
& 1/2A\Delta_q k_{b2}|gamma_1 w_{m1} + 1/2iB\Delta_q k_{b2}\Gamma_1 w_{m1} + 1/2iG^2 k_{b2}\Gamma_1 w_{m1} - 1/2iAk_{b2}\Gamma_1\Gamma_2 w_{m1} \\
& + 1/2Bk_{b2}\Gamma_1\Gamma_2 w_{m1} + 1/2A\Delta_q k_{b1}\Gamma_1 w_{m2} + 1/2iB\Delta_q k_{b1}\Gamma_1 w_{m2} + 1/2iG^2 k_{b1}\Gamma_1 w_{m2} \\
& - 1/2iAk_{b1}\Gamma_1\Gamma_2 w_{m2} + 1/2Bk_{b1}\Gamma_1\Gamma_2 w_{m2} + iA\Delta_q\Gamma_1 w_{m1} w_{m2} - B\Delta_q\Gamma_1 w_{m1} w_{m2} \\
& - G^2\Gamma_1 w_{m1} w_{m2} + A\Gamma_1\Gamma_2 w_{m1} w_{m2} + iB\Gamma_1\Gamma_2 w_{m1} w_{m2}
\end{aligned}
\tag{6.18}
$$

Note: $A = (\frac{\kappa_a}{2} - \frac{G^2 A_1 C}{C^2+D^2})$, $B = (\Delta_a + \frac{G^2 A_1 D}{C^2+D^2} + (g_1 w_1 + g_2 w_2)|a_s|^2)$, $C = 2\Gamma_2(A_1 + A_2|a_s|^2)$, $D = 2\Delta_q(A_1 + A_2|a_s|^2)$, $w_1 = \frac{g_2 J - ig_1}{M_1 M_2 + J^2} + \frac{g_2 J + ig_1}{M_1^* M_2^* + J^2}$, $w_2 = \frac{Jg_1 + ig_2(J^2-1)}{M_1 M_2^2 + J^2 M_2} + \frac{Jg_1 - ig_2(J^2-1)}{M_1^* M_2^{*2} + J^2 M_2^*}$, $M_1 = \frac{\kappa_{b1}}{2} + i\omega_{m1}$ and $M_2 = \frac{\kappa_{b2}}{2} + i\omega_{m2}$

Now, the Routh array can be written as,

$$\begin{array}{ccc} r_5 & r_3 & r_1 \\ r_4 & r_2 & r_0 \\ b_1 & b_2 & b_3 \\ c_1 & c_2 & c_3 \\ d_1 & d_2 & d_3 \\ e_1 & d_2 & d_3 \end{array}$$

where,

$$b_1 = -\frac{1}{r_4}\begin{vmatrix} r_5 & r_3 \\ r_4 & r_2 \end{vmatrix}, b_2 = -\frac{1}{r_4}\begin{vmatrix} r_5 & r_1 \\ r_4 & r_0 \end{vmatrix}, b_3 = -\frac{1}{r_4}\begin{vmatrix} r_5 & 0 \\ r_4 & 0 \end{vmatrix},$$

$$c_1 = -\frac{1}{b_1}\begin{vmatrix} r_4 & r_2 \\ b_1 & b_2 \end{vmatrix}, c_2 = -\frac{1}{b_1}\begin{vmatrix} r_4 & r_0 \\ b_1 & b_3 \end{vmatrix}, c_3 = -\frac{1}{b_1}\begin{vmatrix} r_4 & 0 \\ b_1 & 0 \end{vmatrix},$$

$$d_1 = -\frac{1}{c_1}\begin{vmatrix} b_1 & b_2 \\ c_1 & c_2 \end{vmatrix}, d_2 = -\frac{1}{c_1}\begin{vmatrix} b_1 & b_3 \\ c_1 & c_3 \end{vmatrix}, d_3 = -\frac{1}{c_1}\begin{vmatrix} b_1 & 0 \\ c_1 & 0 \end{vmatrix},$$

$$e_1 = -\frac{1}{d_1}\begin{vmatrix} c_1 & c_2 \\ d_1 & d_2 \end{vmatrix}, e_2 = -\frac{1}{d_1}\begin{vmatrix} c_1 & c_3 \\ d_1 & d_3 \end{vmatrix}, e_3 = -\frac{1}{d_1}\begin{vmatrix} c_1 & 0 \\ d_1 & 0 \end{vmatrix}.$$

After numerically solving the characteristic equation we find that all the coefficients in the first column of the Routh array [216, 217] have the same sign and are non-zero. Therefore, we conclude that our system is stable.

Published Papers

- S. Yeasmin, S. Yadav, A B. Bhattacherjee, and S. Banerjee, Multistability and Fano resonances in a hybrid optomechanical photonic crystal microcavity, Journal of Modern Optics **68** 975-983 (2021).
- S. Yadav, S. Yeasmin, A. B. Bhattacherjee, and S. Banerjee, Far-Infrared frequency mode conversion using bulk acoustic phonon modes, Applied Physics B **128** 46 (2022).
- S. Yeasmin, S. A. Barbhuiya, A. B. Bhattacherjee, and S. Banerjee, Optical bistability and four-wave mixing response of a quantum dot coupled to an optomechanical photonic crystal nanocavity, Photonics and Nanostructures-Fundamentals and Applications **54** 101129 (2023).
- S. Yeasmin, S. A. Barbhuiya, A. B. Bhattacherjee, and S. Banerjee, Coupling of QD-based PhC nanocavity with two mechanical modes: An approach to tunable optical switching and sensing applications, Journal of Optics **25** 085401 (2023).

Conference Proceeding :

- S. Yadav, S. Yeasmin, A. B. Bhattacherjee and S. Banerjee, Engineering two-way photonic current in a solid state qubit-opto-mechanical system, ICEAT 2021, Lords Institute of Engineering and Technology, Hyderabad, 16-17 July 2021, Page:11.

Biography of Sajia Yeasmin

My name is **Sajia Yeasmin**, currently working as a full-time Ph.D. scholar under the supervision of Prof. Souri Banerjee and co-supervision of Prof. Aranya Bhuti Bhattacherjee at BITS Pilani, Hyderabad Campus, India. I was graduated with a bachelor's degree in Physics from Handique Girls' College under Gauhati University in Assam, India, in the year 2015. The following year, in 2018, I completed my post-graduation with Master's in Physics at University of Science and Technology, Meghalaya, India.

I'm interested to work on research projects that provide me with better opportunities for growth and exposure to novel ideas, enabling me to gather new perspectives which will contribute to the progress of my research career as well as uplift our society as a whole.

Along with several international peer-reviewed publications, I have also taken part in a variety of activities during my academic career, including

- Certificate of Participation in One Day ACADEMIC FIELD SURVEY conducted by the Department of Statistics, Handique Girls' College, Guwahati, Assam, India (2013).
- Certificate of Participation in National Level Seminar on NON-EQUILIBRIUM COMPLEX SYSTEMS organized by Handique Girls' College, Guwahati, Assam, India (2014).
- 3rd Position in DREAMPRENEUR in ERTHNITI held at Assam Engineering College, Guwahati, India (2015).
- Certificate of Participation for poster presentation in OSI-International Symposium on Optics (OSI-ISO 2018) at IIT KANPUR.
- Certificate of Participation for a training workshop in preparing a "Ph.D. application in the field of Natural Sciences to German Universities and research centers" held at Hyderabad by German Academic Exchange Service (DAAD) Chennai (2019).

- Certificate of Participation in an online poster presentation, AIP Horizons - Photonics in Chemical Physics Conference, September (2021)

- Certificate of Participation in poster presentation in the XLV symposium of the Optical Society of India on "Conference on Optics, Photonics and Quantum Optics (COPaQ 2022)" held at IIT Roorkee (2022).

During my undergraduate and post-graduate degree, I was also engaged with project work which are mentioned below,

- To design a '5 VOLT REGULATED POWER SUPPLY' - (B.SC 6th semester), 2015.

- 'Investigation of Kerr Nonlinearity at Electromagnetically Induced Transparency Windows in a Four-Level Quantum Well System' (M.Sc 4th Semester),2018.

Biography of Prof. Souri Banerjee

Prof. Souri Banerjee pursued his B.Sc. in Physics and an M.Sc. in Physics at Scottish Church College in Kolkata. He has done his Ph.D. in high-temperature superconductivity and applications of solid-state physics like nanomaterials. During his post-doc in Japan, he worked on device physics. Currently, he holds the position of Senior Professor, Department of Physics at Birla Institute of Technology and Science, Pilani, Hyderabad Campus, India. He also holds the position of Dean of Faculty Affairs (of all the BITS Pilani campuses).

He teaches the following undergraduate(UG) and postgraduate(PG) courses: Physics I (UG), Physics II (UG), Mechanics, Oscillations and Waves (UG), Classical Mechanics (PG), Quantum Mechanics I (PG), Optical Physics and Applications (PG), IC Fabrication Technology (PG), Introduction to Nano-sciences (EL), Modern Physics Lab (PG).

His research experience includes:

Extensive use of Clean Room (Class-100 to 10,000), Photolithography and Mask making, Electron Beam Lithography (Minimum beam spot size of 10nm) equipped with mini-CAD for patterning and transfer of about 30 nm gap pattern, CVD, Etching, Oxidation Technique, Electron Beam Evaporator for very thin metal deposition, Field Emission type SEM to obtain image of narrow quantum well or narrow patterns, Thin film and nanocrystal deposition using different CVD techniques, Sputtering etc.

- Device Fabrication: Successfully fabricated Single Electron Memory Device with short and narrow channel having nanocrystal Si dots as floating gate. The device is operated even at room temperature.

- Instruments for Electrical Characterization: Semiconductor Parameter Analyzers (HP4156), Pulse Generator (HP81105A), Probe Station equipped with close cycle He cryo-cooler (<10 K).

- Scanning Probe Studies : Use of Atomic Force Microscopy equipped with nanolithography techniques (Seiko Instrument, Japan) for making, manipulating and imaging nanometer size features. Various modes of operation; tapping, contact and non-contact mode to inject charge in nanocrystals and their probing, Kelvin Probe Microscopy to image surface potential.

His research Projects that has been completed by him As Co-PI includes,

- BRNS-DAE Funded: 19.5 lakhs (August 2011 onward for 3 yrs) on "Site-specific immobilization of a single DNA molecule"

- CSIR Funded: 22.26 lakhs (January 2013 onward for 3 yrs) on "AC impedance measurement on two-dimensional origami structures of various shapes"

- BRNS-DAE funded, 36 Lacs (With Dr. Souvik Kundu, Dept of EEE) 2017-2020 on "Metal-Oxide and Nanocomposite Based Low-Power Non-volatile Switching Device: A Novel Approach"

His works have appeared in a variety of peer-reviewed international journals, and have earned a number of awards and research positions across the globe.

Biography of Aranya Bhuti Bhattacherjee

Prof. Aranya Bhuti Bhattacherjee pursued his Ph.D. in Physics degree at the University of Delhi, India in the years (1990-1995). Currently, he holds the position of Professor at Birla Institute of Technology and Science, Pilani, Hyderabad Campus, Jawahar Nagar, Kapra Mandal, Medchal District, Hyderabad 500 078, Telangana, India. His previous positions include UGC Associate Professor (Directly Appointed by University Grants Commission, New Delhi) at School of Physical Sciences, Jawaharlal Nehru University, New Delhi, (2013-2018) and Associate Professor at Atma Ram Sanatan Dharma College, University of Delhi,(1993-2013), both of which involve a significant amount of work.

He has taught the following courses in the Undergraduate Level : Solid State Physics, Thermal Physics, Mechanics, Mathematical Physics, Optics, Numerical analysis, Waves and Oscillations, Modern Physics, Electromagnetic theory, Laser Physics, Quantum Optics, Atomic and Molecular Physics and in the Postgraduate Level : Condensed Matter Physics (MSc), Advanced Condensed Matter (MSc), Special topics in condensed matter (Pre-PhD), Laser Physics (MSc), Topics in Classical and Quantum Mechanics (pre-PhD), Computational Physics (MSc), Mathematical Physics (MSc), Atomic and Molecular Physics, Quantum Optics. His area of specialization includes Theoretical Quantum Photonics, Quantum-Optomechanics, Quantum Gases, Low-dimensional physics. Also, his research Projects that has been completed by him As PI includes,

- Electromagnetic properties of atoms moving in an optical Lattice (2001-2003). Sponsoring organization: University Grants Commission.
- Optomechanical control of superfluid properties of a Bose Einstein condensate coupled to a nano-mechanical resonator: detection of weak forces, (2012-2015), Sponsoring organization: Department of Science and Technology, New Delhi.

and As Co - PI he has Completed the project

- Dynamics of coupled quantum dots in a semiconductor micro-cavity : feasibility of building all optical switches. SERB project no. : emr/ 2017/0019870.

He holds numerous awards and research positions across the world and has published in hundreds of peer-reviewed international journals. Additionally, under his capable leadership, he has finished supervising seven PhD fellows and is now working with five more, including me.